

SHOCK FORMATION AND STAR FORMATION  
IN GALACTIC SPIRALS

by

WILLIAM WOODRUFF ROBERTS, JR.

S.B., Massachusetts Institute of Technology  
(1964)

SUBMITTED IN PARTIAL FULFILLMENT  
OF THE REQUIREMENTS FOR THE  
DEGREE OF DOCTOR OF  
PHILOSOPHY

at the

MASSACHUSETTS INSTITUTE OF  
TECHNOLOGY

November, 1968, i. e. Feb. 1969

Signature of Author

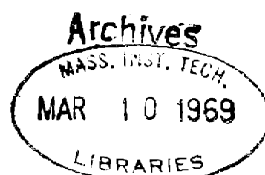
Department of Mathematics, November 14, 1968

Certified by

Thesis Supervisor

Accepted by

Chairman, Departmental Committee on Graduate  
Students



SHOCK FORMATION AND STAR FORMATION  
IN GALACTIC SPIRALS

by

WILLIAM WOODRUFF ROBERTS, JR.

Submitted to the Department of Mathematics on  
November 14, 1968 in partial fulfillment of the  
requirements for the degree of  
Doctor of Philosophy

Abstract

The dynamical problems of shock formation and star formation in a normal spiral galaxy are investigated. The motion considered is that of the continuum of turbulent gas composing the gaseous disk moving in a gravitational field consisting of a two-armed spiral field superposed on the Schmidt model for the Milky Way System. The purpose is to simulate the dynamics of the galactic gaseous disk and to gain further understanding of the problems: (1) why young stars and H II regions lie only along a grand design of spiral structure, (2) why the young stars are always found in associations along the spirals, and (3) what physical mechanism could trigger star formation in such an orderly fashion.

This investigation provides an extension to the linear density wave theory in the form of a nonlinear analysis of the dynamics of the gaseous disk. An asymptotic theory is developed in order to facilitate the description of the nonlinear gas flow along narrow nearly concentric streamtube bands about the galactic center.

The first part of the investigation concerns the possible existence and persistence of a stationary two-armed spiral shock pattern. Numerical calculations for streamtube bands lying at typical radii in the range between 3-4 kpc and 12 kpc confirm the compatibility of two periodically-located shock waves lying along and within the imposed two-armed spiral pattern. The extent of the shock pattern over the galactic disk is confined to the region interior to the circular band near 12 kpc. Inside the inner bound of the shock pattern at inner Lindblad resonance, an exciting theoretical feature of the galactic shock picture is evidenced by the existence of a stationary twice-periodic free mode discovered in the 3 kpc neighborhood of the Galaxy. Although resonance may contribute to the maintenance of the overall two-armed shock pattern over the galactic disk between the radii of

3-4 kpc and 12 kpc, it is only in the 3 kpc neighborhood that a free mode consisting of exactly two shock waves may be maintained entirely by resonance without the contributing influence of the imposed spiral field. Some features of the "3 kpc arm" of observational studies are apparent in this "resonant" free mode.

Once the compatibility of the stationary two-armed spiral shock pattern is confirmed, the problem associated with the possible evolution and development of galactic shock waves is next investigated. An initial value problem in which a given sinusoidal spiral gravitational field is superposed on the gaseous disk is considered in order to determine the possible growth of shocks in the Galaxy. It is found that shocks, both corotating and non-corotating with respect to the imposed spiral field, may develop. Of all the possible developing shocks, there is one mode that evolves into a corotating shock. This mode evolves at a faster rate than any of the others. It is shown that this corotating shock is an outgrowth of the neutral density wave mode which accounts for the grand design of spiral structure in the Lin-Shu density wave theory.

It is suggested that galactic shock waves may very well form the triggering mechanism for the gravitational collapse of gas clouds, leading to star formation. The implication of shock formation on star formation is then investigated. A possible gas cloud model for the turbulent gaseous disk is considered. It is shown that the shock wave may trigger the gravitational collapse of a large cloud which in turn is capable of triggering the subsequent compression and collapse of the individual internal subclouds which are the candidates for proto-stars. In the framework of this gas cloud picture, it is therefore possible for the shock to trigger star formation only in associations. If an upper bound of 30 million years is assumed for the process of formation and evolution of relatively massive stars initiated at the shock, it is shown that the regions of luminous newly-born stars and H II regions lie on the inner sides of the observed gaseous spiral arms, extending from the inner edges to approximately the middle of the arms, in general agreement with observations.

Thesis Supervisor: Chia-Chiao Lin  
Title: Institute Professor; Professor of Applied Mathematics

### Acknowledgements

Much of the credit for this investigation belongs to Professor C.C. Lin whose density wave theory of spiral structure set the foundation for this investigation of shock formation and star formation in galactic spirals. I am very happy to have had the opportunity of working closely with him throughout this work. With his invaluable guidance and direction as my thesis supervisor, I have benefitted deeply.

I would like to thank Dr. F.D. Kahn for his many interesting and fruitful ideas and discussions on star formation. I would also like to thank Professor C. Hunter and Professor A. Toomre who served on my thesis committee for their helpful advice and suggestions on various aspects of this work. To each of these people, I am very grateful.

I pay tribute to my father who instilled in me at an early age the desire to succeed in this endeavor. To my wife, Linda, I express my gratitude for her unceasing patience, help, and understanding.

This work was supported in part by the National Science Foundation and the National Aeronautics and Space Administration. The numerical computations were performed at the M.I.T. Computation Center.

## Table of Contents

Abstract

Acknowledgements

Sections:

### Part I - Synopsis

1. Introduction	9
2. Statement of problem	15
3. Plan of investigation	20

### Part II - Shock Formation

#### Part II A. Gas Flow about a Spiral Galaxy of Trailing Type

4. Dynamical equations governing the gaseous disk	31
5. Asymptotic theory	37
6. Galactic shock waves	42
7. Gas flow along narrow streamtubes through two periodically-located shocks	46
8. Analysis of singular points	50
9. Effects of variation of the galactic parameters	64
10. Gaseous disk: a family of nearly concentric streamtubes	76

Part II B. Gas Flow about a Spiral Galaxy of Leading Type

- 11. Similarity of the gas dynamical equations for spiral galaxies of leading and trailing type 89
- 12. Physical picture for the gaseous disk of a spiral galaxy of leading type 93

Part II C. Resonance and the "Three Kpc Arm"

- 13. Nature of linear and nonlinear resonance 101
- 14. Free spiral mode 106
- 15. Forced spiral mode 112

Part III - Mathematical Theory of the Development of Galactic Shocks

Part III A. Unsteady One Dimensional Gas Flow through a Sinusoidal Perturbation Gravitational Field

- 16. Initial value problem for one dimensional gas flow 121
- 17. Perturbation theory in characteristic coordinates for one dimensional gas flow 124
- 18. Ordinary one dimensional shock development 129
- 19. Shock of most rapid development 136
- 20. Self gravitation of the gas 143

Part III B. Unsteady Gas Flow about a Spiral Galaxy

- 21. Initial value problem for galactic gas flow through a sinusoidal spiral perturbation gravitational field 149
- 22. Perturbation theory in characteristic coordinates for galactic gas flow 153
- 23. Shock development in a spiral galaxy 159
- 24. Spiral shock of most rapid development; the Lin-Shu neutral density wave mode 163

## Part IV - Star Formation

25. Gas clouds: the constituents of the interstellar medium	171
26. Accretion	175
27. Shock wave-triggered gravitational collapse of a large gas cloud	178
28. Gas cloud model; internal region of a galactic shock	190
29. Classic problems associated with star formation	196
30. Subclouds: the candidates for protostars	205
31. Galactic star formation in a grand design of spiral structure	210

## Part V - Conclusions and Implications

32. Summary of results	215
33. Comparison with observations	228

### Appendices:

I. Comparison with earlier work	236
II. Validity of the asymptotic approximation	242
III. Sonic point conditions	246
IV. Procedure of numerical integration	249
V. Closure of gas streamtubes about the galactic disk	251

Bibliography	255
--------------	-----

Biographical Sketch	258
---------------------	-----

Part I - Synopsis



## 1. Introduction

### Grand Design of Spiral Structure

Ever since man first began viewing the universe beyond his own Milky Way System, a classic problem in galactic structure has existed: namely, why most galaxies have a fairly regular grand design of spiral structure over their disks. Oort (1962) viewed this classic problem in terms of the more basic problems of the origin and the persistence of the regular grand design:

"In systems with strong differential rotation, such as is found in all nonbarred spirals, spiral features are quite natural. Every structural irregularity is likely to be drawn out into a part of a spiral. But this is not the phenomenon we must consider. We must consider a spiral structure extending over the whole galaxy, from the nucleus to its outermost part, and consisting of two arms starting from diametrically opposite points. Although this structure is often hopelessly irregular and broken up, the general form of the large-scale phenomenon can be recognized in many nebulae."

Two different spiral theories have been suggested to account for this grand design feature. The first associates each spiral arm with a specified body of matter throughout the course of the arm's evolution. The winding dilemma associated with the disrupting influence of differential rotation is an uncomfortable difficulty arising out of this theory. The second theory regards the spiral structure as

a wave pattern, which remains quasi-stationary in a frame of reference rotating around the center of the galaxy at a given angular speed. This quasi-stationary wave pattern is composed of self-sustained density waves of gas and stars. This theory, as worked out by Lin and Shu (1964, 1966), accounts for the persistence of a regular grand design of spiral structure even in the presence of differential rotation and stellar and gaseous velocity dispersion.<sup>1</sup> In this theory, only a two-armed spiral pattern is possible when the basic rotation curve is similar to that of the Milky Way System.

### Large-Scale Galactic Shocks

Once a self-sustained field of density waves develops in the galactic disk, certain related phenomena of fundamental importance may also arise. Of especial interest is the possible formation of large-scale galactic shocks from the self-sustained field of density waves making up the gaseous disk.

The presence of a marked grand design of spiral structure in many disk-shaped galaxies signifies an even more marked and narrow region for the initiation of star formation within the gaseous spiral arms of

---

<sup>1</sup>The density wave theory of spiral structure was proposed by the late B. Lindblad. His work on the subject may be traced through his last paper in the Stockholm Observatory Annalen (Lindblad, 1963). He placed emphasis on the properties of individual stellar orbits rather than on the behavior of stellar collective modes. On the other hand, P. O. Lindblad (1960, 1962) attempted to study the collective modes by extensive numerical calculation of the orbits of a number of stars. Although density waves of a spiral form were found, they were rather transient and not quasi-stationary.

the grand design. Indeed, G. Westerhout (personal communication with C.C. Lin and coworkers) has recently reported that the most luminous newly-born stars and H II concentrations appear on the inside of the observed gaseous spiral arms of our Galaxy. Since the peak of gas concentration in a density wave extends over a broad region, it is evident that the field of density waves alone as a triggering mechanism for star formation could not provide for narrow spiral strips of newly-born luminous stars. In this situation, we are led to infer the presence of large-scale galactic shocks which would be capable of triggering star formation in narrow spiral regions over the disk.

We might expect self-sustained density waves in the galactic disk to grow and develop in the course of time into disturbances with shock-like nature. If all the self-sustained density waves, which evolve into shocks, together characterize the regular grand design of spiral structure over the galactic disk, then the developing shocks likewise must exhibit a similar grand design. Although plausible, it is by no means certain a priori that two periodically-located spiral shock waves present throughout the galactic disk would be compatible with the general nature of the gas flow about the disk. The compatibility for the existence of two periodically-located shock waves in the galactic disk is just what must be confirmed.

We should distinguish the large-scale galactic shocks from the various types of small-scale shock waves previously considered for the interstellar medium. Wentzel (1966) has studied shock waves in H I regions. Shock waves generated in H I regions by expanding H II regions have been considered by Mathews (1965) and by Lasker (1966a,b). Field,

Rather, Aannestad, and Orszag (1967) have considered shock waves in H I regions further by taking both magnetic fields and radiative losses into account. Axford (1961) has studied shock waves (ionization fronts) in the expansion of a spherically symmetric H II region around a star, and Kahn (1968) has considered shock waves (ionization fronts) in the flow of an ionized gas from a globule in interstellar space. All these investigations actually consider small-scale galactic shocks (or ionization fronts) in that they consider a physical picture which encompasses a relatively small region of the interstellar medium (with a typical scale of 10-100 pc and containing at most a few stars and a few large gas clouds).

On the other hand, large-scale shock waves (with a typical scale of a few kpc) have been considered by Fujimoto (1966) in the flow of gas through a model spiral arm. Fujimoto's calculations represent an important first step in the determination of the nonlinear dynamics of the gaseous component of the galactic disk. Although the gas flow picture considered by Fujimoto contains large-scale shocks, it cannot account for a two-armed galactic shock pattern.<sup>1</sup> Of especial interest in the present investigation is the physical picture of a two-armed grand design of spiral structure which is characteristic of the majority of normal spiral disk-shaped galaxies.<sup>2</sup>

---

<sup>1</sup> Fujimoto's calculations exhibit a multiarmed spiral potential that possesses more than two spiral arms (no fewer than four, and in some cases on the order of ten or twenty).

<sup>2</sup> Unlike Fujimoto's work, this investigation imposes a two-armed spiral gravitational field. In such a picture, if large-scale galactic shocks develop, they must necessarily grow into a two-armed galactic shock wave pattern. Further discussion of Fujimoto's calculations is included in Appendix I. Appendix I also provides a comparison of the basic differences between Fujimoto's work and the present investigation.

## Star Formation in the Galaxy

The implications of the theory of shock formation in galactic spirals bear directly on a fundamental present day problem associated with star formation. The process of star formation undoubtedly has been intriguing to man ever since he first recognized that celestial bodies such as stars existed. In particular, understanding why star formation is occurring for the most part only in regions comprising the spiral arms of a galaxy is being given a great deal of attention by both observationalists and theoreticians alike in this day and age. An understanding of this problem of star formation along spirals may be possible directly from the theory of shock formation.

As pointed out by Kahn (1960), attempts to explain the formation of stellar associations have been faced with two major difficulties: (1) only vague data are known about the physical state and properties of the interstellar medium, and (2) the dynamics of all the processes involved is highly complex. Although present theories make many appeals to physical intuition, none can give very exact answers. Kahn (1960) suggests that neither accretion theory<sup>1</sup> nor any present theory involving a supernova explosion<sup>2</sup> can adequately explain the existence of stellar

---

<sup>1</sup>Accretion, however, may aid in the formation of stellar associations. Section 26 of Part IV - Star Formation contains a discussion of the accretion process.

<sup>2</sup>Supernovae may provide for a secondary regeneration of star formation. This is discussed in Section 31 of Part IV - Star Formation.

associations. In addition, hydromagnetic forces<sup>1</sup> seem to have little to do with the formation of stars in chains and along spirals.

In our nonquiescent picture of the interstellar medium, large gas clouds exist under the influence of their cohesive gravitational forces and their dispersive turbulent pressures. Without the galactic shock wave-triggering mechanism, star formation in stellar associations may occur only when cloud complexes have grown large enough through accretion processes to reach their verges of gravitational collapse. This situation is rather tenuous since the time of evolution of a cloud complex which in general undergoes accretion as well as fragmentation, is rather uncertain. It is reassuring, therefore, when a triggering mechanism such as a large-scale galactic shock wave is present to account for star formation occurring only in stellar associations which lie in chains and along spirals.

---

<sup>1</sup>The author has considered the problem of magnetic fields along spiral arms, but he is convinced that the magnetic field in the Galaxy is an unsatisfactory triggering mechanism for star formation along chains and spirals. Further discussion on the large-scale effects of a magnetic field is included in Section 3. Discussion of the small-scale effects of a magnetic field on star formation is included in Section 29 of Part IV - Star Formation.

## 2. Statement of problem

### Observational Features of Spiral Galaxies

"Normal" spiral galaxies comprise the majority of all the brighter galaxies. A normal spiral consists of two major portions: (1) a very flat disk whose mean thickness is generally only about 1/50 to 1/100 of its diameter and (2) a spheroidal nucleus at its center. Spiral galaxies appear in a wide variety of forms. The openness of spiral arms, the degree of resolution of the arms into stars, and the relative size of the unresolved nuclear region are certain diverse features of spiral galaxies which provide a means for their classification (see Sandage, 1961). Many spiral galaxies have multiple spiral arms; however, two principal arms can generally be traced to the central region and sometimes to the very center of the system. Often they dominate the structural form of the system. While the nucleus of a disk-shaped galaxy may rotate with nearly uniform angular velocity, the disk generally undergoes a differential rotation with the inner parts possessing a higher angular velocity than the outer parts. With these general features in mind, we shall consider some of the striking physical features characteristic of the spiral structure.

Often spiral arms show a very high resolution into "knots" which are generally interpreted as H II regions and associations of stars. The young stars practically always appear in stellar associations.

These young stellar associations with their corresponding H II regions often occur in chains and spiral arcs within the larger grand design of spiral structure. The contiguity of H II regions and spiral arms of a galaxy was first recognized by Baade and Mayall (1951) in their study of the H II regions of M 31. It was Morgan, Sharpless, and Osterbrock (1952) who first detected spiral structure in our Galaxy and who showed that the young stars and H II regions appear like strings of beads. Recently the young stellar associations and brilliant H II regions in our Galaxy were found to lie along the inner side of the observed gaseous spiral arms (personal communication of Westerhout to Lin and coworkers). There is much dust in the spiral arms and usually it lies on the inside of these luminous arcs of spiral structure.

The occurrence of brilliant young stellar associations and brilliant H II regions along spiral chains inside the larger spiral arms of a galaxy causes a striking luminosity contrast between the spiral arms and the interarm regions where no young stars are present. Even though this striking luminosity contrast does exist, the contrast in total mass concentration inside and outside the spiral arms may be only a few percent. The mass in the spiral arms therefore contributes only a small perturbation field to the total gravitational field, which is nearly axisymmetric.

Our Milky Way System contains yet another striking feature. In the region between 3 and 4 kpc from the galactic center, there exist two arc segments of spiral arms that are apparently moving radially outwards at very high speeds on the order of 50 km/s. The closest of these arm segments to the solar vicinity is generally referred to as the "3 kpc arm." This intriguing "3 kpc arm" feature is generally con-



sidered to be associated either with some type of an explosion which originated in the central region or with the inner Lindblad resonance which manifests itself in this region of the galactic disk.

### Development of a Nonlinear Theory

We now reiterate how the linear density wave theory of Lin and Shu sets the stage for a theoretical view of spiral structure, and we indicate the nonlinear theory that is considered in this investigation. In the next subsection we set forth the perplexing problems of spiral structure that may be accounted for in the nonlinear theory.

The linear density wave theory demonstrates how it is possible to have a regular grand design of spiral structure despite the presence of differential rotation and stellar and gaseous velocity dispersion. This spiral structure accounted for by the linear theory persists in both the stellar component and the gaseous component of the disk. These spiral distributions of density give rise to an induced gravitational field. In order that a quasi-stationary spiral structure of density waves may be self-sustained, this induced field is required to equal the original, imposed gravitational field.

In this investigation, we are interested in augmenting this linear density wave picture. One notable improvement to be accomplished would be the formulation of nonlinear theories for the gaseous and stellar components of the galactic disk. The first step toward this goal is the development of a partially nonlinear theory composed of the linear theory for the stellar component together with a nonlinear theory for the gaseous component. In this situation, the total response

which is linear in the stellar component and nonlinear in the gaseous component gives rise to an induced gravitational field which is required to be similar to the original, imposed gravitational field. This is the condition which guarantees that the quasi-stationary spiral pattern composed of the linear density waves in the stellar component together with the nonlinear counterpart of the density waves in the gaseous component be self-sustained. The imposed and induced fields may be regarded as nearly one and the same resultant field of gas, young stars, and moderately-old stars.<sup>1</sup>

#### Scope of the Nonlinear Theory

With such a gaseous nonlinear theory we ask whether we will be able to better understand some of the aforementioned features associated with spiral structure and star formation. We have already seen how the linear density wave theory can account for the persistence of a regular grand design of spiral structure. We now ask if the nonlinear counterpart of the linear theory can account for some further remarkable features.

A most striking phenomenon in our Galaxy is the location of the young stars and associated H II regions, which evidently lie for the most part only along spirals. In addition to this spiral feature of

---

<sup>1</sup>The calculations proceed in two steps. First, the nonlinear response of gas (without self gravitation) to an imposed field is determined. Second, the fundamental component of the gas-induced gravitational field is determined and is shown to lie almost exactly in phase with the imposed field. Therefore, the total induced field due to the (nonlinear) gaseous and the (linear) stellar responses lies almost exactly in phase with the imposed field. The imposed field is therefore almost equivalent to the resultant field of gas, young stars, and moderately-old stars (see Section 9).

star formation, practically all newly-born stars lie in associations with other newly-born stars. We therefore pose a fundamental question to be considered in this investigation: why do the young stellar associations and the corresponding brilliant H II regions occur in chains and knots along spiral arms in our Galaxy?

In some Sc-type galaxies these spirals, where young stellar associations and H II regions lie, are often limited in their radial extent over the galactic disk. Sometimes these spirals do not even extend out to the bands about the galactic center where the maximum H I distribution occurs.<sup>1</sup> It would seem obvious a priori that star formation would most probably take place in those regions where the mass of neutral hydrogen is the largest. To have little or no star formation in the regions of highest H I distribution is indeed perplexing. This is just one further feature of the overall problem of spiral structure and star formation that must be considered.

For an understanding of all these features it is essential to first determine the possible physical mechanism that can trigger star formation with all these aforementioned properties. Once we have determined the physical mechanism that triggers star formation only in a grand design of spiral structure (as outlined by the newly-born luminous stars), perhaps we shall be able to show how all these physical features of star formation are related (see Sections 30,31,32, and 33).

---

<sup>1</sup>M.S. Roberts (1967) has shown for Sc-type galaxies that the regions of highest H I distribution do not coincide with and, in fact, lie well outside of the regions of the newly-born stars and the H II regions. Further discussion of this feature is included in Section 33.

### 3. Plan of investigation

The task before us is an investigation of the problem of shock formation in a disk-shaped galaxy and its possible implication on star formation.

#### Dynamics of a Disk-Shaped Galaxy

A disk-shaped galaxy such as our own Milky Way System consists of two basic portions: a very flat disk which contains all the features of spiral structure on which is superposed a spheroidal nuclear region at the center of the disk. The physical features associated with the galactic disk characterize it as a spiral or non-spiral galaxy. Since the major proportion of gas and stars are evidently located in a layer whose thickness is about  $1/50$  to  $1/100$  of the diameter of the disk, the galactic disk may be imagined as a very thin sheet. In order to eliminate effects due to the variation of the galactic variables with height above or below the median plane of the disk we consider mean values of the physical variables integrated over the sheet thickness. In terms of these mean variables, the dynamics of the disk may be regarded as two-dimensional in nature with the forcing mechanisms and the responses confined entirely within the sheet. Although there are really two separate components of the disk, gaseous and stellar, we shall be primarily concerned with the determination of the response of the gaseous component to an imposed spiral gravitational field which may be attri-

buted to the organization of the more massive stellar component into a spiral pattern.<sup>1</sup> The first goal of this investigation will be a determination of the dynamics of the gaseous disk in the framework of a nonlinear theory.

A variety of forces present in the galactic disk influences the dynamics of the gas and the stars that make up the disk. The predominant forces acting in the differentially rotating galactic disk are the inertial forces associated with the rotation of the disk and the smoothed gravitational force of the system as a whole. The dynamics of the stellar component is primarily governed by these inertial and gravitational forces. When we consider the dynamics of the gaseous component of the galactic disk, other forces should be taken into account. These include the gaseous "pressure" associated with turbulence in the interstellar medium<sup>2</sup> and the hydromagnetic forces due to magnetic fields embedded in the gas. In the gas dynamical picture one should also include the effects due to cosmic rays, supernovae explosions, and stellar radiation, which are the primary sources of turbulent energy for the gas, and the effect of dissipation of turbulence by collisions of gas clouds, which is the primary sink of turbulent energy for the gas. In our picture, which provides a first approximation to the total nonlinear galactic picture, turbulence together with

---

<sup>1</sup>It is shown in Section 9 that the imposed field may actually be regarded as the resultant field of gas, young stars, and moderately-old stars.

<sup>2</sup>If the interstellar medium is indeed a nonquiescent one, the pressures due to turbulence may be much larger than the kinetic pressures.

the inertial and gravitational effects is included in the determination of the dynamics of the gaseous disk.

We envisage the effects of the galactic magnetic field to be of only secondary importance. If the magnetic field energy density is high enough and if the degree of ionization in the interstellar medium is high enough to strongly couple the neutral gas to the magnetic lines of force, the presence of magnetic fields may hinder and distort the gravitational collapse of gas clouds and cloud complexes.<sup>1</sup> However, Yuan (1968) has carried out calculations for the imposition of a magnetic field on the large-scale galactic gas flow in the framework of the linear theory and has shown that for a magnetic field of the order of  $5 \times 10^{-6}$  gauss, the streamlines do not deviate greatly from the streamlines of the gas flow without the presence of a magnetic field. A magnetic field no larger than  $5 \times 10^{-6}$  gauss may be considered to influence only secondary effects in the dynamics of the gas in the nonlinear theory as well as in the linear theory, and therefore such a magnetic field will not be considered further in the large-scale shock investigations.

In the interstellar medium, H I clouds dissipate energy during their inelastic collisions with each other; and unless energy is available from other sources, the turbulence of the cloud medium cannot be maintained. The primary sources of energy for the cloud medium are

---

<sup>1</sup>Further discussion of the small-scale effects of a magnetic field on star formation is included in Section 29 of Part IV - Star Formation.

cosmic rays, supernovae explosions, and stellar radiation. As estimated by Spitzer (1968), the energy dissipation rates of H I clouds may be about  $3.7 \times 10^{-27}$  ergs/cc-s, whereas the three energy sources make energy available at the rates of about  $1.3 \times 10^{-27}$ ,  $14 \times 10^{-27}$ , and  $57 \times 10^{-27}$  ergs/cc-s respectively. A certain fraction (perhaps 1/100) of the energy provided by these three sources may be transferred into the turbulent energy of H I clouds for the overall maintenance of the turbulence of the gaseous disk.<sup>1</sup> Therefore, the maintenance of turbulence does not appear as a serious difficulty; and in a first approximation, the gaseous disk might be visualized to possess a uniform mean turbulent dispersion speed.<sup>2</sup> With this implicit energy balance, the disk is characterized by a uniform mean equivalent temperature. In such a situation, the gas flow is isothermal.<sup>3</sup>

---

<sup>1</sup> Kahn estimates that roughly 1% of the energy available from stellar radiation may be converted into gaseous turbulent energy. This amount of energy in itself would be almost sufficient to maintain the gaseous turbulence against its dissipation. (Personal communication, 1968)

<sup>2</sup> In this investigation a uniform mean turbulent dispersion speed is assumed along each gas streamtube band about the galactic center; and therefore, the mean turbulent dispersion speed is taken as a function of radius from the galactic center.

<sup>3</sup> "Isothermal" refers to the uniformity of the mean equivalent temperature (primarily due to turbulence) over the large-scale gaseous disk. This approximation of a fairly uniform mean turbulent dispersion speed along individual streamtube bands about the disk may not be too bad an approximation since observational studies do not indicate too large deviations from a possibly uniform mean turbulent dispersion speed. In Part IV - Star Formation, we discuss the small-scale picture of a gas cloud at an equivalent temperature (partly kinetic and partly due to turbulence).

## Stationary Galactic Shock Pattern

First, the problem of the existence and persistence of a stationary two-armed spiral shock pattern over the galactic disk is investigated. We consider the steady motion of a turbulent gas with an approximately uniform mean dispersion speed moving in a gravitational field consisting of a two-armed spiral field superposed on the Schmidt Model for the Milky Way System. A pattern speed of 12.5 km/s/kpc determined from other studies of spiral structure<sup>1</sup> is adopted.

We are interested in a particular type of solution of the nonlinear gas flow equations that satisfies several imposed requirements. It shall be: first, a solution that permits the gas to pass through two periodically-located shock waves which lie along gravitational equipotential curves of the imposed two-armed spiral field; second, a solution that describes the gas flow along narrow, nearly concentric streamtube bands that extend circumferentially about the entire galactic disk; and third, a solution that repeats itself through every half revolution of the gas flow about the disk so that exactly two identical shocks and a twice-periodic streamtube are present at each radius.

An asymptotic theory is developed in order to facilitate the solution of the gas flow equations. In this asymptotic approximation the perturbation quantities of velocity, density, and pressure are

---

<sup>1</sup>This pattern speed is obtained from two studies: (1) the distribution of neutral hydrogen and (2) the migration of moderately-young stars (see Lin, Yuan, and Shu, 1968). The value used here is actually a compromise value between 11.5 and 13.5.



taken to be slowly varying in the direction along the contours of constant phase of the spiral field. To the first order in the asymptotic approximation, the only variation in the perturbation quantities is therefore along the coordinate perpendicular to the equipotential contours. In the linear theory this asymptotic approximation makes it possible for an analytical solution in terms of density waves. Since the nonlinear theory is expected to yield streamtubes that are not far different from those of the linear theory, such an asymptotic approximation is expected to be valid for the nonlinear theory as well. This is in fact confirmed by our numerical calculations for the determination of the stationary shock wave pattern.

#### Growth and Development of Galactic Shocks

Having considered the problem associated with the existence and persistence of a stationary two-armed spiral shock pattern, we next investigate the problem associated with the possible evolution and development of the two-armed shock pattern. We consider an initial value problem in which a given two-armed spiral perturbation gravitational field is imposed on the galactic disk from some time onwards, and we determine its influence on the initial purely circular gas flow of the disk. Actually two types of initial value problems are considered: (1) a one dimensional ordinary gas flow problem, and (2) the galactic gas flow problem. The first provides insight for the solution of the second. With such an initial value problem for the galaxy we are able to see the growth of density waves into large amplitude disturbances and eventual shock development from these

disturbances. Within the scope of this analysis, we shall determine the crucial physical parameters which govern such shock development. A determination of the time scale for the evolution of a disturbance in the galactic disk into an evolved shock wave is of considerable interest.

### Implications on Star Formation

Third and finally, we consider the implications of the theory of shock formation on star formation in the galactic disk. We visualize the galactic interstellar medium as very irregular with non-quietest turbulent gas eddies and fragments evidently present on all discernible scales. With such a physical picture in mind, a feasible gas cloud model of the turbulent medium is developed.

In particular, we are primarily interested in an explanation why the young stars and H II regions occur for the most part only in the regions of the spiral arms. This problem is an urgent one in the density wave picture, since a given body of gas remains in the spiral arm only for a short period of time (on the order of perhaps  $3 \times 10^7$  -  $5 \times 10^7$  years). An understanding of the process of star formation therefore may aid in understanding the reason why young stars and H II regions occur in cooperation to form a regular grand design of spiral structure over the galactic disk. The problem why young stars form only in associations is also pursued. Our model for the structure of gaseous clouds in the interstellar medium is compatible with the physical phenomena characteristic of star formation in stellar associations and along spiral arms and with the dynamical features associated

with the collapse of gas cloud complexes.

A galactic shock wave may be visualized as the fundamental triggering mechanism for the gravitational collapse of cloud complexes in the following manner. Before reaching the shock some of the cloud complexes may be on the verge of gravitational collapse. A sudden compression of the clouds in the shock to perhaps ten times their original density could conceivably trigger the gravitational collapse of some of the larger gas cloud complexes, leading to star formation. As the gas leaves the shock region, it is (rather quickly) decompressed, and star formation ceases.

It is shown that star formation is possible only in the regions where the highest concentrations of gas clouds (subclouds) exist in the form of large clouds or large cloud complexes. The shock is capable of triggering the gravitational collapse of only the largest clouds and cloud complexes and cannot trigger directly the candidates for protostars. It is only through the collapse of the large cloud complexes that the constituent subclouds are eventually compressed and collapsed into protostars. The influence of turbulence in the galactic interstellar medium is demonstrated. General agreement exists between observational studies of spiral galaxies and this model of shock wave-triggered star formation along a luminous grand design of spiral structure.

Part II. Shock Formation

Part II A. Gas Flow about a Spiral Galaxy of Trailing Type

The problem of the existence and persistence of a stationary two-armed spiral shock pattern of trailing type over the disk of the Galaxy is to be considered in Part II A. We consider the steady motion of an "isothermal" gas (at a mean equivalent temperature, primarily due to turbulence) moving in a gravitational field consisting of a two-armed spiral field (possibly attributed to a two-armed pattern of spiral structure composed of density waves of moderately-old stars)<sup>1</sup> superposed on the Schmidt model of the Milky Way System. Our goal is to determine if such a stationary two-armed spiral shock pattern is compatible with the general nature of the gas flow about the galactic disk.

In Section 4, we consider the equations of motion for the gaseous component of the galactic disk, and in Section 5, an asymptotic theory is developed for the gas flow. A large-scale galactic shock wave is considered in Section 6. The two aspects: (1) gas flow over the disk apart from shock regions (considered in Sections 4 and 5) and (2) the flow of gas across a shock (considered in Section 6) are combined in Section 7 to form a composite solution for gas flow along a closed, nearly concentric, and twice-periodic streamtube band through

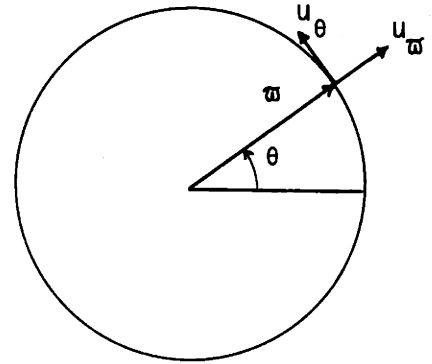
---

<sup>1</sup>In Section 9, we demonstrate that the imposed spiral gravitational field is almost equivalent to the resultant field of gas, young stars, and moderately-old stars.

two periodically-located shock waves. Sections 8 and 9 determine some important physical features of this composite solution. In Section 10, it is shown that the gaseous disk may consist of a family of these nearly concentric gas streamtube bands which pass through and in fact make up the overall two-armed spiral shock pattern in the Galaxy.

4. Dynamical equations governing the gaseous disk

The fundamental equations of motion for gas flow about a circular disk, where  $u_{\varpi}$  and  $u_{\theta}$  represent the velocity components in the  $\varpi$  and  $\theta$  directions respectively, may be written by an observer in an inertial frame of reference as:



$$\frac{\partial \sigma}{\partial t} + \frac{1}{\varpi} \frac{\partial(\sigma u_{\varpi} \varpi)}{\partial \varpi} + \frac{1}{\varpi} \frac{\partial(\sigma u_{\theta})}{\partial \theta} = 0 \quad (4.1)$$

$$\frac{\partial u_{\varpi}}{\partial t} + u_{\varpi} \frac{\partial u_{\varpi}}{\partial \varpi} + \frac{u_{\theta}}{\varpi} \frac{\partial u_{\varpi}}{\partial \theta} - \frac{u_{\theta}^2}{\varpi} = -\frac{a^2}{\sigma} \frac{\partial \sigma}{\partial \varpi} - \frac{\partial \mathcal{U}}{\partial \varpi} \quad (4.2)$$

$$\frac{\partial u_{\theta}}{\partial t} + u_{\varpi} \frac{\partial u_{\theta}}{\partial \varpi} + \frac{u_{\theta}}{\varpi} \frac{\partial u_{\theta}}{\partial \theta} + \frac{u_{\varpi} u_{\theta}}{\varpi} = -\frac{a^2}{\sigma \varpi} \frac{\partial \sigma}{\partial \theta} - \frac{1}{\varpi} \frac{\partial \mathcal{U}}{\partial \theta} \quad (4.3)$$

where

$t$  denotes the time

$\sigma(\varpi, \theta, t)$  is the gas density of the galactic disk

$a$  is the mean turbulent dispersion speed of the gas

$\mathcal{U}(\varpi, \theta, t)$  is the total gravitational potential

### Base State of Motion

We take for the base state of motion an equilibrium state of purely circular gas flow where the total smoothed central gravitational force field is exactly balanced by the inertial force associated with the rotation of the disk as a whole. The gas density of the base state will be taken as  $\sigma_0(\varpi)$  and the smoothed gravitational potential field will be denoted by  $\mathcal{U}_0(\varpi)$ . For purely circular flow, we have  $u_{\varpi} = 0$  and  $u_{\theta} = \Omega(\varpi)\varpi$ ; and therefore  $\mathcal{U}_0(\varpi)$  and  $\Omega(\varpi)$  satisfy a relation which balances radial forces:

$$\Omega^2(\varpi)\varpi = \frac{d\mathcal{U}_0(\varpi)}{d\varpi}$$

For our own Milky Way System the base state of motion which satisfies the above radial force balance is described by the Schmidt model (see Schmidt, 1965).

### Perturbed State

Since we are dealing with a galactic system where the gravitational field consists of a two-armed spiral field superposed on the Schmidt model, we may divide the total gravitational potential into two portions:

$$\mathcal{U}(\varpi, \theta, t) = \mathcal{U}_0(\varpi) + \mathcal{U}_1(\varpi, \theta, t)$$



where

$U_0(\varpi)$  is the smoothed gravitational potential corresponding to the Schmidt model for the Milky Way System, and

$U_1(\varpi, \theta, t)$  is the spiral gravitational potential corresponding to the two-armed spiral pattern.

We take  $U_1(\varpi, \theta, t)$  of the form:

$$U_1(\varpi, \theta, t) = A(\varpi, \theta) \cos \left[ 2\Omega_p t - 2 \left( \frac{1}{\tan i} \ln \left( \frac{\varpi}{\varpi_0} \right) + \theta \right) - \phi \right] + U_2$$

where

$A(\varpi, \theta)$  is a slowly varying function of  $\varpi$  and  $\theta$ ,

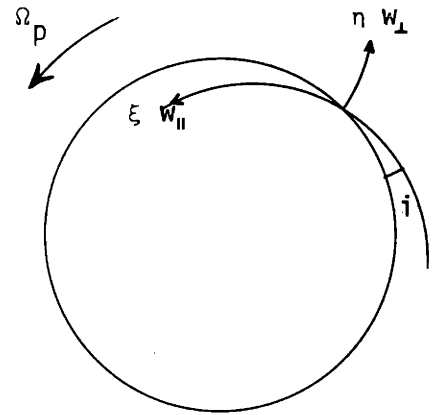
$\phi$  is a constant phase angle,

$U_2$  is a small correction to the spiral potential which will be specified later.

In a similar manner, each physical variable may be divided into a portion corresponding to the axisymmetric equilibrium state of the Schmidt model plus a portion corresponding to the perturbation due to the spiral gravitational field:

$$\begin{aligned} \sigma(\varpi, \theta, t) &= \sigma_0(\varpi) + \sigma_1(\varpi, \theta, t) \\ u_{\varpi}(\varpi, \theta, t) &= 0 + u_{\varpi 1}(\varpi, \theta, t) \\ u_{\theta}(\varpi, \theta, t) &= \Omega(\varpi)\varpi + u_{\theta 1}(\varpi, \theta, t) \end{aligned}$$

Since the spiral pattern rotates as a rigid structure, it would be convenient to describe the gas flow from a vantage point on a rotating coordinate system fixed with respect to the spiral pattern which rotates with angular velocity  $\Omega_p$ . In addition, the form of the spiral potential,  $U_1(\varpi, \theta, t)$ , indicates that a convenient set of coordinates with which to describe the gas flow may be the coordinates fixed in the  $\Omega_p$ -rotating system that are parallel and perpendicular to the spiral equipotential curves. These coordinates may be written as follows:



$$\eta = \ln\left(\frac{\varpi}{\varpi_0}\right) \cos i + (\theta - \Omega_p t) \sin i$$

$$\xi = -\ln\left(\frac{\varpi}{\varpi_0}\right) \sin i + (\theta - \Omega_p t) \cos i$$

The velocity components along these coordinates may be written as:

$$w_{\perp 0} + w_{\perp} = u_{\varpi_1} \cos i + \left\{ (\Omega - \Omega_p) \varpi + u_{\theta_1} \right\} \sin i$$

$$w_{\parallel 0} + w_{\parallel} = -u_{\varpi_1} \sin i + \left\{ (\Omega - \Omega_p) \varpi + u_{\theta_1} \right\} \cos i$$

In terms of these  $\eta$  and  $\xi$  coordinates, the gas flow equations, (4.1), (4.2), and (4.3), may be rewritten as:

$$\begin{aligned}
& \omega \frac{\partial \sigma_1}{\partial t} + \frac{\partial(\sigma_1 w_{\perp})}{\partial n} + \frac{\partial(\sigma_1 w_{\parallel})}{\partial \xi} + \sigma_0 \left( \frac{\partial w_{\perp}}{\partial n} + \frac{\partial w_{\parallel}}{\partial \xi} \right) \\
& + (\Omega - \Omega_p) \omega \left( \sin i \frac{\partial \sigma_1}{\partial n} + \cos i \frac{\partial \sigma_1}{\partial \xi} \right) \\
& + (\sigma_0 + \sigma_1 + \omega \frac{d\sigma_0}{d\omega}) (w_{\perp} \cos i - w_{\parallel} \sin i) = 0 \quad (4.4)
\end{aligned}$$

$$\begin{aligned}
& \omega \frac{\partial w_{\perp}}{\partial t} + w_{\perp} \frac{\partial w_{\perp}}{\partial n} + w_{\parallel} \frac{\partial w_{\perp}}{\partial \xi} + (\Omega - \Omega_p) \omega \left( \sin i \frac{\partial w_{\perp}}{\partial n} + \cos i \frac{\partial w_{\perp}}{\partial \xi} \right) \\
& - 2\Omega \omega w_{\parallel} + \omega^2 \frac{d\Omega}{d\omega} \sin i (w_{\perp} \cos i - w_{\parallel} \sin i) \\
& - w_{\parallel} (w_{\perp} \sin i + w_{\parallel} \cos i) = - \frac{a^2 \omega \cos i}{\sigma_0 + \sigma_1} \frac{d\sigma_0}{d\omega} - \frac{a^2}{\sigma_0 + \sigma_1} \frac{\partial \sigma_1}{\partial n} \\
& - \frac{\partial U_{\perp}}{\partial n} \quad (4.5)
\end{aligned}$$

$$\begin{aligned}
& \omega \frac{\partial w_{\parallel}}{\partial t} + w_{\perp} \frac{\partial w_{\parallel}}{\partial n} + w_{\parallel} \frac{\partial w_{\parallel}}{\partial \xi} + (\Omega - \Omega_p) \omega \left( \sin i \frac{\partial w_{\parallel}}{\partial n} + \cos i \frac{\partial w_{\parallel}}{\partial \xi} \right) \\
& + 2\Omega \omega w_{\perp} + \omega^2 \frac{d\Omega}{d\omega} \cos i (w_{\perp} \cos i - w_{\parallel} \sin i) \\
& + w_{\perp} (w_{\perp} \sin i + w_{\parallel} \cos i) = \frac{a^2 \omega \sin i}{\sigma_0 + \sigma_1} \frac{d\sigma_0}{d\omega} - \frac{a^2}{\sigma_0 + \sigma_1} \frac{\partial \sigma_1}{\partial \xi} \\
& - \frac{\partial U_{\parallel}}{\partial \xi} \quad (4.6)
\end{aligned}$$

where

$$U_1(n, \xi) = A(n, \xi) \cos \left\{ -\frac{2n}{\sin i} - \phi \right\} + U_2(n) \quad (4.7)$$

and where  $A(n, \xi)$  is a slowly varying function of  $n$  and  $\xi$ .

## 5. Asymptotic Theory

Since the imposed spiral potential is oscillatory as cosine in  $n$  and only slowly varying in  $\xi$ , we expect the physical perturbation solution of interest to be likewise oscillatory in  $n$  and only slowly varying in  $\xi$ . Indeed this is precisely the case in the linear density wave theory where all perturbation quantities are of the general form:

$$P(n, \xi) \exp\{iQ(n)\}$$

where  $P(n, \xi)$  is slowly varying in  $n$  and  $\xi$ , and

$$Q(n) = -\frac{2}{\sin i} n$$

Guided by the linear theory we expect the asymptotics of the nonlinear theory not to differ radically from that of the linear theory. In addition, we are interested in stationary, or at least quasi-stationary, gas flow. Therefore, we look for solutions for which the induced perturbation quantities are weakly dependent on  $\xi$  and  $t$  in comparison to their dependence on  $n$ . We exhibit this behavior by introducing the small parameters  $\delta_1$  and  $\delta_2$  and by regarding the physical variables as:

$$\sigma_1(n, \delta_1 \xi, \delta_2 t) \quad w_{\perp}(n, \delta_1 \xi, \delta_2 t) \quad w_{\parallel}(n, \delta_1 \xi, \delta_2 t) \quad (5.1)$$

We therefore make the asymptotic approximation in which the perturbation quantities to first order vary only along the direction normal to the contours of constant phase. Its validity is not a priori certain; and, we therefore demonstrate its validity a posteriori (the validity of this asymptotic approximation is demonstrated in Appendix II).

To first order in the asymptotic scheme, the asymptotic equations of gas flow may be written as:

$$(w_{\perp 0} + w_{\perp}) \frac{\partial \sigma_1}{\partial \eta} + (\sigma_0 + \sigma_1) \frac{\partial w_{\perp}}{\partial \eta} + (\sigma_0 + \sigma_1 + \varpi \frac{d\sigma_0}{d\varpi}) \chi_1 + \mathcal{O}(\delta_1, \delta_2) = 0 \quad (5.2)$$

$$(w_{\perp 0} + w_{\perp}) \frac{\partial w_{\perp}}{\partial \eta} - 2\Omega \varpi w_{\parallel} + \frac{a^2}{\sigma_0 + \sigma_1} \frac{\partial \sigma_1}{\partial \eta} + \frac{\partial U_1}{\partial \eta} + \chi_2 + \mathcal{O}(\delta_1, \delta_2) = 0 \quad (5.3)$$

$$(w_{\perp 0} + w_{\perp}) \frac{\partial w_{\parallel}}{\partial \eta} + (\frac{K^2}{2\Omega}) \varpi w_{\perp} + \chi_3 + \mathcal{O}(\delta_1, \delta_2) = 0 \quad (5.4)$$

where

$$(\frac{K^2}{2\Omega}) = 2\Omega (1 + \frac{\varpi}{2\Omega} \frac{d\Omega}{d\varpi} \cos^2 i) \quad (5.5)$$

and

$$x_1 = (w_{\perp} \cos i - w_{\parallel} \sin i) \quad (5.6)$$

$$x_2 = \omega^2 \frac{d\Omega}{d\omega} \sin i (w_{\perp} \cos i - w_{\parallel} \sin i) - w_{\parallel} (w_{\perp} \sin i + w_{\parallel} \cos i) + \frac{a^2 \omega \cos i}{\sigma_0 + \sigma_1} \frac{d\sigma_0}{d\omega} \quad (5.7)$$

$$x_3 = \omega^2 \frac{d\Omega}{d\omega} \cos i (-w_{\parallel} \sin i) + w_{\perp} (w_{\perp} \sin i + w_{\parallel} \cos i) - \frac{a^2 \omega \sin i}{\sigma_0 + \sigma_1} \frac{d\sigma_0}{d\omega} \quad (5.8)$$

$$U_1 = A \cos\left(-\frac{2}{\sin i} \eta - \phi\right) + U_2(\eta) \quad (5.9)$$

Although the terms containing  $x_1$ ,  $x_2$ , and  $x_3$  in the equations, (5.2), (5.3), and (5.4), are all of secondary importance, they will be retained in the numerical calculations.

Eliminating  $\sigma_1$  between equations (5.2) and (5.3), we can rewrite equations (5.3) and (5.4) in the following form:

$$\frac{\partial w_{\perp}}{\partial \eta} = - \frac{(w_{\perp 0} + w_{\perp}) (2\Omega \omega w_{\parallel} + f - x_2) + a^2 \left(1 + \frac{\omega}{\sigma_0 + \sigma_1} \frac{d\sigma_0}{d\omega}\right) x_1}{a^2 - (w_{\perp 0} + w_{\perp})^2} \quad (5.10)$$

$$\frac{\partial w_{\parallel}}{\partial \eta} = - \frac{\left(\frac{K^2}{2\Omega}\right) \omega w_{\perp} + x_3}{w_{\perp 0} + w_{\perp}} \quad (5.11)$$

where

$$f = A \sin\left(\frac{2}{\sin i} \eta + \phi\right), \quad A = \frac{2}{\sin i} A$$

These are two asymptotic equations to be solved for the two dependent variables,  $w_{\perp}$ ,  $w_{\parallel}$ . Once we have  $w_{\perp}(\eta)$  and  $w_{\parallel}(\eta)$ , we can determine  $\sigma_1(\eta)$  by solving the equation:

$$(w_{\perp 0} + w_{\perp}) \frac{\partial \sigma_1}{\partial \eta} + (\sigma_0 + \sigma_1) \frac{\partial w_{\perp}}{\partial \eta} + \left(\sigma_0 + \sigma_1 + \varpi \frac{d\sigma_0}{d\varpi}\right) \chi_1 = 0 \quad (5.12)$$

and we can determine our position about the disk (specified by  $\xi$ ) by solving the equation:

$$\frac{\partial \xi}{\partial \eta} = \frac{w_{\parallel 0} + w_{\parallel}}{w_{\perp 0} + w_{\perp}} \quad (5.13)$$

Solution of this system of four equations will determine a gas streamtube as well as the gas flow at every point along the streamtube. As in the linear theory, the streamtubes are not expected to deviate greatly from purely circular orbits about the galactic center. In the first approximation,  $w_{\perp 0}(\varpi)$ ,  $w_{\parallel 0}(\varpi)$ , and  $\sigma_0(\varpi)$  therefore may be taken as constants along each particular streamtube lying at an average radius  $\varpi$  from the galactic center. Consequently,  $w_{\perp 0}$ ,  $w_{\parallel 0}$ , and  $\sigma_0$  may be considered as parameters which are related according to their proper values in the Schmidt model and which specify the radius



of the particular gas streamtube under investigation. We have in mind therefore the solution of the above set of four equations, (5.10-(5.13), with these parameters specified at a particular radius according to the Schmidt model. This type of solution characterizes gas flow along closed narrow nearly concentric streamtube bands which extend circumferentially about the entire disk.

## 6. Galactic shock waves

In the galactic disk where the velocity of the gas relative to the pattern much exceeds the mean turbulent dispersion speed associated with the cloud constituents of the interstellar medium, effects of compressibility of the gas are expected to be of prime importance. Indeed, one of the most important distinctive features of supersonic flow (as opposed to subsonic flow) is that shock waves, in which processes of irreversible nature may take place, can occur in the flow. Galactic shocks may thereby appear in the supersonic flow of gas about the Galaxy.

The fundamental laws which govern the flow of gas about the (entire) galactic disk are the conservation laws of mass, momentum, and energy, and the conservation or increase of entropy. In the absence of net creation of mass, momentum, or energy by extraneous mechanisms, these conservation laws directly apply to the gas in the shock regions as well as to the remainder of the gaseous disk (apart from the shock regions). Whereas these laws take the form of differential equations in describing gas flow over the disk apart from shock regions, they become "shock jump" conditions in describing the flow of gas across a shock. The differential equations together with the shock jump conditions therefore suffice to determine a composite gas flow about the galactic disk without describing in detail the irreversible processes across the shocks.

Suppose we consider a composite picture of gas flow in which two large-scale periodically-located shock waves exist over the galactic disk. In addition, suppose we require each shock to lie along a spiral gravitational equipotential curve of the imposed pattern of background matter (primarily the moderately-old stars). Each of these galactic shock waves may have a thickness of only about 50 pc;<sup>1</sup> and such a shock represents a fairly sharp discontinuity since the shock width is practically infinitesimal with respect to the length scale of 4 kpc, which represents a characteristic scale for the interarm spacing of the system.

Since we already have the equations of motion that describe the gas flow over the galactic disk apart from shock regions (the equations of Section 5), we can easily complete the picture by deriving from these equations the form of the conservation laws which describes the flow of gas across the shock regions. Suppose we consider a column of gas which extends across a shock region and whose ends lie outside the shock neighborhood on either side. If we multiply equations (5.10), (5.11), and (5.12) by appropriate quantities, integrate them along  $n$  across the shock, and then take the limit as the length of the column shrinks toward zero, we can determine the shock jump conditions. With the additional requirements of no net creation of mass, momentum, and energy inside the shock region, the conservation laws across the shock take the form:

---

<sup>1</sup>In Section 28, a model for the gas clouds of the interstellar medium and an internal picture of a large-scale galactic shock (which may contain several gas clouds across it along a line of sight) are considered. From these investigations, a typical length scale for a shock width appears to be about 50 pc.

$$(\sigma_0 + \sigma_1(n_2)) (w_{\perp 0} + w_{\perp}(n_2)) = (\sigma_0 + \sigma_1(n_1)) (w_{\perp 0} + w_{\perp}(n_1)) \quad (6.1)$$

$$w_{\parallel}(n_2) = w_{\parallel}(n_1) \quad (6.2)$$

$$\begin{aligned} & (\sigma_0 + \sigma_1(n_2)) (w_{\perp 0} + w_{\perp}(n_2))^2 + (p_0 + p_1(n_2)) \\ &= (\sigma_0 + \sigma_1(n_1)) (w_{\perp 0} + w_{\perp}(n_1))^2 + (p_0 + p_1(n_1)) \end{aligned} \quad (6.3)$$

$$\begin{aligned} & \frac{(w_{\perp 0} + w_{\perp}(n_2))^2}{2} (\gamma-1) + a^2(n_2) \\ &= \frac{(w_{\perp 0} + w_{\perp}(n_1))^2}{2} (\gamma-1) + a^2(n_1) \end{aligned} \quad (6.4)$$

Although these shock jump conditions apply to a spiral shock wave extending about the galactic disk, they are of the same form as the usual shock jump conditions for ordinary one dimensional gas flow.

### Isothermal Shock

We are primarily interested in an "isothermal" shock (see Section 3). For an isothermal shock, we have:

$$a(n_2) = a(n_1) = a = \text{constant}$$

Therefore, we assume that the isothermal gas satisfies the equation

of state:

$$(p_0 + p_1(\eta)) = a^2 (\sigma_0 + \sigma_1(\eta)) \quad (6.5)$$

With equations (6.1), (6.3), (6.4), and (6.5), we may take the limit as  $\gamma \rightarrow 1$  and obtain the isothermal shock jump conditions:

$$(w_{\perp 0} + w_{\perp}(\eta_2)) = \frac{a^2}{(w_{\perp 0} + w_{\perp}(\eta_1))} \quad (6.6)$$

$$(p_0 + p_1(\eta_2)) = \left(\frac{w_{\perp 0} + w_{\perp}(\eta_1)}{a}\right)^2 (p_0 + p_1(\eta_1)) \quad (6.7)$$

$$(\sigma_0 + \sigma_1(\eta_2)) = \frac{m_f^2}{a^2(\sigma_0 + \sigma_1(\eta_1))} \quad (6.8)$$

where  $m_f$  is the constant mass flux across the shock.

7. Gas flow along narrow streamtubes through two periodically-located shocks

In Sections 4 and 5, we determined the equations of motion which describe gas flow along narrow nearly concentric streamtube bands about the galactic center. In Section 6, we determined the shock conditions which describe the flow of gas across an isothermal galactic shock. We now consider a composite picture which combines these two aspects of the flow. This composite picture must satisfy certain requirements:

- (1) It must permit the gas to pass through two periodically-located shock waves which lie coincident with spiral equipotential curves in the galactic disk.
- (2) It should describe the gas flow along narrow nearly concentric streamtube bands about the galactic center.
- (3) It must insure closure of the gas streamtubes so that no net radial transfer of mass, momentum, or energy takes place over the disk.
- (4) The streamtubes must repeat themselves through every half revolution of the gas flow about the disk.

Requirements (1) and (2) specify the general type of gas streamtube solution; requirements (3) and (4) provide periodic boundary conditions on this solution. These boundary conditions specify the

distances between successive shocks in terms of  $\eta$  and  $\xi$  coordinates as:

$$\Delta\eta = \pi \sin i$$

$$\Delta\xi = \pi \cos i$$

This particular type of solution, which is determined by requirements (1), (2), (3), and (4) is a solution for the gas flow in a (closed, nearly concentric, and twice-periodic) streamtube band through two periodically-located shock waves (this solution is hereafter referred to as an STS solution). The composite picture over the whole galactic disk, which is made up of a family of STS solutions (see Section 10), describes gas flow in (closed, nearly concentric, and twice-periodic) streamtube bands which pass through a two-armed spiral shock pattern (this composite picture of gas flow is hereafter referred to as the TASS picture).<sup>1</sup>

To determine whether the STS solution as outlined by these four requirements is actually attainable, an investigation of the possible degrees of freedom in the choice of the parameters versus the number of prescribed conditions is in order. Suppose we consider the various

---

<sup>1</sup>"TASS" refers to gas flow in (closed, nearly concentric, and twice-periodic) streamtube bands through a two-armed spiral shock pattern over the galactic disk between the radii of 3-4 kpc and 12 kpc. In Section 10, it is shown that the inner and outer bounds on the TASS pattern are the radii of 3-4 kpc and 12 kpc respectively.

parameters associated with the gas flow about the galactic disk. We consider first the various parameters associated with the properties of the spiral pattern and second the various galactic parameters associated with the disk as a whole:

(1) Parameters associated with the spiral pattern:

$i$  inclination angle of the spiral pattern to the circumferential direction.

$\Omega_p$  angular speed of the spiral pattern.

$A$  amplitude of the spiral gravitational field taken to be a fixed fraction of the smoothed axisymmetric field in the Schmidt model.

(2) Galactic parameters associated with the disk as a whole:

$\varpi$  average radius of a particular streamtube under consideration. If a gas streamtube does not deviate greatly from a purely circular orbit about the galactic center, the average radius for the streamtube will provide a good estimate of the actual distance of any point along the streamtube from the galactic center.

$\Omega(\varpi)$  the basic equilibrium angular velocity at a radius  $\varpi$  in the Schmidt model. This together with  $\Omega_p$ ,  $\varpi$ , and  $i$  determines the velocity components for the gas flow in the directions normal and parallel to the spiral equipotential curves:

$$w_{\perp o} = (\Omega(\varpi) - \Omega_p)\varpi \sin i$$

$$w_{\parallel o} = (\Omega(\varpi) - \Omega_p)\varpi \cos i$$



If the streamtubes do not deviate greatly from exactly circular orbits, these velocity components may be taken as constants for each particular radius under consideration.

$K(\varpi)$  epicyclic frequency at a radius  $\varpi$  in the Schmidt model.

$a(\varpi)$  mean turbulent dispersion speed of the gas along a streamtube at a radius  $\varpi$  from the galactic center.

These above-mentioned parameters associated with the spiral pattern and with the disk as a whole govern a general gas flow solution which satisfies requirements (1) and (2). With a consideration of two remaining parameters at our disposal, requirements (3) and (4) may be satisfied. These remaining parameters associated with the gas flow about the galactic disk are:

$\phi_s$  the phase of the shock with respect to the spiral field.

$\mathcal{U}_2$  a small potential field correction to the spiral potential field.

There are exactly two such parameters,  $\phi_s$  and  $\mathcal{U}_2$ ; and, there are exactly two boundary conditions (i.e., requirements (3) and (4)) to be satisfied with the proper choice of  $\phi_s$  and  $\mathcal{U}_2$  for each streamtube. In general, these boundary conditions will be satisfied for one value of  $\phi_s$  and one value of  $\mathcal{U}_2$  only. Therefore, the location of the two shocks of an STS solution is predetermined.

## 8. Analysis of singular points

To gain insight into a possible numerical solution of the gas flow about the galactic disk, we now investigate the small amplitude behavior of the velocity components of the gas flow about possible equilibrium states. In such an analysis we neglect all higher order terms of secondary importance in the equations of motion. In addition, we are concerned with possible small amplitude behavior without any influence of forcing; and therefore, the imposed forcing due to a spiral field is neglected.

### Singular Points

The "equilibrium" positions of the system of equations, (5.10) and (5.11), correspond to the singular points of the following differential equation:

$$\frac{\partial w_{\parallel}'}{\partial w_{\perp}'} = - \frac{\left(\frac{K}{2\Omega}\right)^2 w_{\perp}' [w_{\perp 0}' + w_{\perp}' - a'] [w_{\perp 0}' + w_{\perp}' + a']}{(w_{\perp 0}' + w_{\perp}')^2 w_{\parallel}'} \quad (8.1)$$

where each "primed" quantity represents a velocity in nondimensional form:

$$(w_{\perp}', w_{\perp 0}', w_{\parallel}', a') = \frac{1}{2\Omega\bar{\omega}} (w_{\perp}, w_{\perp 0}, w_{\parallel}, a)$$

We therefore investigate the character of the integral curves in the neighborhood of each of the various isolated singular points of the differential equation (8.1). The singular points may be found by inspection:

$$(w_{\perp}' = 0, w_{\parallel}' = 0)$$

$$(w_{\perp}' = a' - w_{\perp 0}', w_{\parallel}' = 0)$$

$$(w_{\perp}' = -a' - w_{\perp 0}', w_{\parallel}' = 0)$$

The integral curves about the singular point,  $(w_{\perp}' = 0, w_{\parallel}' = 0)$ , are given by:

$$w_{\parallel}'^2 + \mu_1^2 w_{\perp}'^2 = \text{constant} \quad (8.1a)$$

where

$$\mu_1^2 = \left(\frac{k}{2\Omega}\right)^2 \left(1 - \left(\frac{a'}{w_{\perp 0}'}\right)^2\right)$$

If  $w_{\perp 0}' - a' > 0$ , which is the situation we are concerned with in the Galaxy, the integral curves (8.1a) are ellipses with the origin,  $(w_{\perp}' = 0, w_{\parallel}' = 0)$ , as the center.

The integral curves about the singular point,  $(w_{\perp}' = a' - w_{\perp 0}', w_{\parallel}' = 0)$ , are given by:

$$w_{\parallel}'^2 + \mu_2^2 (w_{\perp 0}' - a' + w_{\perp}')^2 = \text{constant} \quad (8.1b)$$

where

$$\mu_2^2 = 2 \left( \frac{K}{2\Omega} \right)^2 \left( 1 - \frac{w_{\perp 0}'}{a'} \right)$$

In the situation where  $w_{\perp 0}' - a' > 0$ , the singular point,  $(w_{\perp}' = a' - w_{\perp 0}', w_{\parallel}' = 0)$ , is a saddle point.

The integral curves about the singular point,  $(w_{\perp}' = -a' - w_{\perp 0}', w_{\parallel}' = 0)$ , are given by:

$$w_{\parallel}'^2 + \mu_3^2 (w_{\perp 0}' + a' + w_{\perp}')^2 = \text{constant} \quad (8.1c)$$

where

$$\mu_3^2 = 2 \left( \frac{K}{2\Omega} \right)^2 \left( 1 + \frac{w_{\perp 0}'}{a'} \right)$$

Since  $\mu_3^2 > 0$ , the singular point,  $(w_{\perp}' = -a' - w_{\perp 0}', w_{\parallel}' = 0)$ , is a center.

Integrating the numerator of equation (8.1), we can determine a "potential function:"

$$F(w_{\perp}') = w_{\perp}'^4 + \frac{8}{3} w_{\perp 0}' w_{\perp}'^3 + 2 (w_{\perp 0}'^2 - a'^2) w_{\perp}'^2$$

Suppose we consider a plot of  $F(w_{\perp}')$  versus  $w_{\perp}'$  in order to gain more information about the integral curves. The valleys of  $F(w_{\perp}')$  correspond to situations where the kinetic energy associated with  $w_{\parallel}'$  is at a local maximum. Therefore in the valleys of  $F(w_{\perp}')$  the magnitude of  $w_{\parallel}'$  takes on local maximum values. This relation between  $F(w_{\perp}')$  and  $w_{\parallel}'$  is analogous to the usual type of potential energy plot for an oscillatory system with the maximum values of velocity being realized in the "potential" valleys.

In Figure (8.1), we have plotted  $F(w_{\perp}'/w_{\perp 0}')$  for various values of  $a'/w_{\perp 0}'$ . The base state gas flow in the Galaxy is supersonic so that we are primarily interested in cases for which  $a'/w_{\perp 0}'$  satisfies the condition:

$$0 \leq \frac{a'}{w_{\perp 0}'} \leq 1$$

We can see that the valleys of  $F(w_{\perp}'/w_{\perp 0}')$  correspond to centers, and the peak of  $F(w_{\perp}'/w_{\perp 0}')$  corresponds to a saddle point. The unique saddle point associated with each  $F(w_{\perp}'/w_{\perp 0}')$  curve may be called the "sonic point". Whereas the velocity component,  $w_{\perp}$ , is supersonic if it lies to the right of the sonic point, it is subsonic if it lies to the left. Furthermore, there is a lower bound on  $w_{\perp}'$ , i.e.,  $w_{\perp}'/w_{\perp 0}' = -1$ , beyond which physical gas flow is not possible.

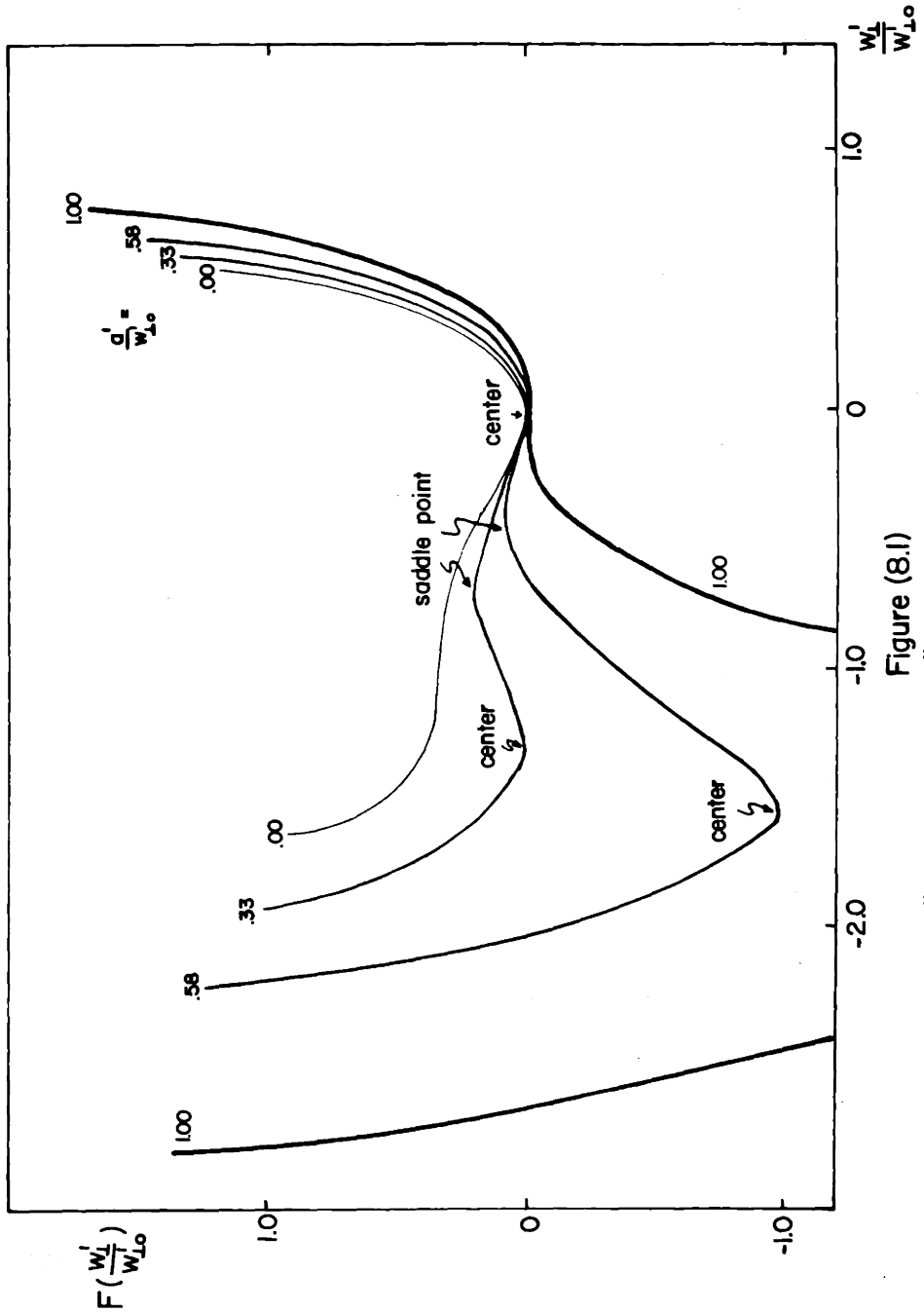


Figure (8.1)  
 "Potential Function" and Singular Points

At this limit, the gas flow must completely reverse direction.

Figure (8.2) illustrates several integral curves of equation (8.1) for the set of parameters:

$$\left(\frac{K}{2\Omega}\right)^2 = .4, \quad w_{\perp 0}' = .049, \quad a' = .034$$

The circumferential streamtube lengths about the galactic disk for these several integral curves are indicated beside each curve. Whereas a value of  $\pi$  radians is a necessary angular length for a streamtube which is exactly twice-periodic about the disk, these integral curves represent streamtubes of angular lengths of about  $.8\pi$  radians, which require a multiple periodicity greater than two.

Passage across the "sonic plane" is possible only at the sonic point and only if a particular state of the gas flow is realized at this point. Otherwise, any solution blows up upon reaching the sonic plane; and therefore, an arbitrary integral curve which does not pass through this point or which passes through this point without the proper slope cannot represent physical gas flow. The quantities,  $w_{\perp}'$ ,  $w_{\parallel}'$ ,  $\partial w_{\perp}'/\partial \eta$ , and  $\partial w_{\parallel}'/\partial \eta$ , are completely specified at the sonic point by the set of parameters.<sup>1</sup>

---

<sup>1</sup>The complete specification of the quantities,  $w_{\perp}'$ ,  $w_{\parallel}'$ ,  $\partial w_{\perp}'/\partial \eta$ , and  $\partial w_{\parallel}'/\partial \eta$ , at the sonic point for the full nonlinear problem is demonstrated in Appendix III.

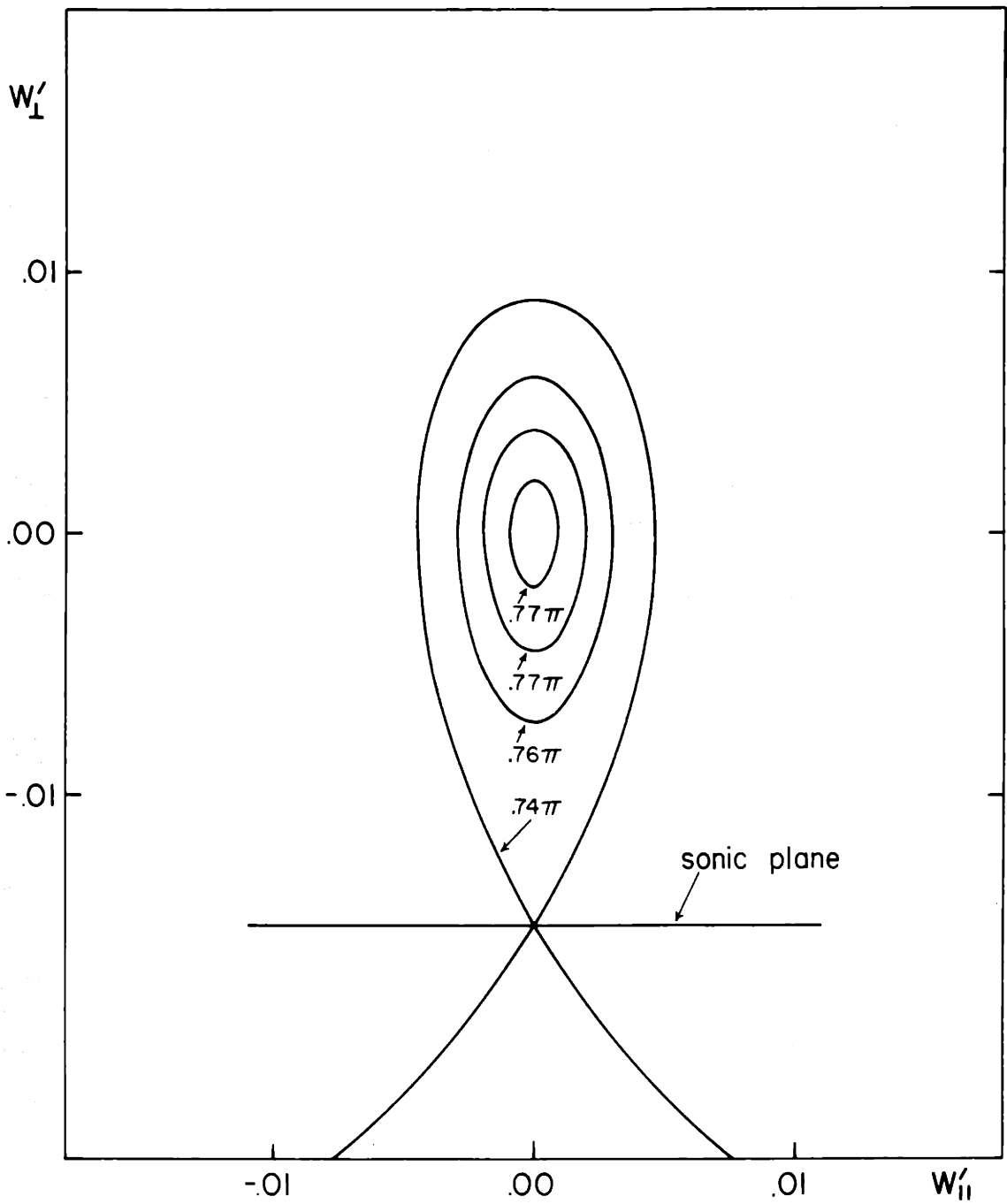


Figure (8.2)  
Integral Curves of Equation (8.1)



## Nonlinear Equations

When higher order nonlinear terms and forcing due to a spiral field are included, new features enter the problem. However, the general nature of the above results remains essentially unchanged even with the addition of these nonlinear effects and forcing.

Suppose we examine the full nonlinear equations (5.10) and 5.11) (in nondimensional form) for singular points. In a similar fashion to the linear singular point analysis, a singular point exists along the nonlinear solution curve where  $w_{\perp}' + w_{\parallel}' = a'$ . This is the "sonic point" where the gas flow exhibits a change from subsonic to supersonic flow. Since our picture of the Galaxy contains shocks, the gas flow must indeed pass from subsonic to supersonic somewhere. The denominator of equation (5.10) is zero at this sonic point. Physically, no discontinuities occur in flow passing from subsonic to supersonic, so we require the numerator of equation (5.10) likewise to equal zero at the sonic point. With this restriction on the numerator, the quantities,  $w_{\perp}'$ ,  $w_{\parallel}'$ ,  $\partial w_{\perp}' / \partial \eta$ , and  $\partial w_{\parallel}' / \partial \eta$ , are all uniquely specified at the sonic point. (c.f. Appendix III). If the sonic point were therefore chosen as a possible point where the integration of the equations of motion may begin, there would be no arbitrariness in the choice of values for the various flow variables (at the initial step of numerical integration). The sonic point is therefore the only convenient point at which the numerical integration of the equations of motion may be initiated.<sup>1</sup>

---

<sup>1</sup>Fujimoto (1966) also arrived at the same conclusion.

With the specification of all the parameters, the sonic point conditions are determined, and numerical integration of the gas flow equations may begin from the sonic point. The basic integration procedure followed is the Runge-Kutta-Gill method contained in the System/360 Scientific Subroutine Package (p. 118-). At each step of the integration process, an automatic error analysis scheme for satisfactory integration within specified error limits is carried out before passage to the next step. If the error limits are exceeded in any one step, the grid size is reduced appropriately before passage to the next step. A detailed treatment of the integration process is given in Appendix IV.

Along the solution curve in the positive  $n$  direction, the flow is supersonic, whereas the flow is subsonic along the solution curve in the negative  $n$  direction. Because of the nature of the integral curve on the supersonic side of the sonic plane in Figure (8.2), the supersonic branch of the solution curve circles about its center point and finally reaches the sonic plane once again at a point other than the sonic point. In such a situation,  $\partial w_{\perp}' / \partial n$  must be infinite. To avoid this unphysical consequence, a shock is imposed between the supersonic and subsonic branches of the solution curve at some point before the supersonic branch again touches the sonic plane. There is in general only one point along the supersonic branch where a shock will be compatible with the gas flow. The composite solution curve thereby represents periodic gas flow which (1) begins from a shock and passes along the subsonic branch toward the sonic point, (2) becomes supersonic at the sonic point, and (3) after remaining supersonic for some time reaches the next successive shock along its

path. At the next shock, the cycle begins once again.

By proper specification of the parameters, an STS solution may be determined at a given radius (the effects of variation of the parameters will be discussed in Section 9). A typical STS solution is sketched in Figure (8.3); and the projection of this solution in  $w_{\perp}'-w_{\parallel}'$  space is sketched in Figure (8.4).<sup>1</sup> For given radius in the Schmidt model, and for given dispersion speed, field strength, pattern speed, and inclination angle, only a particular value for the shock phase,  $\phi_s$  will insure an exactly twice-periodic shock solution.

Closure of gas streamtubes is insured by a second order correction to the spiral field.<sup>2</sup> Although it is shown in Appendix V that a small second order correction,  $U_2$ , to the spiral potential is necessary to insure streamtube closure, it is also shown that this small correction causes only a slight shifting of the streamtube. In addition, it is shown that the second order correction is of a smaller percentage correction to the basic field than is the percentage error involved in the neglect of stellar dispersion in the determination of the purely circular base state gas flow.

---

<sup>1</sup> Figure (8.4) also sketches a "shock jump curve". At every point along the supersonic branch, subsonic values of the physical variables are calculated by the shock jump conditions (as if a shock were possible at every point along the supersonic branch). The resulting curve, which indicates the possible shock jumps from every point of the supersonic branch, may be denoted the "shock jump curve." The point where the shock jump curve intersects the subsonic branch of the solution curve is the only point on the subsonic branch where a physical shock may actually exist.

<sup>2</sup> In Appendix V, the condition for closure of gas streamtubes about the galactic disk is investigated in detail.

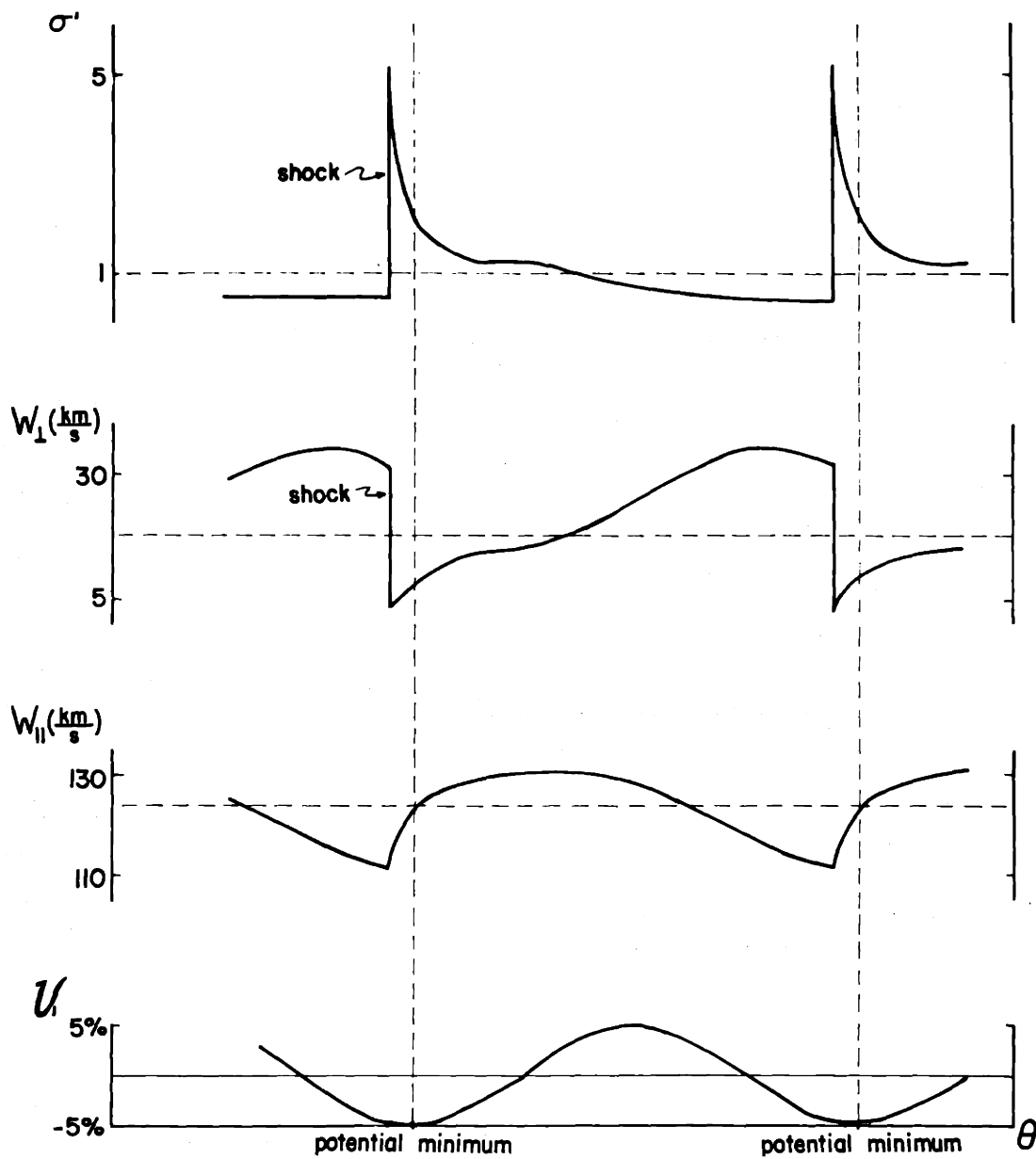


Figure (8.3)  
A Typical STS Solution

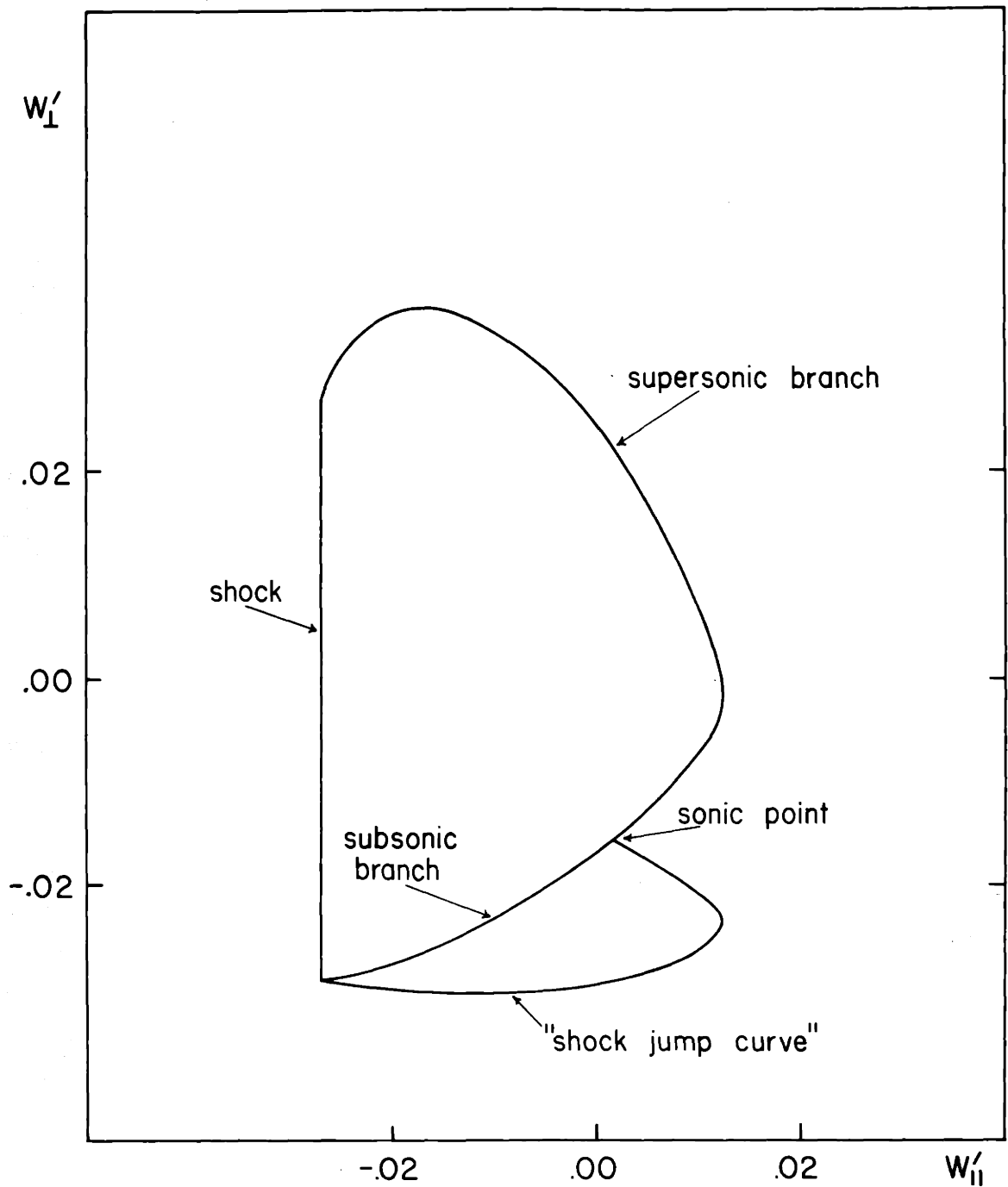


Figure (8.4)  
A Typical STS Solution

The effect of the higher order nonlinear terms (i.e.,  $x_1$ ,  $x_2$ , and  $x_3$  in equations (5.10) and (5.11) ) is yet another important aspect of the STS solution. Figure (8.5) provides a sketch of an STS solution that corresponds to the set of parameters:<sup>1</sup>

$$\tan i = 1/7 \quad \left(\frac{K}{2\Omega}\right)^2 = .4 \quad w_{\perp 0}' = .049$$

$$a' = .034 \quad A = 5\%$$

The nonlinear STS solution and the linear STS solution (i.e.,  $x_1 = x_2 = x_3 = 0$ ) both for 5% perturbation field, and the linear, zero-field integral curve that passes through the sonic plane (see Figure (8.2) ) are all sketched in Figure (8.5). Whereas each 5%-field curve represents an exactly twice-periodic streamtube whose length is  $\pi$  radians between successive shocks, a typical zero-field integral curve may extend only about  $.8\pi$  radians about the disk. It is quite apparent that the spiral field plays a significant role in governing the gas flow. On the other hand, the contiguity of the linear and nonlinear 5%-field curves indicates how small is the influence of the higher order terms,  $x_1$ ,  $x_2$ , and  $x_3$ .

---

<sup>1</sup>A set of five independent parameters that completely specifies an STS solution is:  $i$ ,  $(K/2\Omega)$ ,  $w_{\perp 0}'$ ,  $a'$ , and  $A$ . Another set of five independent parameters that completely specifies the STS solution is:  $i$ ,  $\Omega_p$ ,  $\pi$ ,  $a$ , and  $A$  (see Section 9).

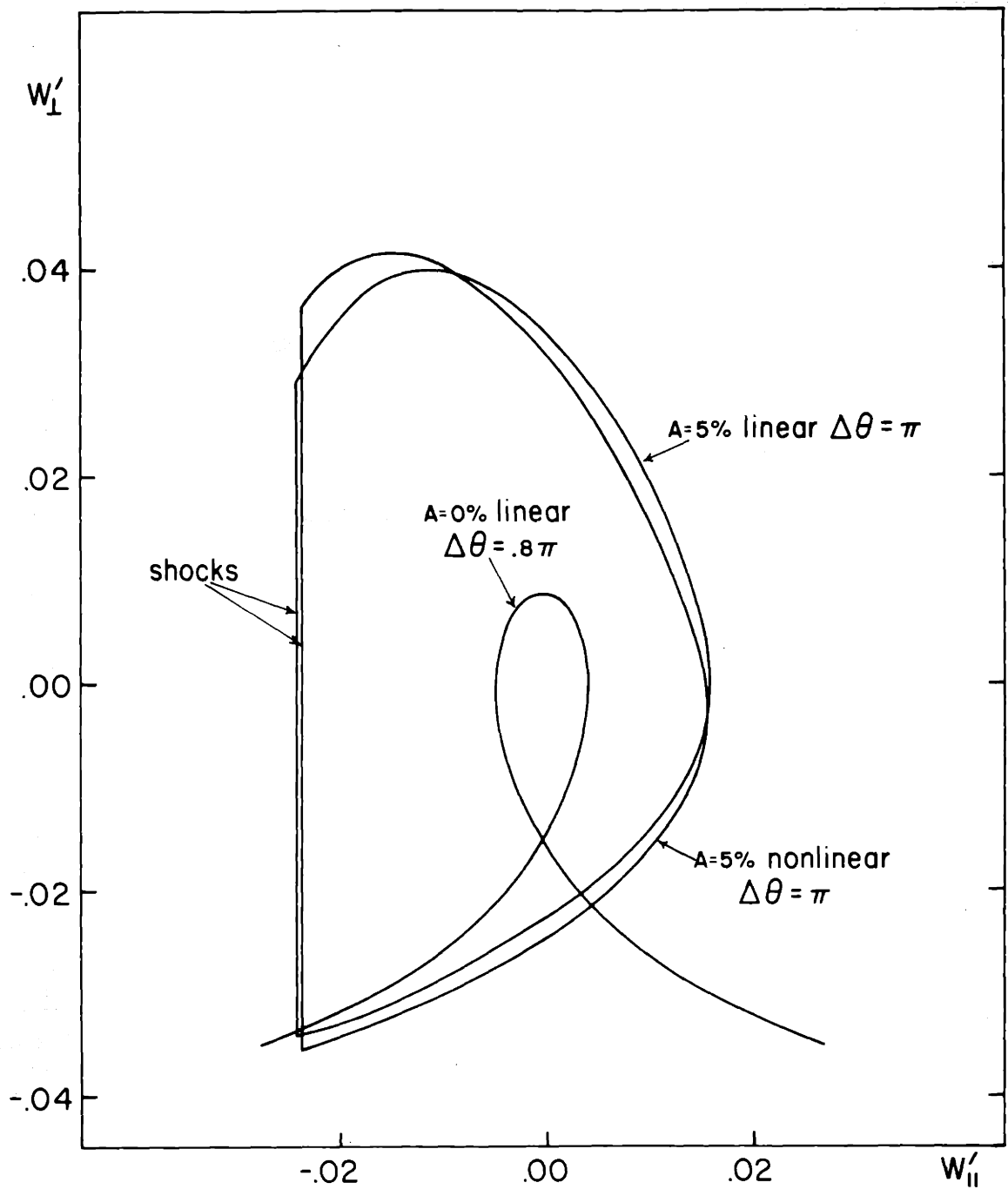


Figure (8.5)  
Forcing and Nonlinear Terms

## 9. Effects of variation of the galactic parameters

We now direct our attention to the features of an STS solution which are governed by the various parameters of the system.<sup>1</sup> The various galactic parameters include:

$i$	$\Omega_p$	$\varpi$	$\Omega(\varpi)$	$K(\varpi)$
$w_{\perp o} = (\Omega(\varpi) - \Omega_p)\varpi \sin i$			$w_{\parallel o} = (\Omega(\varpi) - \Omega_p)\varpi \cos i$	
$a$	$A$	$U_2$	$\phi_s$	

The parameter,  $U_2$ , must be chosen in such a manner to insure stream-tube closure.<sup>2</sup> Of all these parameters, the Schmidt model specifies  $\Omega(\varpi)$  and  $K(\varpi)$  for a particular  $\varpi$ ; and once an inclination angle,  $i$ , and a pattern speed,  $\Omega_p$ , are chosen,  $w_{\perp o}$  and  $w_{\parallel o}$  can be determined as well. Therefore, the parameters,  $i$ ,  $\Omega_p$ ,  $\varpi$ ,  $a$ , and  $A$ , may be considered as the important independent parameters of the system. An inclination angle,  $i$ , such that  $\tan i = 1/7$  and a pattern speed,  $\Omega_p$ , of 12.5 km/s/kpc determined from other observa-

---

<sup>1</sup>"STS" refers to the particular type of solution determined by requirements (1), (2), (3), and (4) of Section 7 that describes gas flow in a (closed, nearly concentric, and twice-periodic) streamtube band through two-periodically-located shock waves.

<sup>2</sup>see Appendix V.



tional studies (see Lin, Yuan, and Shu, 1968) are adopted. Therefore, we are primarily interested in the effects on an STS solution of variation of the remaining independent parameters,  $\varpi$ ,  $a$ , and  $A$ .

### Parameter Space

Suppose we now consider the influence of these galactic parameters on an STS solution. Each one of the parameters,  $\varpi$ ,  $a$ , and  $A$ , may be allowed to vary separately (with corresponding variation of the shock phase  $\phi_s$  in order to retain a twice-periodic solution); and the effect of such variation of each parameter on an STS solution may be determined.

For fixed values of  $\varpi$  and  $A$ , there exists a family of STS solutions which describe a curve in  $a$ - $\phi_s$  space, each such solution being associated with a point of the curve. Two such curves of STS solutions for fields of 5% and 7.5% of the symmetrical field are sketched in Figure (9.1).<sup>1</sup> The shock of an STS solution for  $\phi_s = \pi$  radians coincides with the potential minimum of the imposed field (i.e., the density maximum of the imposed spiral pattern.)

An increase in perturbation field influences a corresponding increase in  $\phi_s$  if  $a$  is held constant and a corresponding increase in  $a$  if  $\phi_s$  is held constant. A larger perturbation field is necessary to maintain an STS solution when dispersion effects are stronger corresponding to a more enhanced state of turbulence in the

---

<sup>1</sup>The values of the fixed galactic parameters for these two families of STS solutions are:  $\tan i = 1/7$ ,  $\Omega_p = 12.5$  km/s/kpc,  $\varpi = 10$  kpc, and  $A = 5\%$ ,  $7.5\%$  respectively.

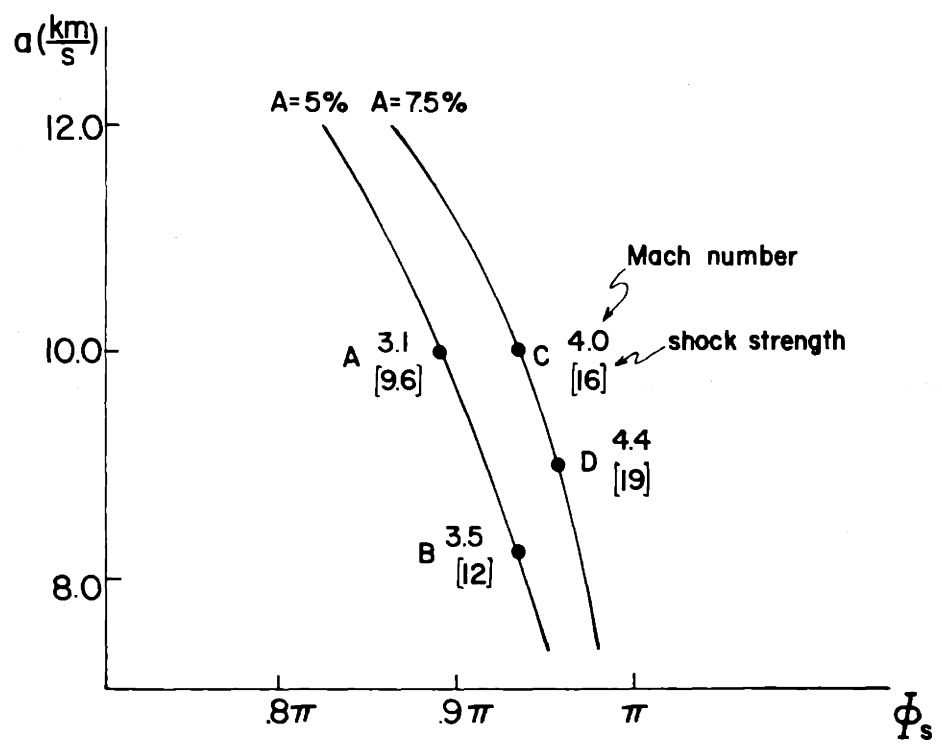


Figure (9.1)  
Two Families of STS Solutions

interstellar medium.

Suppose we consider the STS solution at each one of several points, A, B, C, D, along these curves in Figure (9.1). For an isothermal shock,<sup>1</sup> the pressure jump and density jump are equivalent; and therefore, the shock strength is a measure of both density and pressure jumps. The supersonic and subsonic Mach numbers associated with the gas flow before and after passage through the isothermal shock are directly and inversely proportional respectively to the square root of the shock strength:<sup>2</sup>

$$M_1^2 = M_2^{-2} = \frac{p(2)}{p(1)} = \frac{\sigma(2)}{\sigma(1)}$$

The Mach numbers (supersonic) and shock strengths are indicated beside the various points, A, B, C, D, in Figure (9.1). The behavior of the density distribution of an STS solution which is associated with each of these points, is sketched in Figure (9.2). All the shocks lie close together within a spacing of less than  $.05\pi$  radians on the front side of the potential minimum. The larger the gaseous turbulent dispersion in the interstellar medium, the smaller the shock strength that can be maintained. On the other hand, with larger field strength, a shock of greater strength can be supported.

---

<sup>1</sup>The galactic shock in these calculations is taken as isothermal (see Section 3).

<sup>2</sup>see Section 6.

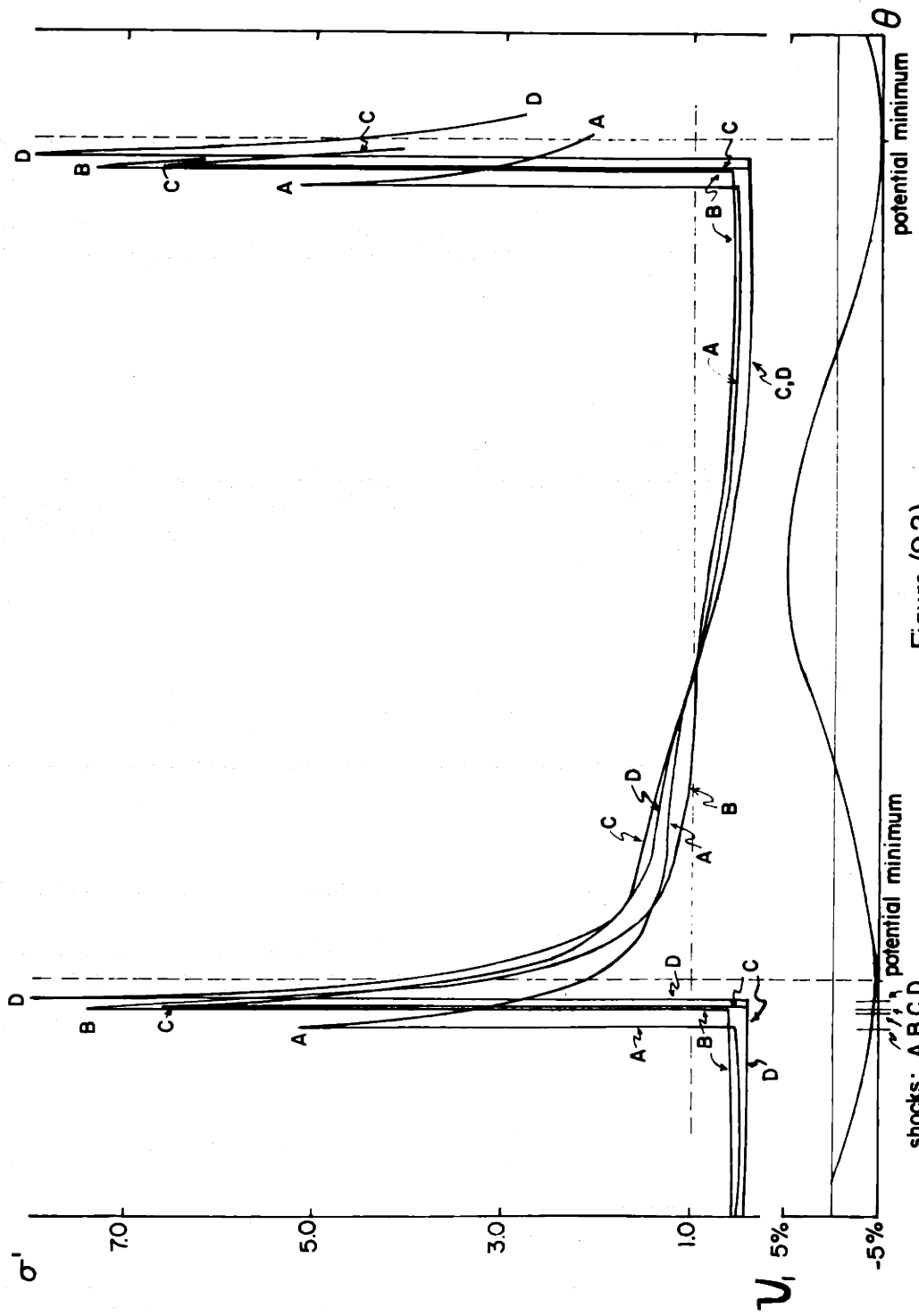


Figure (9.2)

Density Distributions of Four STS Solutions: A,B,C,D

### Fundamental Component of the Density Distribution

Suppose we ask how the (nonlinear) density distribution of an STS solution compares with the density distribution in the linear theory. We are interested in possible features of similarity and difference between the linear and nonlinear theories. The amount of phase shift between the fundamental component of the density distribution of an STS solution and the linear density harmonic would be one such important feature. Figure (9.3) sketches this fundamental component for each of the points, A, B, C, D. In the linear theory, the peak of gaseous density distribution lies exactly at the potential minimum of the imposed field. On the other hand, for each of the points, A, B, C, D, the peak of the fundamental component lies slightly on the back side of the potential minimum, whereas the shock itself lies slightly on the front side. This is, in general, the situation for all STS solutions. An STS solution therefore gives rise to an induced self gravitational field which lies nearly in phase with the imposed field.

The peak of the fundamental component for a smaller perturbation field lies even closer to the potential minimum. This feature might lead us to expect that as the imposed field is reduced, the phase of the peak may approach the potential minimum. Such a tendency would indicate that the nonlinear theory may approach the linear theory in the limit of smaller and smaller field.<sup>1</sup>

---

<sup>1</sup>A similar limit for an STS solution is considered in the following subsection.

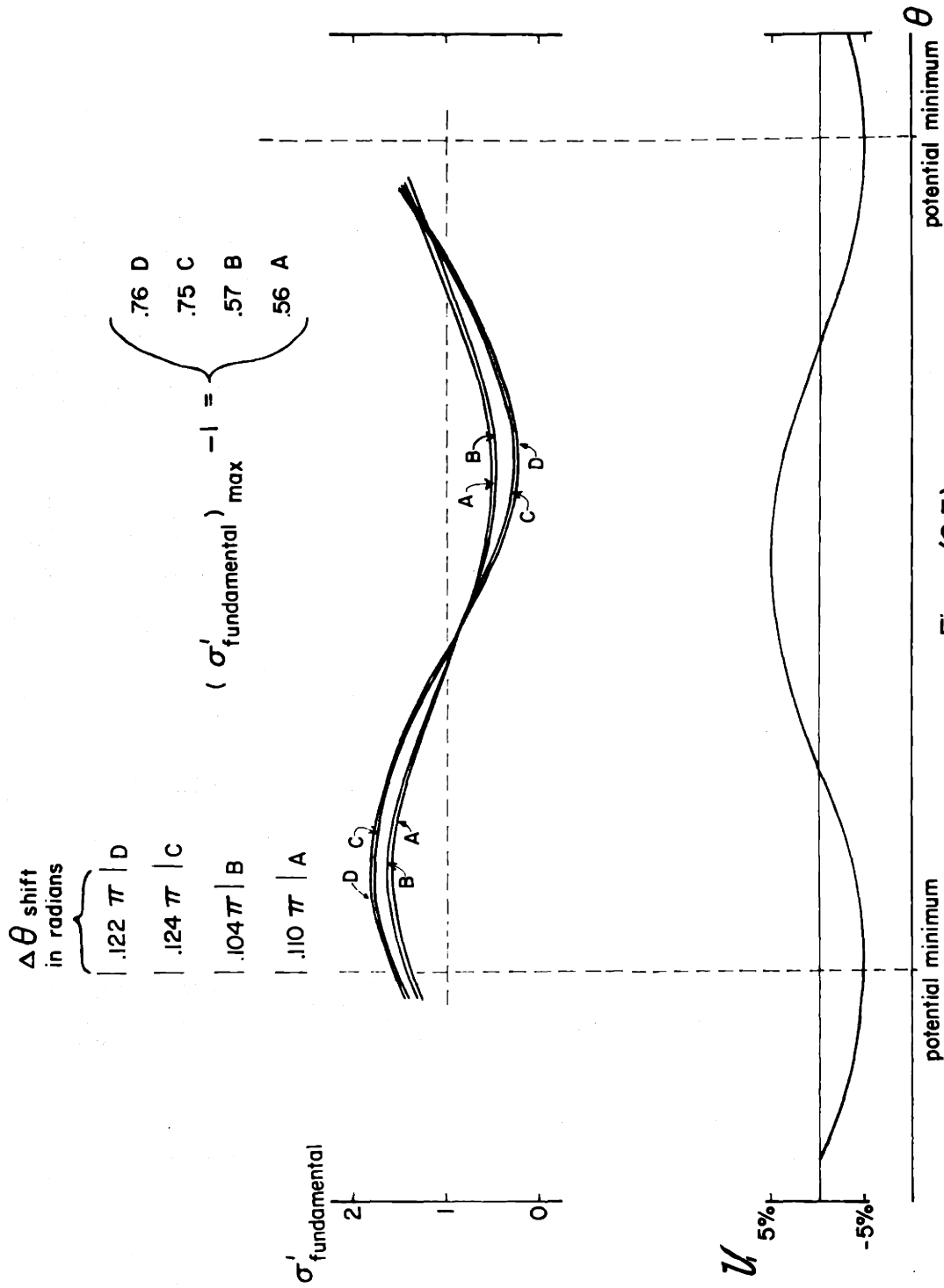


Figure (9.3)  
Fundamental Components of Density Distributions of Four STS Solutions: A, B, C, D

According to Poisson's equation, the total stellar and gaseous mass participation in the solar neighborhood necessary to support a spiral field of 5% of the symmetrical field is about  $9.8 M_{\odot} / \text{pc}$  or about .096 of the total material density of  $94 M_{\odot} / \text{pc}$  in the solar vicinity. If the relative amounts of gas and stellar mass in the solar neighborhood is given as:  $\sigma_0 / \sigma_{*} = 1/9$ , and if the stellar reduction factor is about .07, the gaseous reduction factor then is about .40. Therefore, the gaseous mass to stellar mass participation in the support of the perturbation field may be a little greater than 1:2 (i.e. .65). This is a typical value of the relative gaseous to stellar mass participation in the nonlinear galactic shock picture.

The Limit of Weak Shock Strength and of  
Weak Spiral Perturbation Gravitational Field

In the preceding subsection, it is shown that the phase of the fundamental component of density distribution in an STS solution approaches the phase of the linear density solution as the field decreases. In this subsection, another important limiting process is considered: namely, whether an STS solution (and a two-shock pattern composed of STS solutions) can persist in the limit of zero field. It would be very interesting to determine if a limit for decreasing field (at constant dispersion speed) does exist below which no two-shock gas streamtube solution is possible. Indeed, we shall find this to be the case.

It is clear from the preceding work that in order to retain the STS solution as the field decreases, the shock phase,  $\phi_S$ , must also decrease. Projections of an STS solution in  $w_{\perp}' - w_{\parallel}'$  space

for the set of parameters:  $\tan i = 1/7$ ,  $(K/2\Omega)^2 = .4$ ,  
 $w_{\perp o}' = .049$ , and  $a' = .034$ , and for several values of the  
field strength,  $A = 7.5\%$ ,  $5\%$ ,  $2\%$ ,  $1.28\%$ ,  $1.16\%$ ,  $1.04\%$ , and  $.8\%$ , are  
sketched in Figure (9.4). The shock strength and the Mach number  
(supersonic) decrease as the strength of the field decreases.  
Table (9.1) provides the various shock strengths and Mach numbers  
(supersonic) under these respective field strengths.

For the above set of values of the parameters, a limit is found  
for the field below which no STS solution is possible. This limit of  
finite shock strength is

$$\frac{\sigma(2)}{\sigma(1)} = 1.45 \quad M_1 = 1.2$$

and occurs for a field of about 1.04% of the symmetrical field. If  
the perturbation field strength decreases below this limiting value,  
the STS solution can no longer be sustained. For example, in the case  
of the curve which corresponds to  $A = .8\%$  (sketched in Figure (9.4) ),  
no shock can be constructed between the supersonic and subsonic branches  
of the curve.

In general, for every other set of values of the parameters,  
similar lower bounds exist on the field and the shock strength of the  
associated STS solution.<sup>1</sup> For every radius between 3-4 kpc and 12 kpc

---

<sup>1</sup> Something exceptional occurs in the 3 kpc region of the galactic disk.  
We shall see later (Section 14) that for an STS solution at a radius  
of 3 kpc the lower bound for the field is zero while the corresponding  
lower bound for the shock strength is still finite. The bound on per-  
turbation field strength reaches zero before the bound on shock strength.  
Therefore, it is possible for an STS free mode to exist in the 3 kpc  
region of the galactic disk.



Table (9.1)

The Limit of Decreasing Field and Shock Strength of an SIS Solution

A	$\sigma(2)/\sigma(1)$	$M_1$
7.5%	9.2	3.0
5.0%	6.2	2.5
2.0%	2.4	1.6
1.28%	1.9	1.4
1.16%	1.5	1.22
1.04%	1.45	1.2

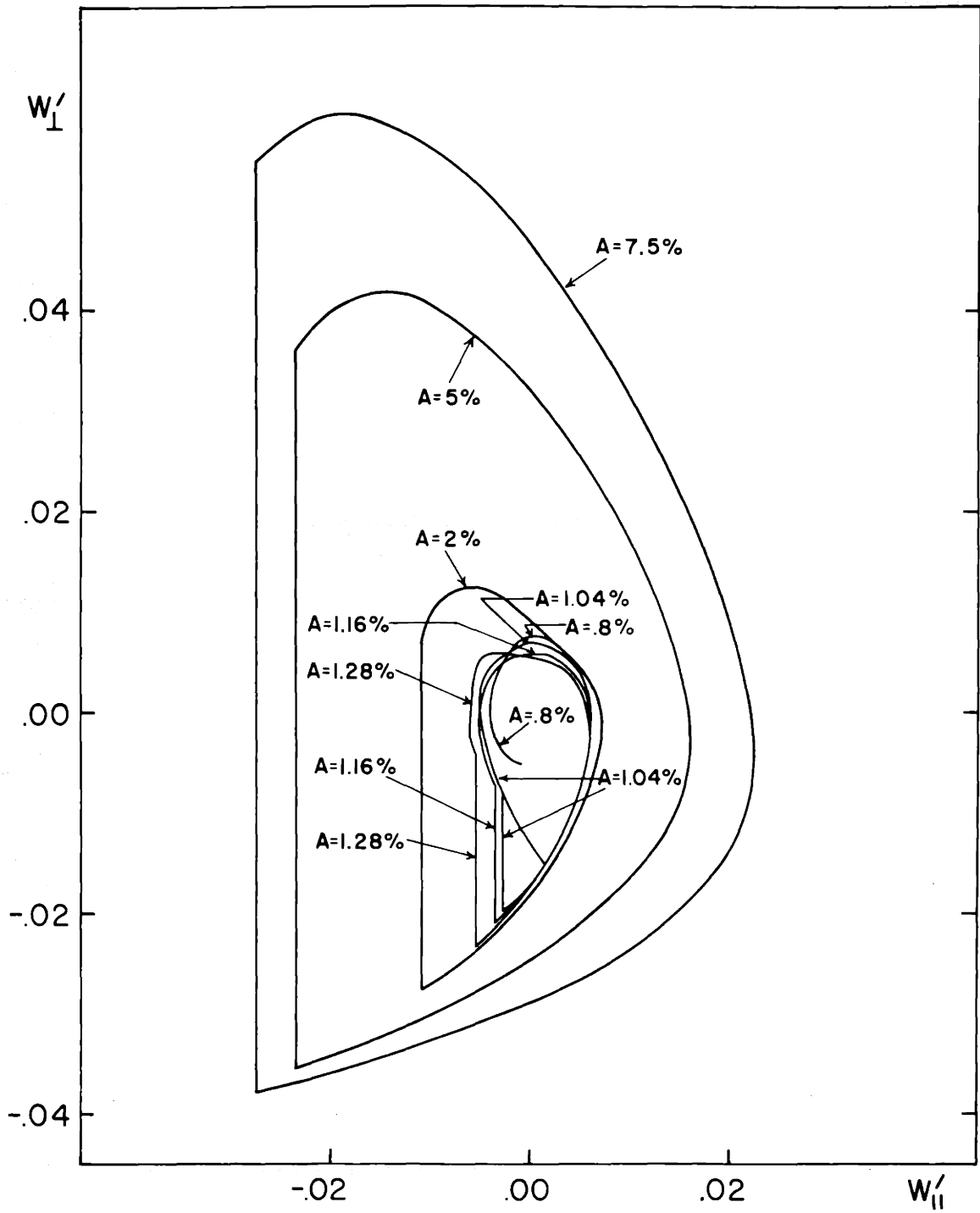


Figure (9.4)  
 Lower Bound on Shock Strength and Perturbation Field  
 for a Typical STS Solution

in the galactic disk, there is a positive lower bound on shock strength for every STS solution and a positive lower bound for the spiral perturbation field which is necessary to support the STS solution.

10. Gaseous disk: a family of nearly concentric<sup>1</sup> streamtubes

In order to simulate the gas flow picture over the whole galactic disk a family of STS solutions that covers all radii of the disk and that is compatible with the galactic parameters over the disk must be constructed.

STS Solutions at Various Radii

Numerical calculations<sup>2</sup> for the determination of such a family of STS solutions that describes the gas flow about the Galaxy have been carried out for streamtube bands lying at typical radii stretching from 3-4 kpc to 12 kpc in the Schmidt model of the Milky Way System.<sup>3</sup>

---

<sup>1</sup>Nearly concentric refers to streamlines (and streamtubes) about the galactic center, which are not exact circles but rather are pointed ovals (e.g., see Figures (10.2) and (10.3) ).

<sup>2</sup>Values of the fixed parameters that have been adopted for these numerical calculations (of Section 10) are:  $\tan i = 1/7$ ,  $\Omega_p = 12.5$  km/s/kpc, and  $A = 5\%$ .  $\omega$  varies over the disk, and  $a$  varies with  $\omega$ .

<sup>3</sup>These calculations where a spiral field is imposed in the 3 kpc neighborhood of the Schmidt model are of general exploratory character since the density wave pattern, which gives rise to such a spiral field does not extend further inwards than inner Lindblad resonance at about 3.5 kpc according to the linear density wave theory. We shall later see however in the nonlinear theory (Section 14) that the gaseous component organizes itself into a free mode and maintains a shock pattern in the 3 kpc region without a supporting perturbation field. This nonlinear organization of a gaseous free mode signifies as well the organization of an induced gravitational field due to the gas alone (which is not included in the calculations), although this induced field can be at most of the order of only a few percent of the symmetrical field.

Values of various parameters at typical radii in the Schmidt model are listed in Table (10.1). Curves representing families of STS solutions at these typical radii in the galactic disk are sketched in  $a-\phi_s$  space in Figure (10.1). As STS solution corresponds to each point of every curve.

A most interesting feature is evident in Figure (10.1); namely, the lack of variation of the shock phase,  $\phi_s$ , along the curves of STS solutions for all radii between 3-4 kpc and 10 kpc. If the dispersion speed of gas in the Galaxy were to vary over a typical range of, perhaps, 7 km/s to 11 km/s, then the range of shock phase for the entire family of possible STS solutions between the radii of 3-4 kpc and 10 kpc would cover only the narrow range between  $\phi_s = .86\pi$  radians and  $\phi_s = 1.01\pi$  radians. We note that the potential minimum of the imposed spiral field is at  $\phi_s = \pi$  radians.

We will refer to a shock of the STS solution in two different ways. While it is sometimes convenient to consider the shock strength which is the ratio of gas density on the back side of the shock,  $\sigma(2)$ , to that on the front side,  $\sigma(1)$  (i.e.,  $\sigma(2)/\sigma(1)$ ); at other times, it is convenient to consider the effective overall gas compression along a streamtube which may be taken as the ratio of the maximum gas density,  $\sigma(2)$ , to the average gas density,  $\sigma_0$  (i.e.,  $\sigma(2)/\sigma_0$ ). Values of the shock strength and the effective gas compression along a gas streamtube are indicated at various points along each of the curves of Figure (10.1). Both of these quantities decrease with increasing gaseous turbulent dispersion speed. In other words, the greater the mean gaseous turbulent dispersion speed in the interstellar medium, the weaker the shocks that can be maintained.

Table (10.1)

1965 Schmidt model

$\sigma$	$\Omega$	K	$(\frac{K}{2\Omega})^2$
3	65	100	.59
4	53	85	.64
6	40	62	.61
8	32	47	.53
10	25	32	.40
12	20	22	.30

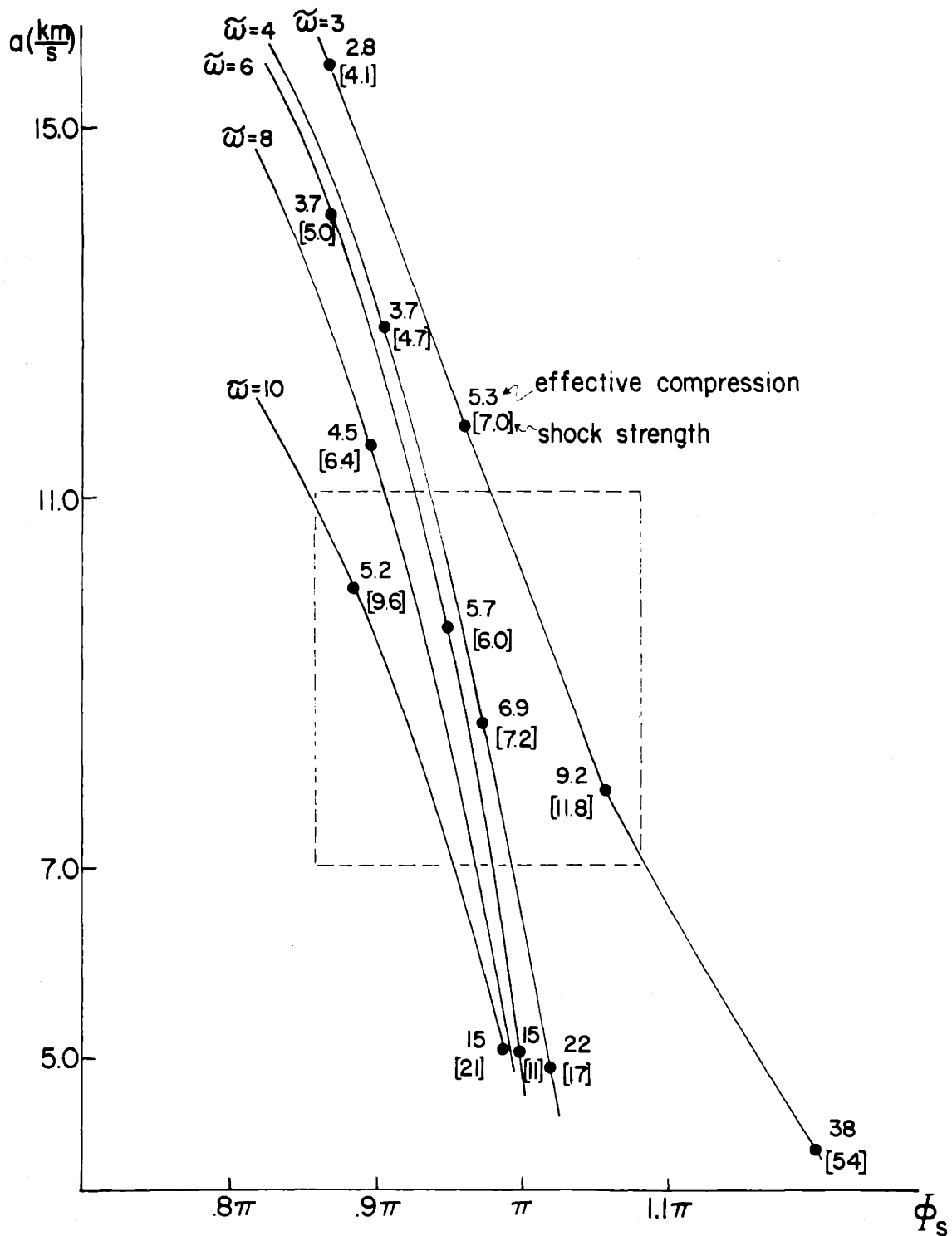


Figure (10.1)  
Families of STS Solutions at Various Radii in the Galactic Disk

A family of STS solutions, which are compatible with the parameters of the galactic disk at their respective radii, will now be chosen. Suppose we assume that a mean turbulent dispersion speed of about 10 km/s may be adopted for our solar neighborhood. In this case, the STS solution that is characteristic of our solar vicinity (at a radius of 10 kpc) is the one associated with the point of the 10 kpc curve where  $a = 10$  km/s. This particular STS solution possesses two shocks, each of which lies slightly in front of a potential minimum of the imposed field (i.e., one of these shocks lies at about  $\phi_S = .89\pi$  radians in Figure (10.1) ).

There are several possible ways to proceed with the selection of the STS solutions for all other radii in our Galaxy. First, it would be possible to select only those STS solutions which have a fixed shock phase,  $\phi_S$ , with respect to the imposed spiral field. In this case, the two-armed spiral shock pattern (which is hereafter referred to as the TASS pattern or the TASS picture)<sup>1</sup> exactly coincides with the equipotential curves of the imposed spiral pattern over the whole disk. This selected family of STS solutions forms a TASS pattern whose shock strength and effective compression decrease slightly from the 10 kpc region toward the 3-4 kpc region.

Alternatively, we might select a family of STS solutions which possess uniform turbulent dispersion speed over the galactic disk (instead of constancy of shock phase over the disk). In this case,

---

<sup>1</sup>The family of streamtube solutions which make up the TASS pattern (and picture) is a subset of the much larger family of STS solutions.



only those STS solutions, which correspond to points (of the various curves of Figure (10.1) ) that lie near a mean turbulent dispersion speed of 10 km/s,<sup>1</sup> are chosen. This alternative picture for the Galaxy possesses a TASS pattern that deviates somewhat from equipotential curves of the imposed spiral pattern. However, because of the narrowness of the range of shock phase variation (as indicated in Figure (10.1) ), the deviation between the TASS pattern and the imposed spiral pattern is very small. This possible TASS picture (with uniform turbulent dispersion speed) of the Galaxy therefore appears to be quite satisfactory also.

This alternative TASS picture for the Galaxy of nearly uniform turbulent dispersion speed except perhaps in the inner region of the disk exhibits some curious features. If the spiral shock pattern is followed inwards from 10 kpc, the shock strength decreases slightly until it reaches a minimum value somewhere in the vicinity of 6-7 kpc. As a spiral shock is followed further inwards from 6-7 kpc, the shock strength rises. Towards the 3-4 kpc region, the shock strength becomes large again.

Although the shock strength shows a slight dip in the 6-7 kpc region, the effective gaseous compression (  $\sigma(2)/\sigma_0$  ) rises monotonically with decreasing radius from 10 kpc to 3-4 kpc. It is likely that the effective gaseous compression rather than the shock strength has the more direct influence on possible star formation, since the

---

<sup>1</sup>Since a mean turbulent dispersion speed of 10 km/s is adopted for the solar neighborhood, such a uniform turbulent dispersion speed over the whole disk would also be 10 km/s.

effective gaseous compression is a measure of the actual maximum gaseous compression along a streamtube. It is the maximum value of gas density,  $\sigma(2)$ , that suggests the actual degree of gas cloud compression and possibly the relative amounts of star formation and H II concentrations at various radii. It is interesting in this respect that the effective gaseous compression at 3-4 kpc appears to be nearly twice its value at 10 kpc. Comparison of this theoretical behavior of the effective gaseous compression versus radius shows general agreement with observational evidence of the mean H II distribution plotted with respect to radius over the galactic disk between 3-4 kpc and 10 kpc.<sup>1</sup>

#### Outer Bound Cutoff of the TASS Pattern in the Galaxy

Calculations have been carried out over the galactic disk out to the outer bound of 12 kpc where the TASS pattern terminates. Evidence of this outer bound cutoff of the TASS pattern near 12 kpc may be seen in Figure (10.1). First of all, no 12 kpc curve in  $a - \phi_s$  space exists. In addition, the 10 kpc curve terminates at an upper bound for dispersion speed of about 12 km/s. Even the curves for streamtubes at 8 kpc and 6 kpc have upper bounds for dispersion speed of 15 km/s and 17 km/s respectively. Termination of these curves signifies a termination of the TASS pattern at these

---

<sup>1</sup>Agreement with observational evidence is further enhanced when the possible increase in turbulent dispersion speed toward the galactic center is taken into consideration (see Section 33 - Comparisons with observations).

values of the parameters and a lack of the TASS pattern for all values beyond. Since we are primarily interested in mean turbulent dispersion speeds in the range from about 7 km/s to 11 km/s, the cutoff in  $a - \phi_s$  space is not reached until gas streamtubes at larger radii than 10 kpc are considered. For a larger spiral field, the outer bound cutoff of the TASS pattern would lie at an even larger radius in the disk. For example, the outer bound cutoff of the TASS pattern for a 7.5% field lies at approximately 14 kpc.<sup>1</sup>

### TASS Pattern in our Galaxy

The overall TASS pattern superposed on the imposed spiral perturbation pattern of background matter is indicated in Figure (10.2). Streamlines which turn sharply at each shock are drawn for several typical radii. The total radial excursion of a given streamtube at a radius between 3-4 kpc and 10 kpc is generally less than 1/10 of the average streamtube radius from the galactic center. Each shock lies along and well within each imposed background spiral arm which gives rise to the imposed spiral field. The shock waves are actually located slightly inwards from the center axes of the imposed spiral arms of trailing type.<sup>2</sup> By the nature of these shocks, the highest gas

---

<sup>1</sup>Observational studies by M.S.Roberts (indicated in Section 2) provide observational evidence for an outer bound cutoff of the TASS pattern in many Sc-type galaxies. It is shown in Section 33 that the theoretical TASS picture with its outer bound cutoff is in good agreement with the observational studies of M.S.Roberts.

<sup>2</sup>A (leading) TASS picture in a spiral galaxy of leading type is considered in Sections 11 and 12.

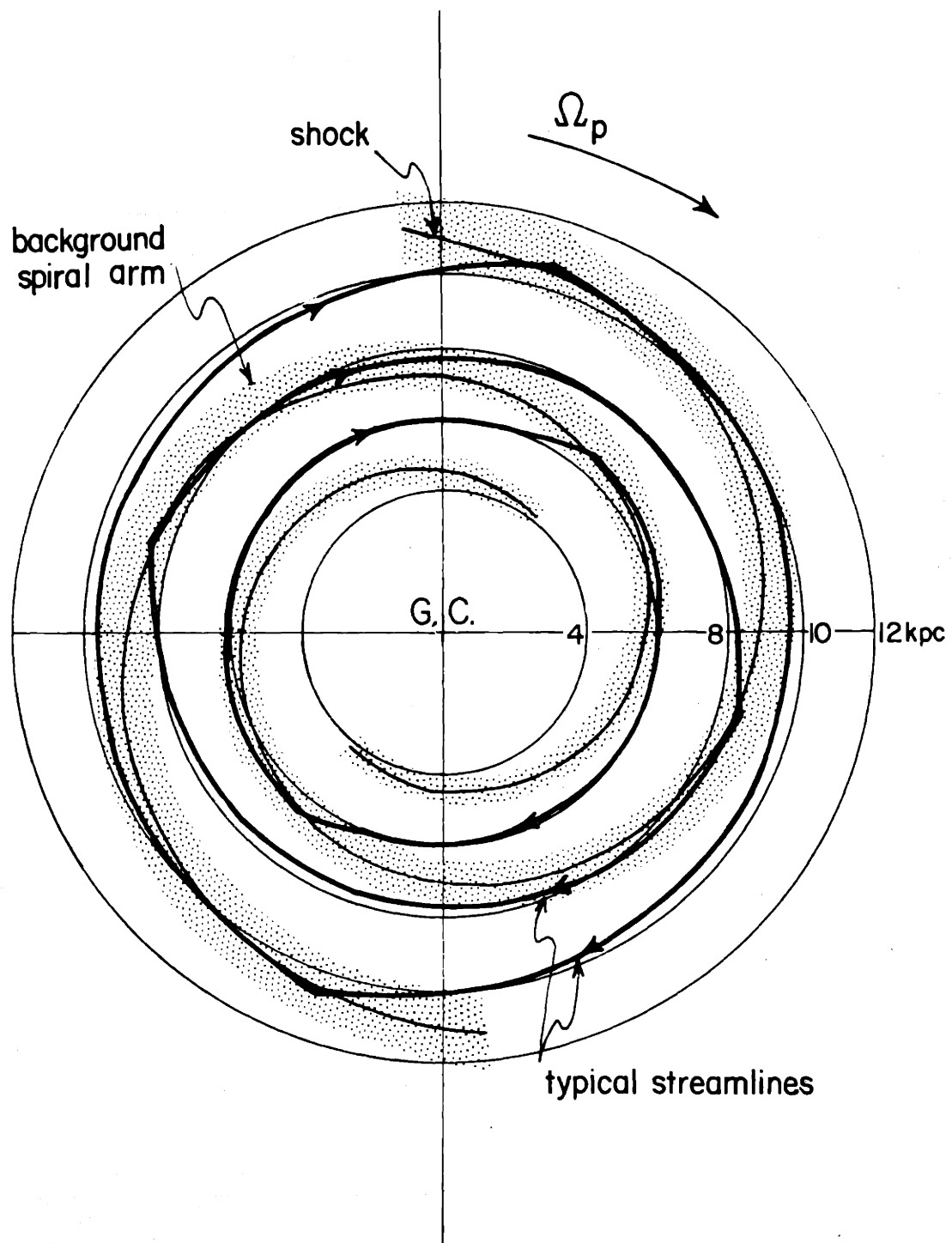


Figure (10.2)  
Shock and Background Spiral Pattern in the Galaxy

concentration in the disk occurs just directly outside the shock where the flow is subsonic. Consequently, the fundamental component of the induced potential field due to the gaseous arm is almost exactly in phase with the imposed background stellar arm, and the two fields enhance each other for the maintenance of the overall TASS pattern.

Figure (10.3) sketches the observable picture of the galactic disk as seen in observational studies. In this picture the imposed background stellar spiral arms are not sketched since they actually exhibit very little luminosity and are not seen in observational studies. What is seen in observational studies is the observable gaseous spiral arms that contain the newly-born stars and most luminous H II regions. The shocks lie on the inner edges of the observed gaseous spiral arms. Regions of most prominent star formation and most brilliant H II concentration occur in the observable gaseous spiral arms, extending from the shocks on the inner edges to approximately the centers of the gaseous arms.

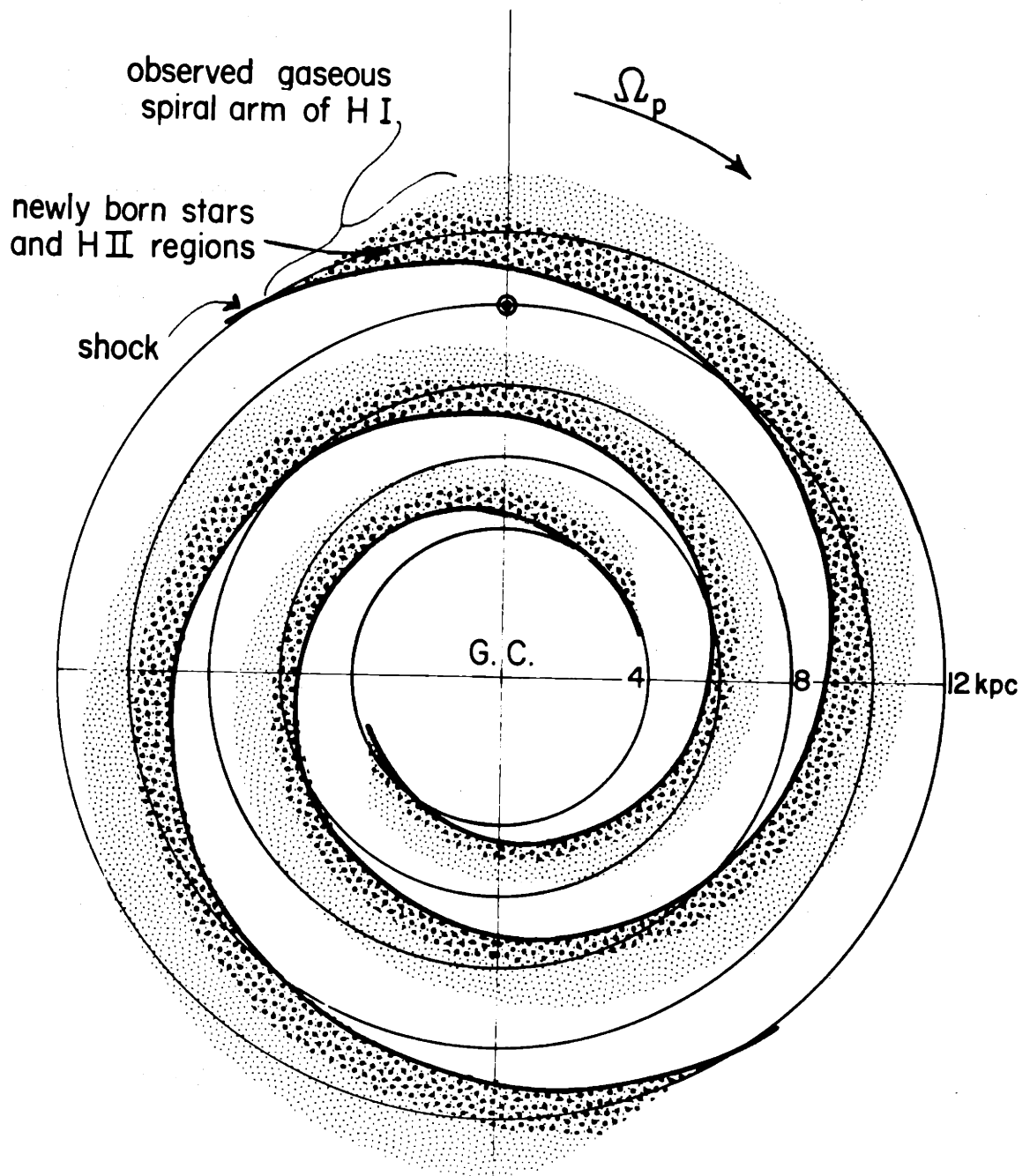


Figure (10.3)  
Spiral Pattern in the Galaxy

## Part II B. Gas Flow about a Spiral Galaxy of Leading Type

The problem of the existence and persistence of a TASS pattern over a spiral galaxy of trailing type is considered in Part II A. In fact, it is demonstrated that a TASS pattern of trailing type is compatible with the general nature of gas flow about a galactic disk made up of a two-armed spiral density wave pattern of background matter of trailing type superposed on the Schmidt model of the Milky Way System.

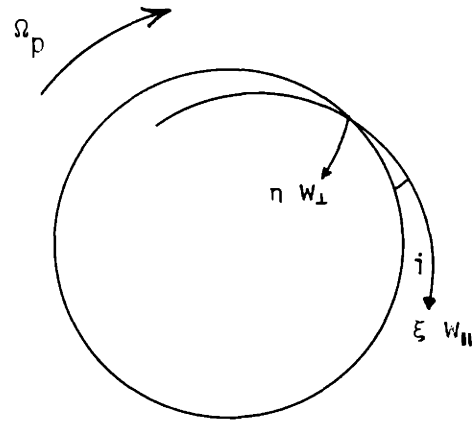
In Part II B, the problem of the existence and persistence of a TASS pattern over a spiral galaxy of leading type is investigated. We ask how greatly different is the picture of a spiral galaxy of leading type from the picture of a spiral galaxy of trailing type (in Part II A). Although the physics of the two situations is the same, we shall soon discover that the TASS pictures of leading and trailing type are quite different. For example, it is shown that the relative location of a shock, a gaseous spiral arm, and the regions of prominent star formation (and H II regions) inside the gaseous spiral arm of leading type in the TASS picture of Part II B is strikingly different from the relative location of these features in the TASS picture of a spiral galaxy of trailing type (in Part II A). An important implication of these results of the theoretical TASS picture for spiral galaxies of leading and trailing type is therefore suggested; namely, by observational studies of spiral galaxies and in particular

of their luminous regions of prominent star formation (and H II regions), it may be possible to distinguish spiral galaxies as leading or trailing type systems and to determine their sense of rotation as well.



11. Similarity of the gas dynamical equations for spiral galaxies of leading and trailing type

In this investigation of a spiral galaxy of leading type we make the same asymptotic approximation that is made in the investigation of a spiral galaxy of trailing type (in Part II A). In this asymptotic approximation the perturbation quantities are assumed to vary more rapidly in the direction normal to the equipotential curves than in the direction parallel to the equipotential curves of the spiral pattern. Verification of this asymptotic approximation is given in Appendix II. The final form of the asymptotic gas dynamical equations for a spiral galaxy of leading type may be written as:



$$\frac{\partial w_{\perp}}{\partial \eta} = [+] \frac{(w_{\perp 0} + w_{\perp}) (2\Omega w_{\parallel} + [-]f - \chi_2) + a^2 \left(1 + \frac{\omega}{\sigma_0 + \sigma_1} \frac{d\sigma_0}{d\omega}\right) \chi_1}{a^2 - (w_{\perp 0} + w_{\perp})^2} \quad (11.1)$$

$$\frac{\partial w_{\parallel}}{\partial \eta} = [+] \frac{\left(\frac{K^2}{2\Omega}\right) \omega w_{\perp} + \chi_3}{w_{\perp 0} + w_{\perp}} \quad (11.2)$$

where the various symbols denote the same physical quantities as for the spiral galaxy of trailing type, but with the velocity directions indicated in the diagram on the preceding page for the spiral galaxy of leading type. The quantities,  $\chi_1$ ,  $\chi_2$ , and  $\chi_3$ , are given by equations (5.6), (5.7), and (5.8); and

$$f = A \sin\left(\frac{2}{\sin i} n + \phi\right)$$

Once the above two equations, (11.1) and (11.2), are solved for  $w_{\perp}$  and  $w_{\parallel}$ , the following equation may be solved for the perturbation gas density,  $\sigma_1$ :

$$(w_{\perp 0} + w_{\perp}) \frac{\partial \sigma_1}{\partial n} + (\sigma_0 + \sigma_1) \frac{\partial w_{\perp}}{\partial n} + [-](\sigma_0 + \sigma_1 + \omega \frac{d\sigma_0}{d\omega}) \chi_1 = 0 \quad (11.3)$$

The following equation may be solved to yield the position,  $\xi$ , along the gas streamtube about the disk:

$$\frac{\partial \xi}{\partial n} = \frac{w_{\parallel 0} + w_{\parallel}}{w_{\perp 0} + w_{\perp}} \quad (11.4)$$

The only differences between this above set of equations, (11.1), (11.2), (11.3), and (11.4), for a spiral galaxy of leading type and the set of equations, (5.10), (5.11), (5.12), and (5.13), for a spiral galaxy of trailing type are simply a few sign changes indicated in the brackets, [ ], above.

These gas flow equations for a spiral galaxy of leading type have been derived from the basic set of equations, (4.1), (4.2), and (4.3). However it is a relatively simple matter to derive the equations for a spiral galaxy of leading type, (11.1) - (11.4), from the equations for a spiral galaxy of trailing type, (5.10) - (5.13), by a transformation between the trailing and leading type pictures that involves no more than sign changes of the variables. We now consider a transformation between the trailing (tr) and leading (ld) pictures that involves a sign reversal of all velocity components and all spatial coordinates:

$$w_{\perp tr} \rightarrow -w_{\perp ld} \quad w_{\parallel tr} \rightarrow -w_{\parallel ld} \quad a_{tr} \rightarrow -a_{ld}$$

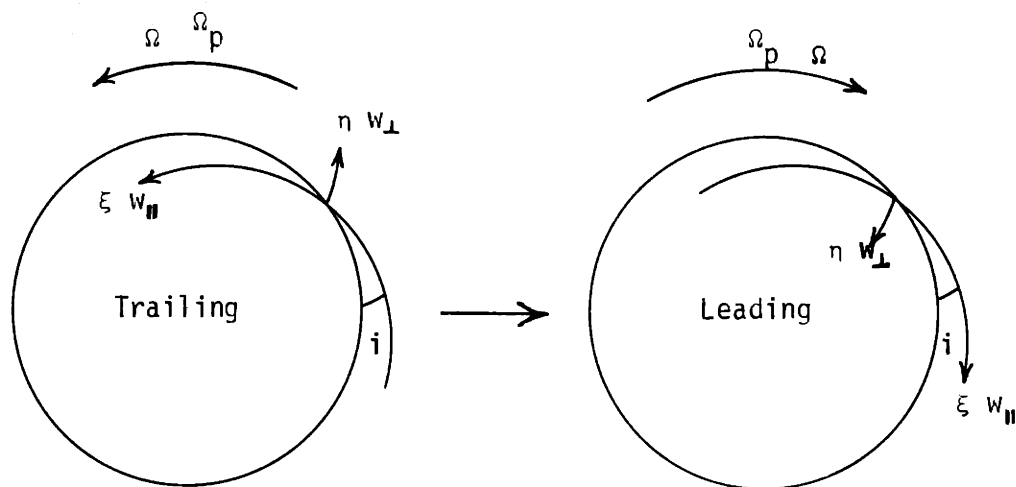
$$\Omega_p tr \rightarrow -\Omega_p ld \quad \Omega_{tr} \rightarrow -\Omega_{ld} \quad K_{tr} \rightarrow -K_{ld}$$

$$\eta_{tr} \rightarrow -\eta_{ld} \quad \xi_{tr} \rightarrow -\xi_{ld} \quad \sigma_{tr} \rightarrow \sigma_{ld}$$

$$x_{1tr} \rightarrow -x_{1ld} \quad x_{2tr} \rightarrow x_{2ld} \quad x_{3tr} \rightarrow x_{3ld}$$

$$f_{tr} \rightarrow -f_{ld} \quad \phi_{tr} \rightarrow -\phi_{ld}$$

This transformation may be represented in diagrammetrical form as:



Therefore, the above variable transformation takes us from the gas flow picture of a spiral galaxy of trailing type to the gas flow picture of a spiral galaxy of leading type.

12. Physical picture for the gaseous disk of a spiral galaxy of leading type

Suppose we adopt the Schmidt model of the Milky Way System as the basic equilibrium state in our theoretical picture. In addition, suppose we adopt values of the basic independent parameters,  $i$ ,  $\Omega_p$ ,  $\pi$ ,  $a$ , and  $A$ , that are adopted for the typical STS solution considered in Part II A (i.e.,  $\tan i = 1/7$ ,  $\Omega_p = 12.5 \text{ km/s/kpc}$ ,  $\pi = 10 \text{ kpc}$ ,  $a = 10 \text{ km/s}$ ,  $A = 5\%$ ). Under these circumstances, we may determine an STS solution at a typical radius in the gaseous disk of a spiral galaxy of leading type and compare it with the corresponding STS solution in the gaseous disk of a spiral galaxy of trailing type.

A Typical STS Solution

The STS solution for the spiral galaxy of leading type which corresponds to this above set of values for the parameters is sketched in  $w_{\perp}'$ - $w_{\parallel}'$  space in Figure (12.1). The corresponding STS solution for a spiral galaxy of trailing type is also sketched. The symmetry of the two curves of leading and trailing type is apparent as expected. One is nearly the exact mirror image of the other reflected through the  $w_{\perp}'$  axis. This symmetry between STS solution curves of leading and trailing type is a feature which is in general present for any set of values of the basic independent parameters. Figure (12.2) illustrates

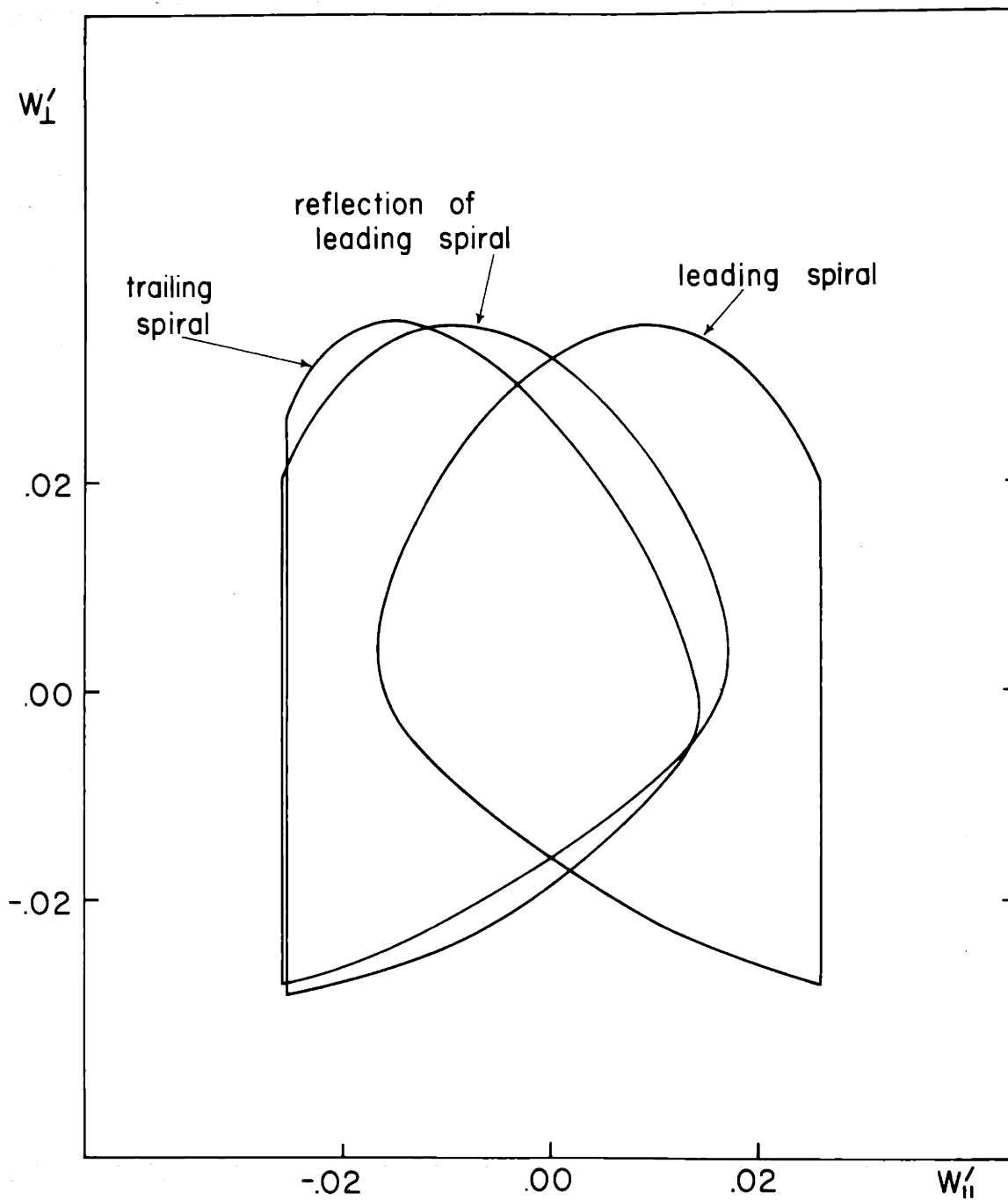


Figure (I2.1)  
 An STS Solution of Leading and Trailing Type

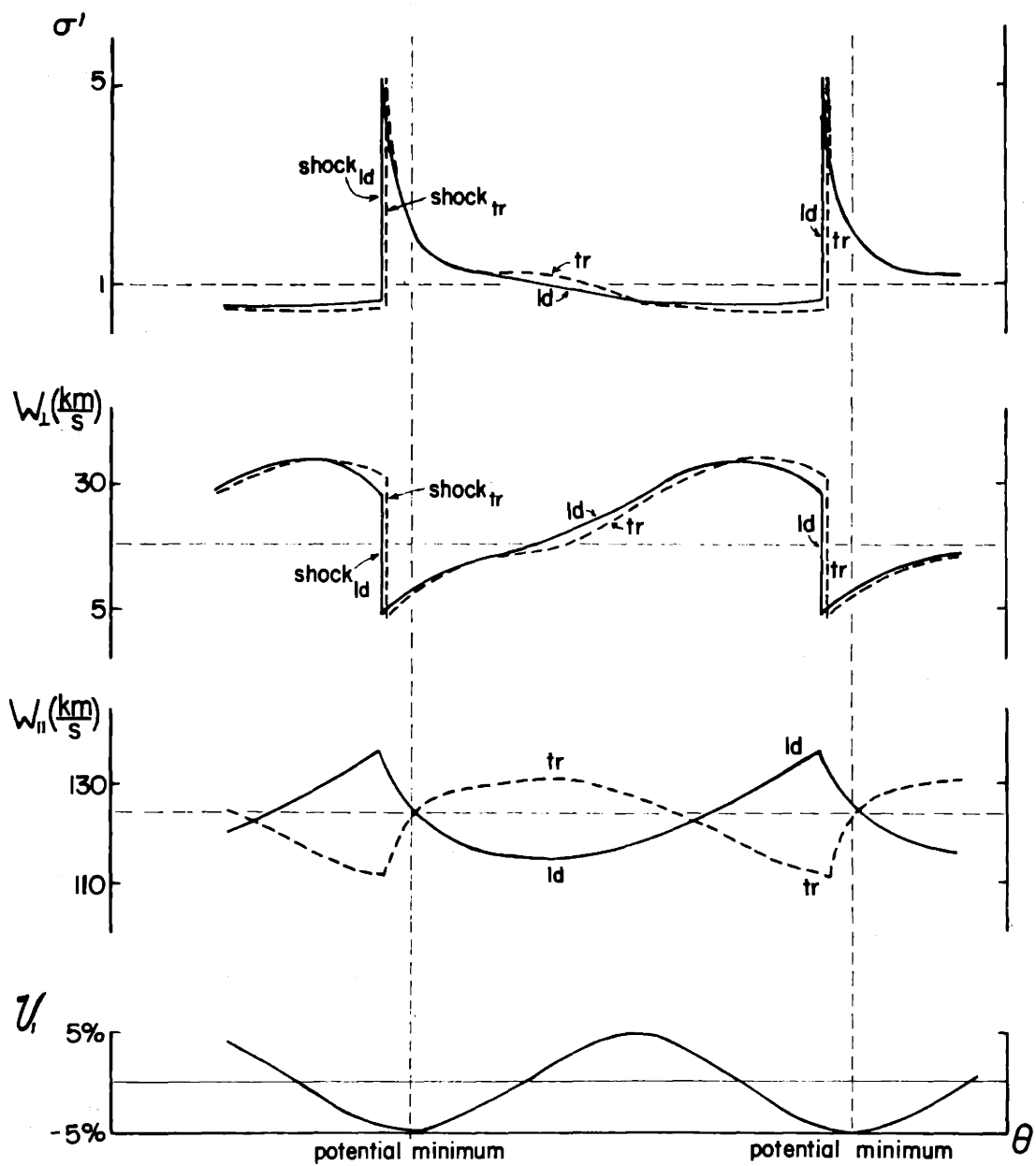


Figure (I2.2)  
 A Typical STS Solution of Leading and Trailing Type

the nature of the gas density,  $\sigma'$ , and the velocity components perpendicular and parallel to the spiral equipotential curves of the imposed spiral pattern for this STS solution in spiral galaxies of leading and trailing type. The symmetry of the two cases is again very striking.<sup>1</sup>

### TASS Pattern of Leading Type

Numerical calculations between the radii of 3-4 kpc and 12 kpc in the Schmidt model have confirmed that a TASS pattern of leading type is indeed compatible with the general nature of gas flow about the galactic disk of leading type. In this TASS picture of leading type, a shock occurs near the density maximum of an imposed spiral arm of background matter (of moderately-old stars) but is shifted slightly on the outer side of the imposed spiral arm. The reverse is true for a spiral galaxy of trailing type in which a shock occurs near the density maximum of the imposed spiral arm of background matter but is shifted slightly on the inner side of the imposed spiral arm. Figure (12.3) (to be compared with Figure (10.2) for a spiral galaxy of trailing type) illustrates the TASS pattern in a spiral galaxy of leading type and demonstrates that the shock occurs well within and actually on the outer side of the imposed background spiral arm.

---

<sup>1</sup>Because of this symmetry (which is characteristic of an STS solution for any set of parametric values), the numerical calculations for the picture of a spiral galaxy of trailing type in Part II A can be applied to the spiral galactic model of leading type as well.



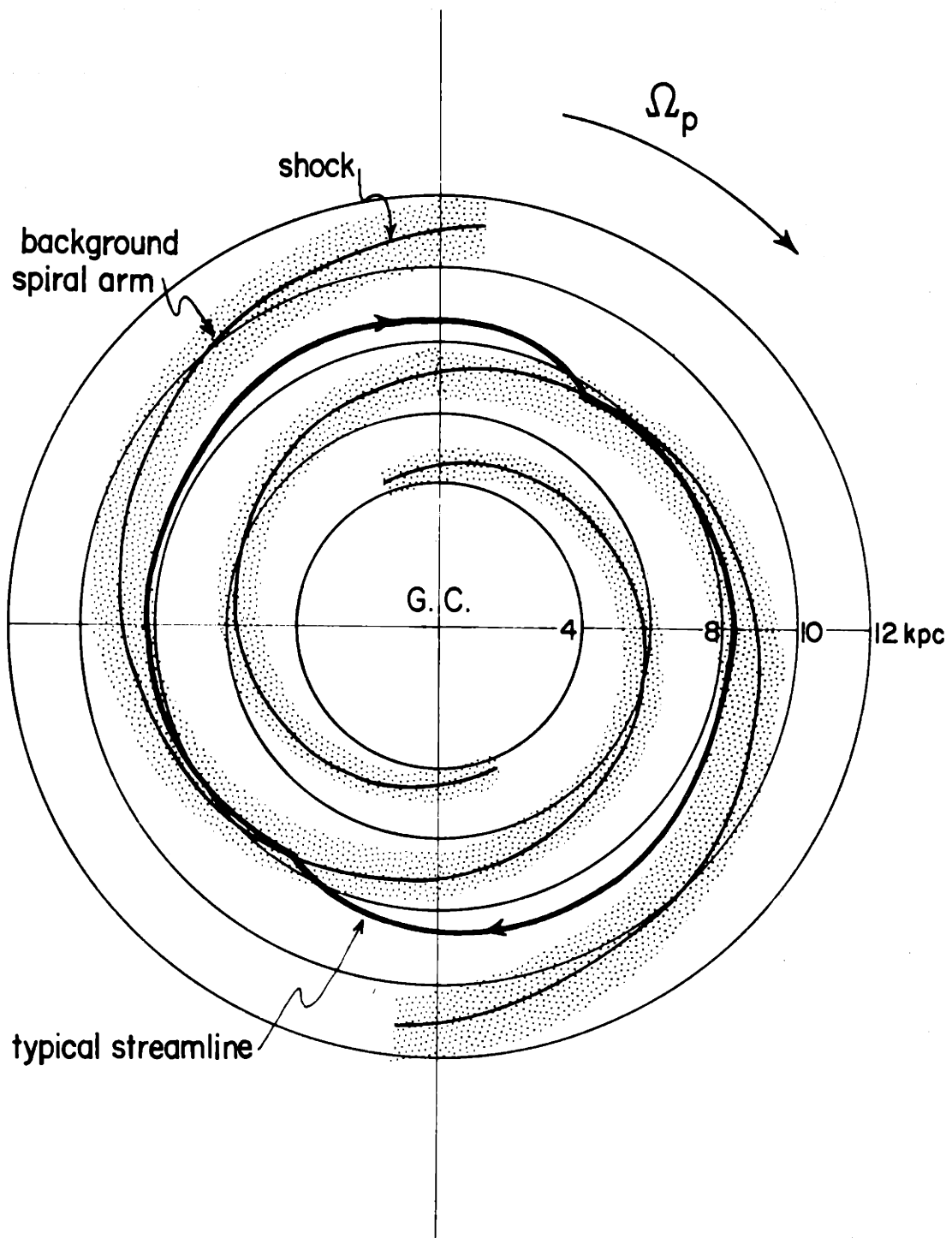


Figure (12.3)  
 Shock and Background Spiral Pattern  
 in a Galaxy of Leading Type

Since the gas flow across a shock of leading type has an inwards radial motion, the regions of largest gaseous concentration occur inside the shock. Therefore, the shocks of a spiral galaxy of leading type lie on the outer edge of the observed gaseous spiral arms, whereas the shocks of a spiral galaxy of trailing type lie on the inner edge of the observed gaseous spiral arms. Figure (12.4) (to be compared with Figure (10.3) for a spiral galaxy of trailing type) provides an observable physical picture of a spiral galaxy of leading type. In this picture, the regions of prominent star formation and the brilliant H II regions lie on the outer side of an observed gaseous (H I) spiral arm of leading type, and each shock lies at the common outer edge of all these spirals of H I, H II, and most prominent star formation.

A shift in the position of shocks, of regions of most prominent star formation, and of most luminous H II regions therefore exists between the outer and inner edges of the observed gaseous spiral arms in spiral galaxies of leading and trailing type respectively. By observational studies of spiral galaxies (and in particular of the locations of the most luminous regions with respect to the observed spiral arms of the galaxies), it may be possible to distinguish spiral galaxies as leading or trailing type systems and to determine their sense of rotation as well, according to the locations of the regions of most prominent star formation and most luminous and brilliant H II regions on the outer or inner edges of the observed gaseous spiral arms.

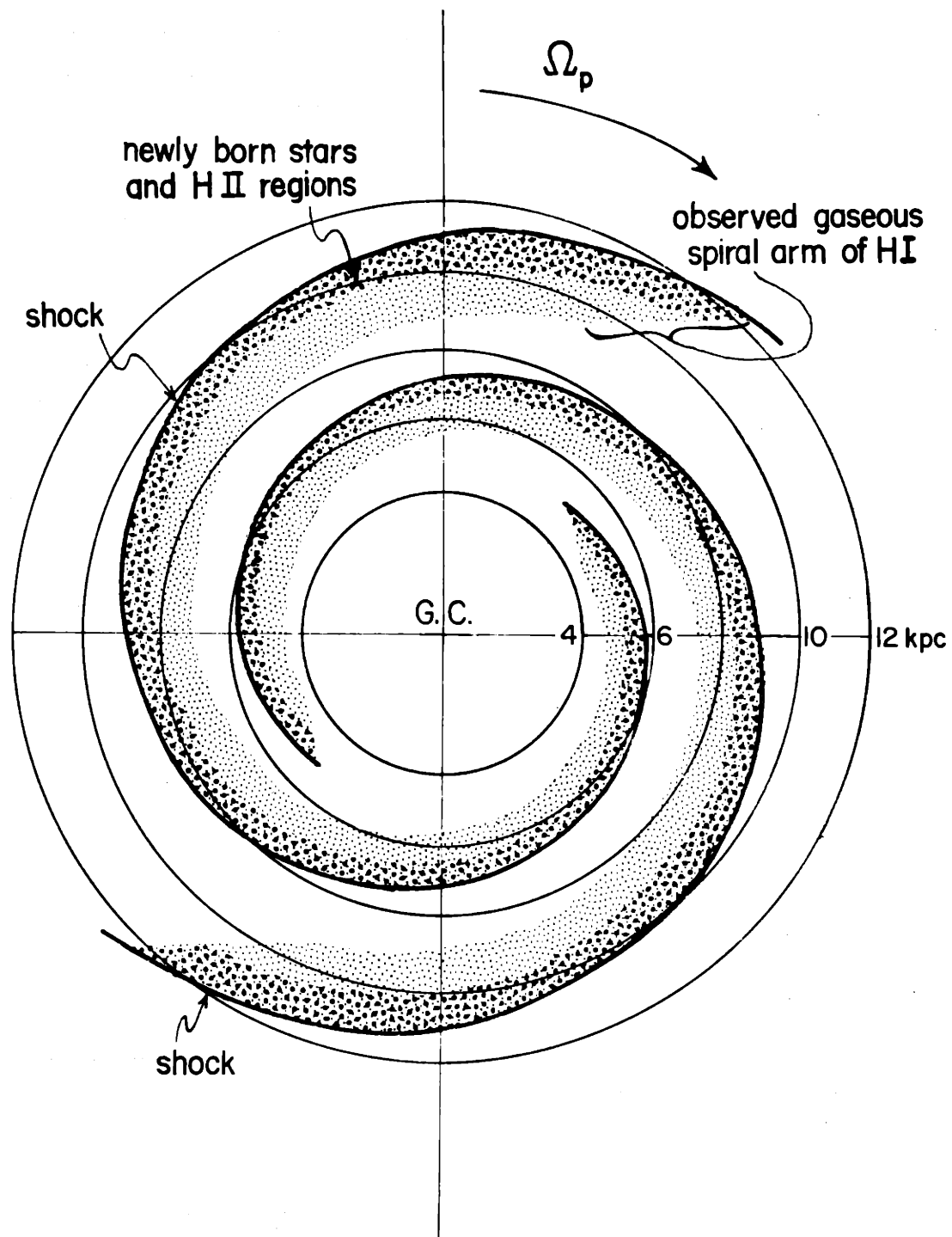


Figure (12.4)  
Spiral Pattern in a Galaxy of Leading Type

## Part II C. Resonance and the "Three Kpc Arm"

The motion and distribution of interstellar gas near the central region of our Galaxy is as intriguing to the theoretician as to the observationalist. It is known that a continuous gaseous arm is present in the velocity profile of the 3 kpc neighborhood of our Galaxy. J.H. Oort (1965) points out that for a spiral arm it is exceptionally homogeneous over its whole arc length of some  $23^\circ$  in longitude and that the variation of its mean velocity with longitude is remarkably smooth. A most curious feature is the arm's apparent high radial velocity of about 53 km/s/kpc away from the galactic center. In addition to this "3 kpc arm" which lies between the galactic center and the solar neighborhood, another spiral arm of similar arc length lies at roughly the same radius on the opposite side of the galactic center.

In Part II C, it is shown that shock formation together with resonance in the 3 kpc neighborhood of the galactic disk may play an important role in this "3 kpc arm" phenomenon. In Section 13, resonance in the inner portion of the Galaxy is investigated. An exciting feature is found in the theoretical shock picture in Section 14; namely, it is shown that a gaseous free mode is possible in the 3 kpc region even without the presence of a sustaining spiral pattern of background matter. Some features of the "3 kpc arm" are apparent in this free mode. In Section 15, the effects of forcing on the free mode are considered.

### 13. Nature of linear and nonlinear resonance

We now direct our attention to resonance, a phenomenon which is present in the 3-4 kpc region of the disk of our Galaxy. Resonance in the nonlinear TASS picture has the same basic characteristics as resonance in the linear density wave theory. However, unlike linear resonance, nonlinear resonance manifests itself in the gaseous component as well as the stellar component of the galactic disk.

#### Resonance in the Linear Density Wave Theory

In the linear density wave theory, resonance is sustained by the stellar component alone. When a star rotates about a disk-shaped galaxy at an angular speed,  $\Omega(\varpi)$ , such that the difference between the angular speed and the wave pattern speed,  $\Omega_p$ , is equal to some submultiple of the epicyclic frequency of the star,  $K(\varpi)$ , then the star may be said to be in resonance with the wave pattern. This type of resonance has come to be known as Lindblad resonance. Any given equipotential curve of the wave pattern repeatedly meets such a "resonant" star at the same phase of its epicyclic oscillation.

The gravitational fields of the wave pattern and a star constitute the mechanism for transferring energy between the wave pattern and the star. When a star moves against the direction of attraction of the pattern's gravitational field, the star loses energy to the wave pattern. Energy is gained by the star from the wave pattern when the

star moves in the direction of attraction of the pattern's gravitational field.

Nearly exact Lindblad resonance is realized over a circular band in the 3-4 kpc neighborhood of the galactic disk. The tendency toward resonance in the presence of both the gaseous and the stellar components in the linear density wave picture is discernible from the Lin-Shu dispersion relationship:

$$k_{L-S} = \frac{\kappa^2 (1 - v^2)}{2\pi G [\sigma_g F_v(x_g) + \sigma_* \mathcal{F}_v(x)]}$$

where

$$v = \frac{m (\Omega_p - \Omega)}{\kappa}, \quad m \text{ is an integer}$$

$F_v(x_g)$  is the gaseous reduction factor

$\mathcal{F}_v(x)$  is the stellar reduction factor

In the limit as  $|v| \rightarrow 1$ , the various functions of  $v$  appearing in the dispersion relationship exhibit the following behavior close to resonance:

$$F_v(x_g) \rightarrow (1 - v^2)^2$$

$$\mathcal{F}_v(x) \rightarrow (1 - v^2)^{3/2}$$

$$k_{L-S} \rightarrow (1 - v^2)^{-1/2}$$

If Lindblad resonance occurs in the presence of both gaseous and stellar components, a limit of the spiral density wave pattern toward shorter and shorter wavelength exists:

$$\lambda_{L-S} \rightarrow (1 - v^2)^{1/2}$$

It is indeed the stellar component in the linear theory that sustains resonance in the 3-4 kpc neighborhood (where  $|v| = 1$ ) and provides for the short wavelength limit in this neighborhood.

A galaxy of stars alone without any gaseous component would exhibit resonance in the same manner as the galaxy which contains both gas and stars since the limit toward shorter and shorter wavelength is provided with or without gas (in the linear theory). Whereas density perturbations increase in magnitude in the limit toward resonance (i.e.,  $|v| = 1$ ), the radial and circumferential perturbation velocity components remain small and exhibit no tendency toward larger amplitudes in the resonance limit. Therefore, linear resonance is characterized not by large amplitudes of the perturbation velocities but rather by a shift toward shorter and shorter wavelength of the spiral density wave pattern in the 3-4 kpc neighborhood.

Lin and Shu (1966) have shown that the linear theory for a galaxy of gas alone and for a galaxy of stars alone yield quite similar results except in the vicinity of  $|v| = 1$ . For a gaseous galactic model without any stellar component, the Lin-Shu dispersion relationship may be solved for  $\lambda_{L-S}$  explicitly:

$$\frac{\lambda_{L-S}}{\lambda_0} = \frac{1}{2} \frac{1}{1 \pm v}$$

Of the two branches of the solution for  $\lambda_{L-S}$ , the shorter wavelength branch corresponds more closely than the longer wavelength branch to the corresponding  $\lambda_{L-S}$  solution for a galaxy which contains stars and no gas. In the limit as  $|v| \rightarrow 1$ , the shorter wavelength branch approaches the finite limit:

$$\lambda_{L-S} = \frac{\lambda_0}{4}$$

Therefore, unlike the linear stellar theory where  $\lambda_{L-S} \rightarrow 0$ , in the linear gaseous theory,  $\lambda_{L-S}$  remains finite. The gaseous density and the radial and circumferential perturbation velocity components all remain of small magnitudes in this limit as  $|v| \rightarrow 1$ . Hence, in the linear theory, no resonance appears for a galaxy which contains only a gaseous component. It is indeed the pressure due to gaseous turbulence that tends to disperse all organized gaseous motion and tends to suppress resonance.



### Resonance in the Nonlinear TASS Picture

The above linear density wave picture portrays the nature of linear resonance in disk-shaped galaxies containing gas alone, stars alone, and gas and stars together. In similarity to linear resonance which cannot be exact, exact nonlinear resonance cannot be realized because of the effect of the radial excursion of the material particles (gas and stars) in their oval (noncircular) streamtubes about the disk.

The nonlinear TASS picture provides for resonance in a little different fashion from the linear theory. In contrast to the linear theory of a gaseous galactic disk in which no resonance is possible, gaseous resonance in the nonlinear TASS picture manifests itself in the form of a free spiral mode which is sustained without the influence of a stellar component and without any imposed spiral field due to the stellar component. In further contrast to the linear theory where the limit to shorter and shorter wavelength of the spiral density wave pattern is necessary for the realization of Lindblad resonance, in the nonlinear TASS picture the gaseous free mode requires no such limit of wavelength. We now direct our attention toward the 3 kpc region of the TASS picture of the Galaxy in an effort to view this "resonant" gaseous free mode.

#### 14. Free spiral mode

We now consider the possibility of an STS free mode at various radii in the Schmidt model of the Galaxy. In Section 9, we investigated the limits of decreasing shock strength and decreasing field for an STS forced mode solution and demonstrated that below a given lower bound of spiral field (which is a function of radius) no STS solution is in general possible.<sup>1</sup> For zero field, a free mode may exist; but its periodicity may be necessarily greater than two (i.e.,  $\Delta\theta < \pi$ ).

Figure (14.1) illustrates some curves in "a- $\Delta\theta$  parameter" space for the family of possible free modes (of arbitrary periodicity) at various radii,  $\varpi$ , in the Schmidt model. A free mode is associated with each point of every curve; however, an STS free mode is possible only when the periodicity is two (i.e., at  $\Delta\theta = \pi$  radians). For reasonable values of the gaseous turbulent dispersion speed in the galactic disk (i.e.,  $a = 4-5$  km/s), it is apparent that only in the 3 kpc neighborhood and interior to the 3 kpc neighborhood of the disk is an STS free mode possible (see Figure (14.1)). In the 3-4 kpc neighborhood, if  $\tan i$  is decreased to 1/14 (corresponding to more tightly wound spirals), an STS free mode may exist in the presence of as large a

---

<sup>1</sup>In Section 14, we demonstrate what is indicated in Section 9; namely, an STS free mode is not possible in the Schmidt model between the radii of 3-4 kpc and 12 kpc for typical values of the dispersion speed (as a function of the radius).

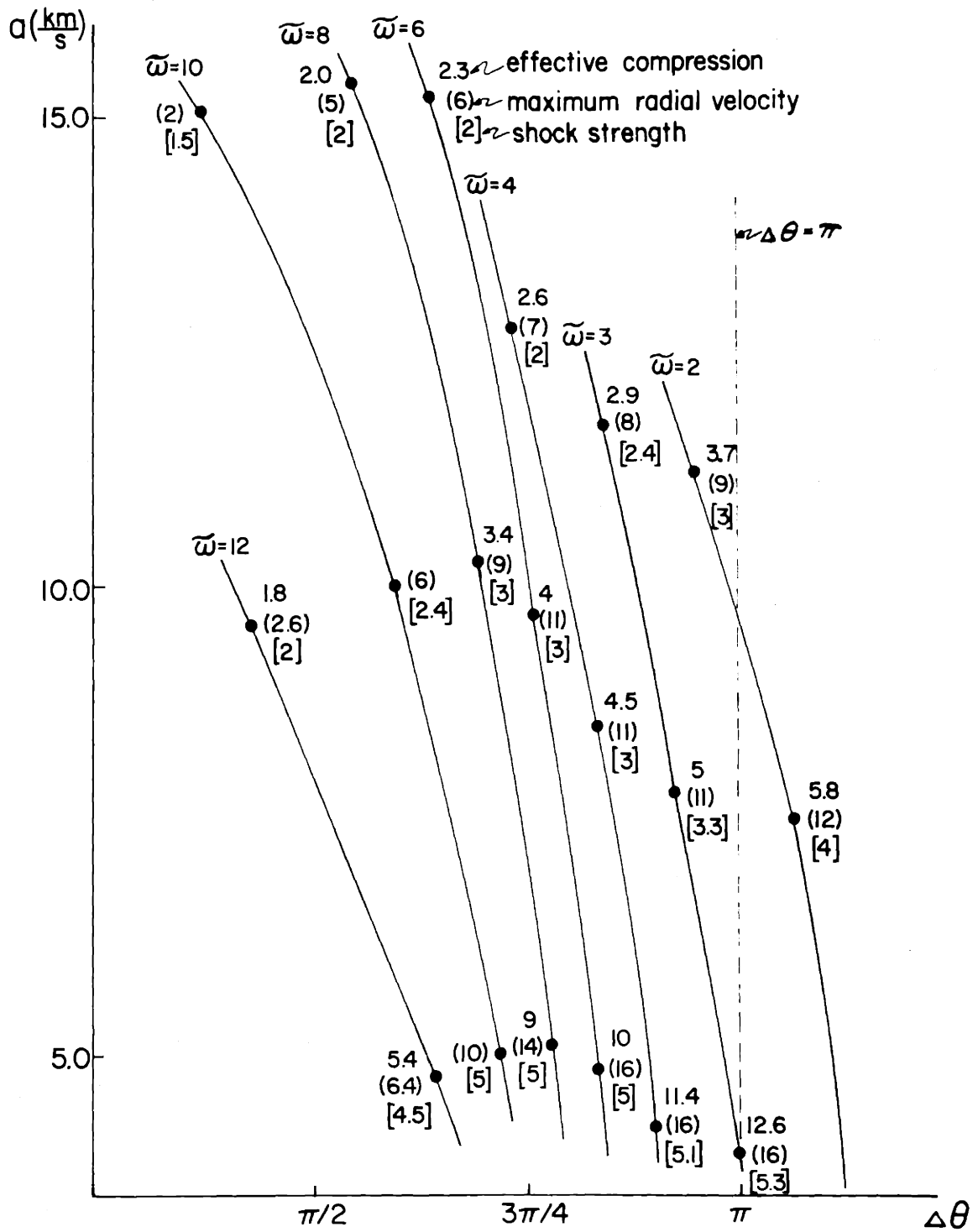


Figure (14.1)  
Families of Possible Free Modes over the Galactic Disk

gaseous turbulent dispersion speed as 5-10 km/s.

It is exciting that the STS free mode, which is apparently sustained entirely by resonance, can in fact exist. Such a self-sustained gaseous STS free mode provides a direct indication of non-linear resonance in the 3 kpc neighborhood of the galactic disk. Since no background spiral pattern of leading or trailing type is necessary for the support of the gaseous STS free mode, the leading or trailing nature of the STS free mode is not necessarily predetermined by any imposed background spiral pattern. Therefore, an STS free mode of both leading type and trailing type is possible.

#### STS Free Mode of Trailing and Leading Type

Figure (14.2) provides a picture of the "resonant" STS free mode of trailing type in the 3 kpc neighborhood of the galactic disk. The radial velocity along the streamtube is large and positive over two short arcs lying directly across the galactic center from one another. These regions of large positive radial velocity (of about 16-20 km/s) coincide with the least dense regions along the streamtube of this STS free mode of trailing type. Just before the gas reaches a shock of trailing type, the gas density is low and the radial velocity is outwards; whereas just after passage through the shock, the gas density is high and the radial velocity is inwards.

A "resonant" free mode of leading type is illustrated in the 3 kpc neighborhood of the galactic disk in Figure (14.3). The streamtube radial velocity is large and positive over two short streamtube arcs lying directly across the galactic center from one another. These

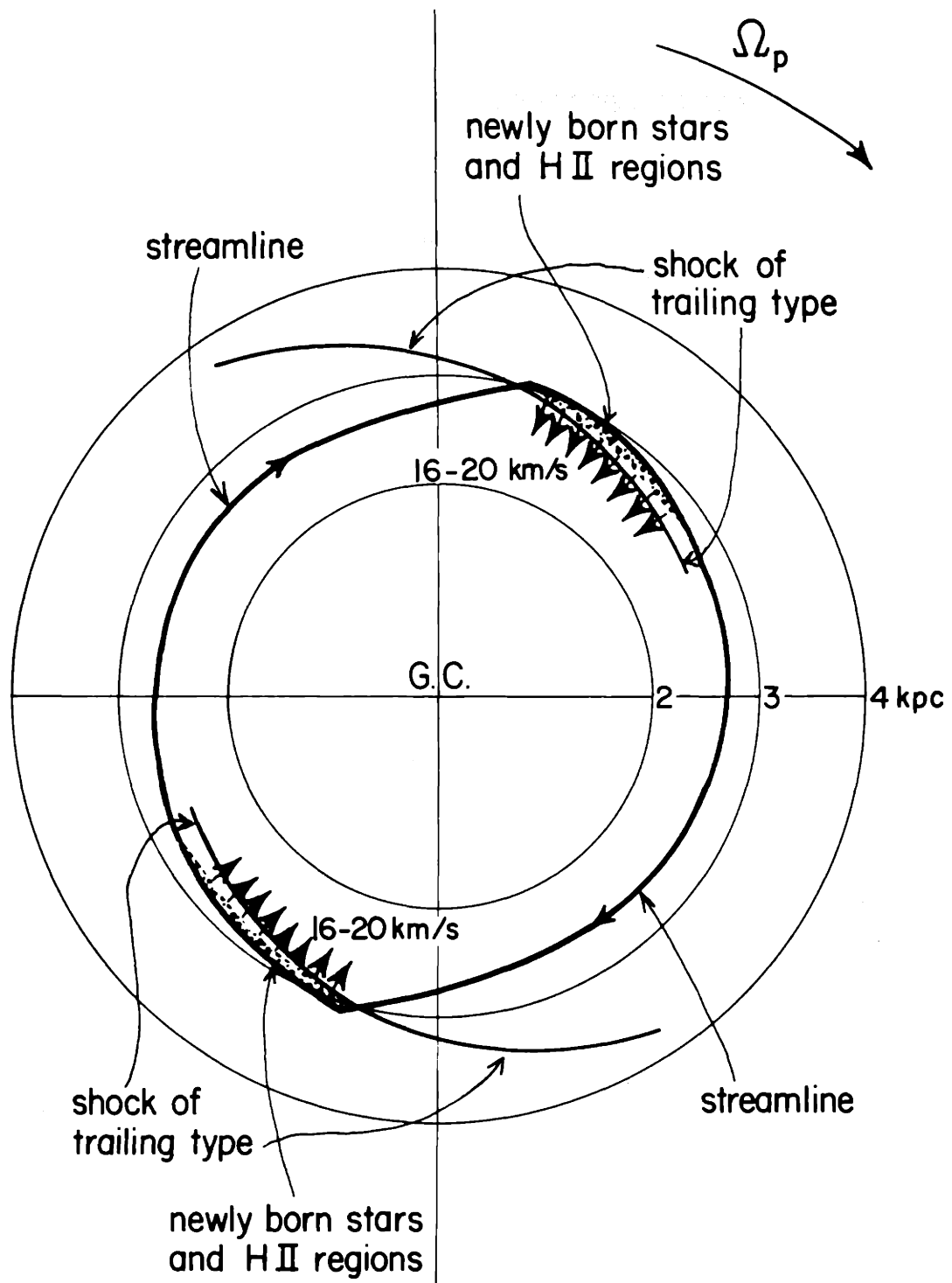


Figure (14.2)  
 The Free Mode of Trailing Type in the 3 Kpc Neighborhood

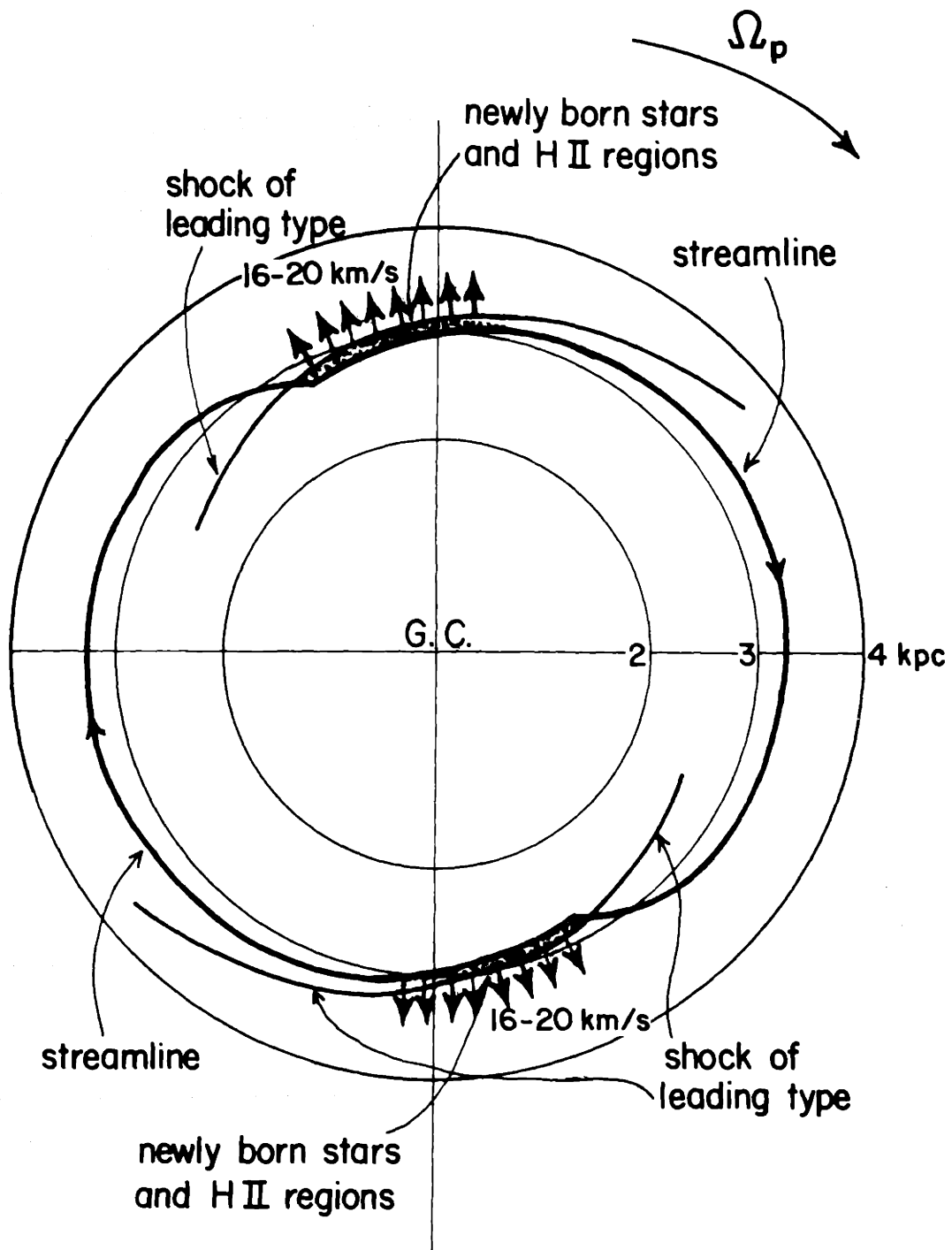


Figure (14.3)

The Free Mode of Leading Type in the 3 Kpc Neighborhood

regions of large positive radial velocity (of about 16 to 20 km/s) coincide with the most dense regions along the streamtube of this STS free mode of leading type. Just before the gas reaches a shock of leading type, the gas density is low and the radial velocity is inwards, whereas just after passage through the shock, the gas density is high and the radial velocity is outwards.

It is a very curious coincidence that in both theoretical STS free mode pictures regions of large positive radial velocity occur only in two relatively short arcs which have lengths similar to the length of the "3 kpc arm" of observational studies and which are located at the same radius on opposite sides of the galactic center from one another. In fact, the regions of positive radial velocity occur only over short arc segments which lie directly in front of and directly behind the shock.

In the STS free mode picture of trailing type the least dense regions move radially outwards, while the most dense regions move radially inwards. On the other hand, in the STS free mode picture of leading type, the most dense regions move radially outwards, while the least dense regions move radially inwards. This latter picture for an STS free mode of leading type better accounts for the "3 kpc arm" in the Galaxy which is apparently undergoing rapid radial expansion away from the galactic center toward the solar neighborhood. On the other hand, if the "3 kpc arm" of observational studies were actually located on the far side of the galactic center from the solar neighborhood, the STS free mode of trailing type would better account for its rapid inwards expansion toward the galactic center (and toward the solar neighborhood).

## 15. Forced spiral mode

Having investigated the STS free mode phenomenon which is apparently sustained by resonance alone, we now direct our attention to a situation in which a perturbation gravitational field is superposed on the STS free mode in the 3 kpc region of the galactic disk.<sup>1</sup> We ask if the response to this combined effort of resonance and the perturbation field may well simulate the "3 kpc arm" phenomenon of observational studies.

The excitation of an STS free mode under a perturbation gravitational field cannot result in an infinite response primarily because of the effects of large nonlinear velocity variation and of the radial excursion of the streamtubes away from exact resonance. However, such excitation may be large, and the question is how large might it be when both resonance and the perturbation field complement the efforts of one another. Section 10 demonstrates that a spiral field with a magnitude of 5% of the symmetrical field can give rise to STS

---

<sup>1</sup>These calculations in which a spiral field is superposed in the 3 kpc neighborhood of the Schmidt model are of general exploratory character since no such spiral background pattern and therefore no imposed spiral field is possible in this region of the galactic disk according to the linear density wave theory. However, in the nonlinear theory, the gaseous component organizes itself into a free mode and maintains galactic shocks in the 3 kpc region of the TASS picture without the presence of a sustaining field. This nonlinear organization of the gaseous free mode signifies as well the organization of an induced gravitational field due to the gas alone, however this induced field due to the gas can be at most of the order of only a few percent of the symmetrical field.



solutions in the 3 kpc region with shock strengths as large as 50 and with radial velocities as large as 20 km/s over two short arc lengths of the streamtubes. These quantities are considerably larger than the corresponding quantities in the solar neighborhood.

Even larger excitation and response may be possible in the presence of a greater field. Therefore, in addition to the calculations for zero and 5% field, numerical calculations have been carried out for STS solutions in the 3 kpc neighborhood under fields with magnitudes of 10% and 15% of the symmetrical field. Figure (15.1) provides a sketch of the three parametric curves (in  $a - \phi_s$  space) of the families of STS solutions in the 3 kpc neighborhood which correspond to the three imposed fields of 5%, 10%, and 15% of the symmetrical field. An STS solution is associated with each point of every parametric curve. The degree of excitation and response in the presence of these fields is suggested by the effective gaseous compression, the maximum radial velocity along a streamtube, and the shock strength, all of which are indicated at various points along the curves.

For a given field, the effective gaseous compression, the maximum radial velocity, and the shock strength all decrease with increasing turbulent dispersion speed. This behavior indicates that the pressure due to gaseous turbulence tends to disperse all organized gaseous motion as well as weaken the galactic shocks. On the other hand, as the field increases, the effective gaseous compression, the maximum radial velocity, and the shock strength all increase as well. This behavior, therefore, indicates that the shock pattern is strengthened by the imposed spiral field. An effective gaseous compression of about 65,

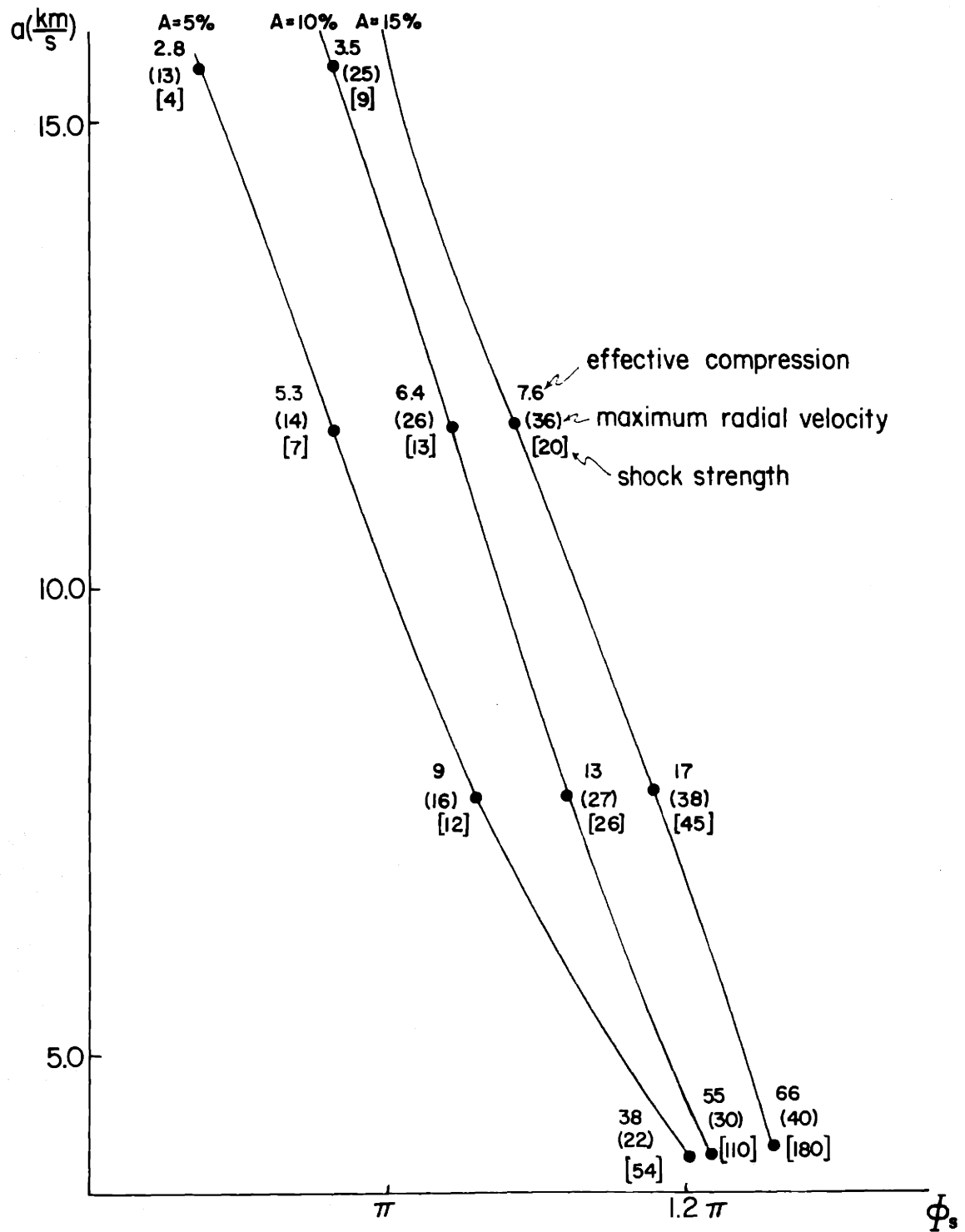


Figure (I5.1)  
Families of STS Solutions in the 3 Kpc Neighborhood under Forcing

a maximum radial velocity of about 40 km/s, and a shock strength of about 180 are all typical estimates for an STS solution under a 15% field and for a turbulent dispersion speed of about 4 km/s. If the turbulent dispersion speed is taken a little smaller, radial velocities as large as 50 km/s are possible.

### Part III. Mathematical Theory of the Development of Galactic Shocks

In part II we investigated the nonlinear dynamics of the gaseous component of the galactic disk and confirmed the compatibility of two periodically-located shock waves over the disk. In fact, it was demonstrated that a stationary galactic shock pattern may be maintained between the radii of 3-4 and 12 kpc over the disk.

In view of the significance of the results of Part II, we pose the following question: How may such large-scale galactic shock waves form in the first place? We therefore direct our attention from the problem of the existence and persistence of a two-armed spiral galactic shock pattern to the problem of the evolution and development of density waves into galactic shocks in the course of time. Of considerable interest is the evolutionary process of how a coherent gaseous density wave pattern may evolve into a coherent galactic shock pattern.

To gain insight into possible galactic shock formation the following initial value problem is considered: a grand pattern of spiral structure which rotates at a given pattern speed and which embodies a sinusoidal spiral perturbation gravitational field is superposed from some time onwards on the gaseous component of the Schmidt model of our Galaxy. Our goal is to determine the resultant nonlinear response of the gaseous disk to the imposed spiral perturbation field. By the method of characteristics we can view the formation of galactic shocks. Of

especial interest is the evolution and development of those galactic shocks which corotate with the imposed spiral pattern (i.e., those considered in Part II).

The linear density wave theory of Lin and Shu provides a theoretical picture of a spiral disk-shaped galaxy by the construction of a quasi-stationary grand design of spiral structure composed of self-sustained density waves. In this theoretical picture the nature of the grand pattern of spiral structure is precisely defined by the Lin-Shu dispersion relationship (which at any radius of the disk determines the wave number associated with the grand pattern at that radius in terms of the pattern speed and the galactic parameters of angular velocity, epicyclic frequency, and the base state density (which is reduced by the proper reduction factor), all defined at that radius). In this investigation, an exciting phenomenon is discovered: namely, only large-scale galactic shocks, which corotate with the pattern, may develop in the theoretical Lin-Shu picture of spiral disk-shaped galaxies. It is demonstrated that corotating galactic shocks (and no others) may develop when the galactic parameters of the grand design and the smoothed disk satisfy the Lin-Shu dispersion relationship (of the linear density wave theory).

In Part III A, we consider the initial value problem for unsteady one dimensional gas flow through a sinusoidal perturbation gravitational field which is superposed on the gas flow from some time onwards. The solution of the one dimensional initial value problem provides insight for the solution of the initial value problem for a model spiral galaxy which is considered in Part III B.

In both Part III A and Part III B, we consider gas flow at an arbitrary base state velocity and determine the types of shocks that develop for various ranges of base state velocity. In Part III B, it is shown that a particular critical speed (as a function of radius) is in fact selected for the base state gas flow about the galactic disk by the theoretical Lin-Shu picture of a spiral galaxy; and it is demonstrated that corotating galactic shocks are possible only at this particular critical speed of the base state gas flow through the spiral pattern.

Part III A. Unsteady One Dimensional Gas Flow through a Sinusoidal Perturbation Gravitational Field

In one dimensional acoustics, disturbances propagate forwards and backwards at the local acoustic speed throughout the gaseous medium. It is therefore natural to expect a small gravitational field, which is initially superposed on the gas flow, to excite at least two small disturbances of different propagation speeds. The crucial question may be stated as follows: Over a sufficiently long time, can these small disturbances grow into shocks? Our first goal is to find the answer to this question and to determine how the formation of one dimensional shocks is possible.

If the base state flow is less than the dispersion speed of the gas, both disturbances propagate through the perturbation field; one propagates backwards and the other forwards through the field.<sup>1</sup> If the base state flow is equal to the dispersion speed of the gas, one disturbance remains fixed and comoves with the field, while the other propagates forwards through the field at twice the dispersion speed (and twice the base state velocity). If the base state flow is greater than the dispersion speed, both disturbances propagate forwards through

---

<sup>1</sup>One disturbance travels backwards through the field at a speed equal to the difference of the base state velocity and the dispersion speed, whereas the other disturbance travels forwards through the field at a speed equal to the sum of the base state velocity and the dispersion speed.

the field. If a shock grows from a disturbance, the shock may be expected to propagate at the same speed as the disturbance. All three cases of subsonic, sonic,<sup>1</sup> and supersonic base state gas flow are considered, and the nature of shock formation in each case is determined.<sup>2</sup>

In Part III A, our attention is then directed toward the initial value problem in which a fixed sinusoidal perturbation gravitational field is superposed from some time onwards on a homogeneous stream of (turbulent) gas moving at a uniform velocity with respect to the field. There is no loss in generality for the one dimensional initial value problem if the contours of constant phase of the field lie perpendicular to the direction of the base state flow.

---

<sup>1</sup>It will be shown that a shock grows much faster from a comoving density wave than from a density wave that propagates through the field.

<sup>2</sup>In Part III B, we shall see that a particular critical base state velocity is preferred for the gas flow by the theoretical Lin-Shu picture of a spiral disk-shaped galaxy; and therefore, those shocks that are associated with this particular critical base state velocity (which is determined in Part III B) are the shocks that may be expected to be characteristic of a spiral disk-shaped galaxy. Curiously enough as we shall see, the corotating galactic shock, which grows fastest and which travels with the pattern, is the one selected by the theoretical Lin-Shu picture of a spiral galaxy.



## 16. Initial value problem for one dimensional gas flow

We consider the initial value problem in which a sinusoidal perturbation gravitational field is superposed from a time,  $t = 0$ , onwards on a homogeneous sheet of turbulent gas moving at a uniform velocity in the plane of the sheet. The basic equations of motion for the gas may be written as:

$$\frac{\partial \sigma}{\partial t} + u \frac{\partial \sigma}{\partial x} + \sigma \frac{\partial u}{\partial x} = 0$$

$$\frac{\partial u}{\partial t} + u \frac{\partial u}{\partial x} + \frac{a^2}{\sigma} \frac{\partial \sigma}{\partial x} = f$$

$$a^2 = \kappa \gamma \sigma^{\gamma-1}; \quad \gamma \neq 1$$

where

$t$  denotes time

$x$  denotes the spatial direction along which the gas flows

$u = u(x,t)$  denotes the gas velocity in the  $x$  direction

$a = a(x,t)$  denotes the mean gaseous turbulent dispersion speed

$\sigma = \sigma(x,t)$  denotes the density of the gas sheet

$f = f(x,t)$  denotes the imposed perturbation gravitational field

$\kappa, \gamma = \text{constants}; \quad \gamma \neq 1.$ <sup>1</sup>

---

<sup>1</sup>The limit of  $\gamma = 1$  may be taken for consideration of the situation of isothermal gas flow at an equivalent turbulent temperature. We later consider isothermal gas flow as a special case.

The initial gas flow at time,  $t = 0$ , is given by:

$$u(x,0) = u_0 \quad a(x,0) = a_0 \quad \sigma(x,0) = \sigma_0$$

Eliminating  $\sigma$ , we may write the basic equations in the following form:

$$\left( \frac{\partial}{\partial t} + (u + a) \frac{\partial}{\partial x} \right) \left( u + \frac{2a}{\gamma-1} \right) = f \quad (16.1)$$

$$\left( \frac{\partial}{\partial t} + (u - a) \frac{\partial}{\partial x} \right) \left( u - \frac{2a}{\gamma-1} \right) = f \quad (16.2)$$

These two nonlinear partial differential equations, (16.1) and (16.2), for the two unknowns,  $u(x,t)$  and  $a(x,t)$ , together with the initial conditions at  $t = 0$ :

$$u(x,0) = u_0 \quad a(x,0) = a_0$$

and the condition for the imposition of the perturbation force field:

$$f(x,t) = \begin{cases} 0 & t < 0 \\ \epsilon k V \sin kx & t \geq 0 \end{cases}$$

where  $\epsilon, k, V = \text{constants}; \quad \epsilon \ll 1$

constitute the initial value problem under consideration. Later we shall

add the effect of self gravitation of the gas. Let us now proceed to solve the above initial value problem in the framework of a perturbation theory in characteristic coordinates.

17. Perturbation theory in characteristic coordinates for one dimensional gas flow

Initial Value Problem in Characteristic Coordinates<sup>1</sup>

Choosing  $\alpha$  and  $\beta$  as characteristic coordinates and setting:

$$a \frac{\partial}{\partial \alpha} = \frac{\partial}{\partial t} + (u + a) \frac{\partial}{\partial x}$$

$$-a \frac{\partial}{\partial \beta} = \frac{\partial}{\partial t} + (u - a) \frac{\partial}{\partial x}$$

we may write equations (16.1) and (16.2) as:

$$a \frac{\partial}{\partial \alpha} \left( u + \frac{2a}{\gamma-1} \right) = f(\alpha, \beta) \quad \frac{\partial x}{\partial \alpha} = (u + a) \frac{\partial t}{\partial \alpha} \quad (17.1)$$

$$-a \frac{\partial}{\partial \beta} \left( u - \frac{2a}{\gamma-1} \right) = f(\alpha, \beta) \quad \frac{\partial x}{\partial \beta} = (u - a) \frac{\partial t}{\partial \beta} \quad (17.2)$$

The initial conditions become:

$$t = 0 \quad x = 2\alpha = 2\beta \quad a = a_0 \quad u = u_0$$

---

<sup>1</sup>Fox (1955) considers by the method of characteristics a similar initial value problem of ordinary one dimensional gas flow subject to initial conditions on the perturbation quantities rather than subject to an imposed perturbation force field.

and  $f$  becomes:

$$f(x(\alpha, \beta), t(\alpha, \beta)) = \begin{cases} 0 & t(\alpha, \beta) < 0 \\ \epsilon k V \sin kx(\alpha, \beta) & t(\alpha, \beta) \geq 0 \end{cases}$$

### Solution by Perturbation Series

A solution to equations (17.1) and (17.2) together with the initial conditions will be attempted in the form of a perturbation series in which each of the quantities,  $u$ ,  $a$ ,  $\sigma$ ,  $t$ ,  $x$ , is expressed as:

$$q(\alpha, \beta) = q^{(0)}(\alpha, \beta) + \epsilon q^{(1)}(\alpha, \beta) + \epsilon^2 q^{(2)}(\alpha, \beta) + \dots \quad (17.3)$$

At this point we assume an approximate perturbation gravitational field that will be adequate for an indication of possible shock development and will facilitate the solution of the initial value problem. We adopt an approximate perturbation force field of the form:

$$f(\alpha, \beta) = \begin{cases} 0 & t^{(0)}(\alpha, \beta) < 0 \\ \epsilon k V \sin[k x^{(0)}(\alpha, \beta)] & t^{(0)}(\alpha, \beta) \geq 0 \end{cases} \quad (17.4)$$

If equations (17.1) and (17.2) are rewritten in the form of the perturbation series (17.3), and if terms of like powers of  $\epsilon$  are equated, the nonlinear equations (17.1) and (17.2) reduce to a series of systems of four linear equations each. The solution of this series of systems of linear equations to  $\mathcal{O}(\epsilon^2)$  for the physical quantities may be written in the form of the perturbation series (17.3):

$$\begin{aligned}
u(\alpha, \beta) = u_0 + \epsilon \frac{V}{2a_0} & \left\{ \frac{1}{\lambda + 1} \cos 2k\beta + \frac{1}{\lambda - 1} \cos 2k\alpha \right. \\
& \left. - \frac{2\lambda}{\lambda^2 - 1} \cos k( (\lambda + 1)\alpha - (\lambda - 1)\beta ) \right\} \\
& + O(\epsilon^2) \qquad (17.5)
\end{aligned}$$

$$\begin{aligned}
a(\alpha, \beta) = a_0 + \epsilon \left( \frac{\gamma - 1}{2} \right) \frac{V}{2a_0} & \left\{ \frac{1}{\lambda + 1} \cos 2k\beta - \frac{1}{\lambda - 1} \cos 2k\alpha \right. \\
& \left. + \frac{2}{\lambda^2 - 1} \cos k( (\lambda + 1)\alpha - (\lambda - 1)\beta ) \right\} \\
& + O(\epsilon^2) \qquad (17.6)
\end{aligned}$$

$$\begin{aligned}
\sigma(\alpha, \beta) = \sigma_0 + \epsilon \frac{\sigma_0 V}{2a_0^2} & \left\{ \frac{1}{\lambda + 1} \cos 2k\beta - \frac{1}{\lambda - 1} \cos 2k\alpha \right. \\
& \left. + \frac{2}{\lambda^2 - 1} \cos k( (\lambda + 1)\alpha - (\lambda - 1)\beta ) \right\} \\
& + O(\epsilon^2) \qquad (17.7)
\end{aligned}$$

$$\begin{aligned}
t(\alpha, \beta) &= \frac{1}{a_0} (\alpha - \beta) + \epsilon \frac{1}{2a_0^2} \left\{ (C_{1+} \cos 2k\alpha - B_{1+} \cos 2k\beta) (\alpha - \beta) \right. \\
&+ \frac{1}{2k} (B_{1-} - C_{1-}) (\sin 2k\alpha - \sin 2k\beta) \\
&+ \frac{1}{k} \left( \frac{A_{1+}}{\lambda - 1} \sin 2k\alpha - \frac{A_{1-}}{\lambda + 1} \sin 2k\beta \right) \\
&+ \left. \frac{1}{k} \left( \frac{A_{1-}}{\lambda + 1} - \frac{A_{1+}}{\lambda - 1} \right) \sin k( (\lambda + 1)\alpha - (\lambda - 1)\beta ) \right\} \\
&+ \mathcal{O}(\epsilon^2(\alpha - \beta)) \tag{17.8}
\end{aligned}$$

$$\begin{aligned}
x(\alpha, \beta) &= (\lambda + 1)\alpha - (\lambda - 1)\beta \\
&+ \epsilon \frac{1}{2a_0} \left\{ ( (\lambda + 1) C_{1+} \cos 2k\alpha - (\lambda - 1) B_{1+} \cos 2k\beta ) (\alpha - \beta) \right. \\
&+ \frac{1}{2k} ( (\lambda + 1) B_{1-} - (\lambda - 1) C_{1-} ) (\sin 2k\alpha - \sin 2k\beta) \\
&+ \frac{1}{k} \left( \frac{\lambda + 1}{\lambda - 1} A_{1+} \sin 2k\alpha - \frac{\lambda - 1}{\lambda + 1} A_{1-} \sin 2k\beta \right) \\
&+ \left. \frac{1}{k} \left( \frac{\lambda - 1}{\lambda + 1} A_{1-} - \frac{\lambda + 1}{\lambda - 1} A_{1+} \right) \sin k( (\lambda + 1)\alpha - (\lambda - 1)\beta ) \right\} \\
&+ \mathcal{O}(\epsilon^2(\alpha - \beta)) \tag{17.9}
\end{aligned}$$

where

$$A_{1\pm} = \frac{v}{a_0} \left( \frac{\lambda \pm \frac{\gamma-1}{2}}{\lambda^2 - 1} \right) \quad B_{1\pm} = \frac{v}{2a_0} \left( \frac{1 \pm \frac{\gamma-1}{2}}{\lambda + 1} \right) \quad C_{1\pm} = \frac{v}{2a_0} \left( \frac{1 \pm \frac{\gamma-1}{2}}{\lambda - 1} \right)$$

We could continue with the calculation of the solutions of the  $\mathcal{O}(\epsilon^2)$  system of equations in order to make the perturbation series complete up to  $\mathcal{O}(\epsilon^3)$ , and so on. However, for our purposes of indicating the possible formation of shocks, this continuation to higher orders is not necessary. The reason for this is that only the first power of  $(\alpha - \beta)$  appears in the terms,  $t^{(2)}$  and  $x^{(2)}$ , and in fact only the first power of  $(\alpha - \beta)$  appears in all the higher order terms also. This is important because as  $(\alpha - \beta)$  becomes of  $\mathcal{O}(\epsilon^{-1})$ , which is the case when shock development sets in, the second terms,  $t^{(1)}$  and  $x^{(1)}$ , still remain of larger order than all the remaining higher order terms, and the perturbation series remains valid. As  $(\alpha - \beta)$  becomes of  $\mathcal{O}(\epsilon^{-1})$ , the second terms,  $t^{(1)}$  and  $x^{(1)}$ , become large enough that the characteristics cross and a shock region appears, but the convergence of the perturbation series is not destroyed and the flow is described up to the shock and a little beyond. Fox (1955) demonstrates this important result in a similar type of initial value problem of ordinary one dimensional gas flow subject to initial conditions on the perturbation quantities rather than subject to an imposed perturbation force field.



## 18. Ordinary one dimensional shock development

The perturbation series solution for the physical variables in the case,  $\lambda \neq 1$ , contains both a comoving wave (i.e., a wave which travels with the field) and two waves which propagate through the field. Although the comoving density wave cannot provide for the development of shocks, the other two waves can. Portions of each of these waves where the local Mach number is greater than  $\lambda$  will tend to catch up with portions where the local Mach number is less than  $\lambda$ . Consequently, the "non-comoving" density waves over a long enough time become distributed along the  $x$  direction in the form of compression and rarefaction regions. As a plane wave propagates, the compression portions tend to steepen and develop into shock fronts, whereas the rarefaction portions tend to smooth out more continuously. Therefore, after sufficient time has elapsed, shocks may be expected to develop at periodic locations along the  $x$  direction.

The development of a shock in the gas flow is characterized by the fact that the mapping from the characteristic plane to the physical plane ceases to be single-valued. The image of the characteristic plane folds over to form a three-sheeted surface in the  $(x,t)$  plane. Along the edges of this fold the Jacobian:

$$J = \frac{\partial x}{\partial \alpha} \frac{\partial t}{\partial \beta} - \frac{\partial x}{\partial \beta} \frac{\partial t}{\partial \alpha}$$

is equal to zero. Within the region of the fold the velocity and density at any point  $(x,t)$  are triple-valued. This paradox is resolved by the introduction of a shock at the point where the characteristics cross and the fold begins; for, the velocity and density jumps between the outermost sheets are reconciled if a shock intervenes. (For a detailed description, see Fox (1955) ).

To determine approximately where the shocks develop, we must find the values of  $\alpha$  and  $\beta$  for which the Jacobian,  $J$ , equals zero. First, it is possible to make  $J = 0$  at some point by taking  $t_\beta = 0^1$  at that point; for, if  $t_\beta = 0$  at some point, then also  $x_\beta = 0$ , and  $J = 0$  at that point. In order to have  $t_\beta = 0$ , the first term of the perturbation expansion for  $t_\beta$  must be cancelled by one or more higher order terms of the expansion. If this cancellation is possible, then shock development may be realized; if not, shocks will not form. Suppose we now consider the expansion for  $t_\beta$  to determine whether shocks may be possible:

$$\begin{aligned}
 t_\beta(\alpha, \beta) = & -\frac{1}{a_0} + \epsilon \frac{1}{2a_0^2} \left\{ 2k B_{1+} \sin 2k\beta (\alpha - \beta) + B_{1+} \cos 2k\beta \right. \\
 & - C_{1+} \cos 2k\alpha + (C_{1-} - B_{1-}) \cos 2k\beta - \frac{2 A_{1-}}{\lambda + 1} \cos 2k\beta \\
 & \left. + (A_{1+} - \frac{\lambda - 1}{\lambda + 1} A_{1-}) \cos k((\lambda + 1)\alpha - (\lambda - 1)\beta) \right\} \\
 & + \mathcal{O}(\epsilon^2(\alpha - \beta))
 \end{aligned}$$

---

<sup>1</sup> $t_\beta$  refers to  $\frac{\partial t}{\partial \beta}$

For  $\epsilon \ll 1$ , only the first two terms are significant for large time. Hence, if these two terms cancel one another, the condition:

$$t_{\beta} = 0 + O(\epsilon)$$

will be insured, and this condition in turn insures the existence of a shock. Balancing these two terms, we find:

$$(\alpha - \beta) = \frac{a_0}{\epsilon k B_{1+}} \frac{1}{\sin 2k\beta}$$

If  $t_{\alpha} \neq 0$  at the point of shock formation, then it may be shown that the condition:

$$t_{\beta\beta} = 0 + O(\epsilon)$$

is satisfied there. Making use of this latter condition, we then may determine the locations of the shocks as:

$$2k\beta = \frac{\pi}{2} + n\pi \quad n = \pm 0, \pm 1, \pm 2, \dots$$

$$(\alpha - \beta) = \frac{a_0}{\epsilon k B_{1+}} \frac{1}{(-1)^n}$$

Since time is an increasing quantity, only the positive values of  $(\alpha - \beta)$  correspond to physical shocks.  $(\alpha - \beta)$  positive implies  $n = 0, \pm 2, \pm 4, \dots$  if  $B_{1+} > 0$ . Shock development of this type (i.e.,  $t_{\beta} = 0$ ) for both subsonic and supersonic base state flow (i.e.,  $\lambda \neq 1$ ) is indicated in Figure (18.1).

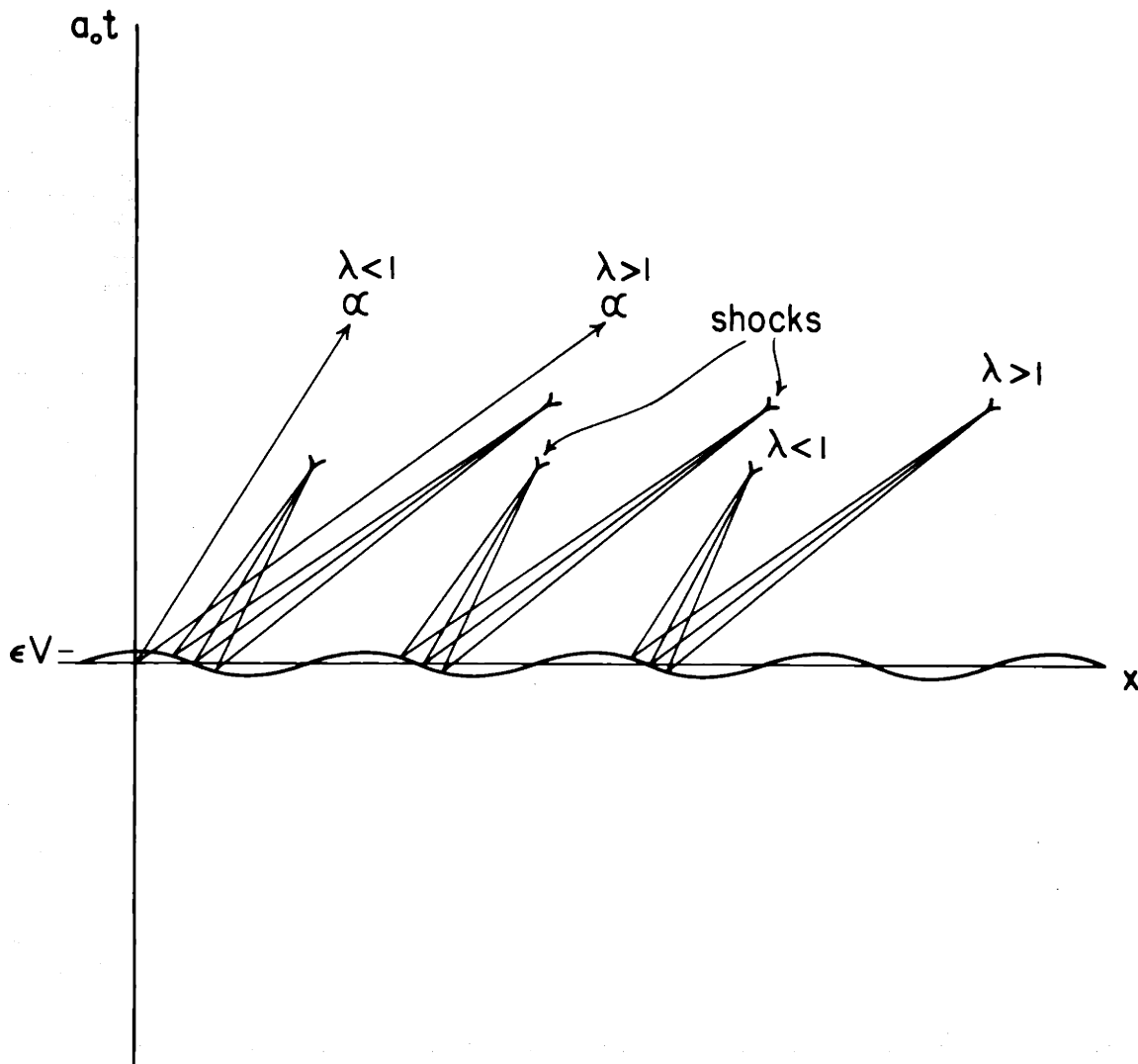


Figure (18.1)  
 The Development of Shocks Propagating at a Speed  
 ( $u_0 + a_0$ ) Through the Field

There is another possible way to make the Jacobian,  $J$ , equal to zero. The Jacobian can be set equal to zero at some point by taking  $t_\alpha = 0$  at that point. If  $t_\alpha = 0$  at some point, then also  $x_\alpha = 0$ , and  $J = 0$  at that point. In order to have  $t_\alpha = 0$ , we require cancellation of the largest terms in the perturbation series of  $t_\alpha$ . Following an analysis similar to the preceding one (i.e., for  $t_\beta = 0$ ), we determine the locations of the shocks as:

$$2k\alpha = \frac{\pi}{2} + n\pi \quad n = 0, \pm 1, \pm 2, \dots$$

$$(\alpha - \beta) = \frac{a_0}{\epsilon k C_{1+}} \frac{1}{(-1)^n}$$

Again, since time is an increasing quantity, only positive values of  $(\alpha - \beta)$  correspond to physical shocks.  $(\alpha - \beta)$  positive implies  $n = 0, \pm 2, \pm 4, \dots$  if  $C_{1+} > 0$ , and  $n = \pm 1, \pm 3, \dots$  if  $C_{1+} < 0$ . Shock development of this type (i.e.,  $t_\alpha = 0$ ) for both subsonic and supersonic base state flow (i.e.,  $\lambda \neq 1$ ) is indicated in Figure (18.2).

Therefore, the two non-comoving density waves give rise to two types of shocks. After a sufficiently long time given by:

$$t_s = \frac{2a_0 |\lambda - 1|}{\epsilon k V \left(1 + \frac{\gamma - 1}{2}\right)} \quad (18.1)$$

the density wave propagating at a speed  $(u_0 - a_0)$  gives rise to shocks propagating at the same speed. After a somewhat longer time

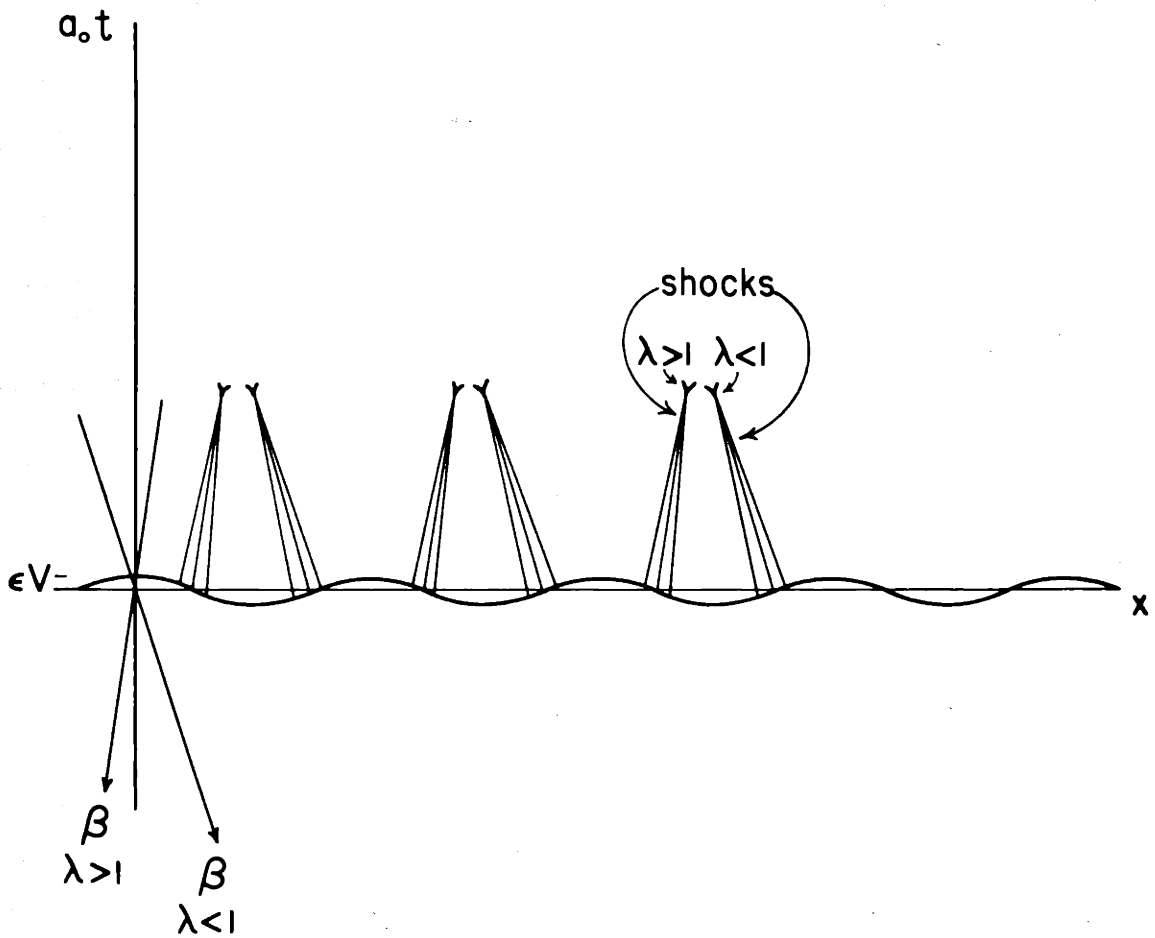


Figure (18.2)  
 The Development of Shocks Propagating at a Speed  
 $(u_0 - a_0)$  Through the Field

given by:

$$t_s = \frac{2a_0 (\lambda+1)}{\epsilon k V (1 + \frac{\gamma-1}{2})} \quad (18.2)$$

the density wave propagating at a speed  $(u_0 + a_0)$  gives rise to shocks propagating at the same speed. The time it takes for the formation of shocks becomes longer; the smaller the amplitude of the sinusoidal gravitational field, or the larger the wavelength of the sinusoidal field, or the larger the base state dispersion speed. For example, a large amplitude and short wavelength of the sinusoidal field may induce relatively rapid formation of shocks.

## 19. Shock of most rapid development

So far we have not examined the possibility of the formation of comoving shocks.<sup>1</sup> For both base state subsonic flow and base state supersonic flow, we have only shown that non-comoving shocks, which propagate through the field, may develop. Suppose we now consider the case in which the base state flow is equal to the acoustic speed of the gas (i.e.,  $\lambda = 1$ ). For this case, either we may take the limit of the preceding solution as  $\lambda \rightarrow 1$  or we may begin again from the basic set of equations (17.1) and (17.2) with  $\lambda$  set equal to unity.<sup>2</sup>

The solution of the physical quantities for the case,  $\lambda = 1$ , to  $\mathcal{O}(\epsilon^2)$  may be written in the form of the perturbation series (17.3) as:

$$u(\alpha, \beta) = u_0 + \epsilon \frac{V}{4a_0} \left[ 2k \sin 2k\alpha (\alpha - \beta) - \cos 2k\alpha + \cos 2k\beta \right] + \dots + \mathcal{O}(\epsilon^n (\alpha - \beta)^n) + \dots \quad n = 2, 3, \dots \quad (19.1)$$

---

<sup>1</sup>In Part III B, we shall see how a spiral galaxy selects the magnitude of its base state flow and thereby selects the type of shocks that it may possess (which correspond to that base state flow). It is demonstrated that only corotating galactic shocks are selected in the theoretical Lin-Shu picture of spiral galaxies.

<sup>2</sup>The author has considered both methods of procedure and has shown that they yield the same results.



$$\begin{aligned}
a(\alpha, \beta) = & a_0 + \varepsilon \frac{\gamma - 1}{2} \frac{V}{4a_0} \left[ -2k \sin 2k\alpha (\alpha - \beta) - \cos 2k\alpha \right. \\
& \left. + \cos 2k\beta \right] + \dots + \mathcal{O}(\varepsilon^n (\alpha - \beta)^n) + \dots \quad (19.2)
\end{aligned}$$

$$\begin{aligned}
\sigma(\alpha, \beta) = & \sigma_0 + \varepsilon \frac{\sigma_0 V}{4a_0^2} \left[ -2k \sin 2k\alpha (\alpha - \beta) - \cos 2k\alpha \right. \\
& \left. + \cos 2k\beta \right] + \dots + \mathcal{O}(\varepsilon^n (\alpha - \beta)^n) + \dots \quad (19.3)
\end{aligned}$$

$$\begin{aligned}
t(\alpha, \beta) = & \frac{1}{a_0} (\alpha - \beta) + \varepsilon \frac{1}{2a_0^2} \left[ kB_{1+} \sin 2k\alpha (\alpha - \beta)^2 \right. \\
& \left. - B_{1+} \cos 2k\beta (\alpha - \beta) + \frac{B_{1+}}{2k} (\sin 2k\alpha - \sin 2k\beta) \right] \\
& + \dots + \mathcal{O}(\varepsilon^n (\alpha - \beta)^{1+n}) + \dots \quad (19.4)
\end{aligned}$$

$$\begin{aligned}
x(\alpha, \beta) = & 2\alpha + \varepsilon \frac{1}{a_0} \left[ kB_{1+} \sin 2k\alpha (\alpha - \beta)^2 \right. \\
& \left. - B_{1-} \cos 2k\alpha (\alpha - \beta) + \frac{B_{1-}}{2k} (\sin 2k\alpha - \sin 2k\beta) \right] \\
& + \dots + \mathcal{O}(\varepsilon^n (\alpha - \beta)^{1+n}) + \dots \quad (19.5)
\end{aligned}$$

This perturbation series solution for the case,  $\lambda = 1$ , breaks down as  $(\alpha - \beta)$  increases to  $\mathcal{O}(\epsilon^{-1})$ . However, we shall see that shock formation occurs before this condition is reached, and that the perturbation series, (19.1) - (19.5), remains valid up to the shock region and a little beyond. Indeed, it will be shown that the time period for shock development is  $\mathcal{O}(\epsilon^{-1/2})$ .

Suppose we now search for possible locations where shocks may develop in this "sonic" case where the base state flow through the field is equal to the mean dispersion speed. There are two possible cases for which  $J = 0$ . First, the case in which  $x_\alpha = t_\alpha = 0$ , and second, the case in which  $x_\beta = t_\beta = 0$ . In the first case, we examine the explicit form of  $t_\alpha$ :

$$\begin{aligned}
 t_\alpha(\alpha, \beta) = & \frac{1}{a_0} + \epsilon \frac{1}{2a_0^2} \left\{ 2k^2 B_{1+} \cos 2k\alpha (\alpha - \beta)^2 \right. \\
 & + 2k B_{1+} \sin 2k\alpha (\alpha - \beta) + B_{1+} (\cos 2k\alpha - \cos 2k\beta) \left. \right\} \\
 & + \mathcal{O}(\epsilon^2 (\alpha - \beta)^3)
 \end{aligned}$$

For  $\epsilon \ll 1$  and  $(\alpha - \beta) \gg 1$ , the terms of largest magnitude are the first two terms. In order to have  $t_\alpha = 0$ , these two terms must cancel. In addition, if  $t_\beta \neq 0$  at the point of shock formation, then it may be shown that  $t_{\alpha\alpha} = 0$  there. This latter condition yields the relation:

$$2k\alpha = n\pi \quad n = 0, \pm 1, \pm 2, \dots$$

and with these values for  $\alpha$  the condition,  $t_\alpha = 0$ , that determines the locations of shock formation becomes:

$$(\alpha - \beta)^2 = \frac{a_0}{\epsilon k^2 B_{1+}} \frac{1}{(-1)^{n-1}}$$

Figure (19.1) indicates the nature and the locations of shocks of this type (i.e.,  $t_\alpha = 0$ ) with respect to the potential field. Since time is an increasing quantity, we must take  $n = \pm 1, \pm 3, \dots$  for the realization of physical shocks. These are the comoving shocks that we have been searching for. Only when the base state flow is sonic does it appear that comoving shocks develop. Their development takes only a time:

$$t_s = \frac{1}{(\epsilon V)^{1/2}} \frac{2}{k(1 + \frac{\gamma-1}{2})^{1/2}} \quad (19.6)$$

whereas all the other shocks evolve only after a longer time of  $\mathcal{O}(\epsilon^{-1})$ . It is easily seen that in this time period for the formation of comoving shocks the perturbation series, (19.1)-(19.5), remains valid up to the shock regions and a little beyond (i.e., the perturbation series remains valid a little beyond the time when  $(\alpha - \beta) = \mathcal{O}(\epsilon^{-1/2})$ ).

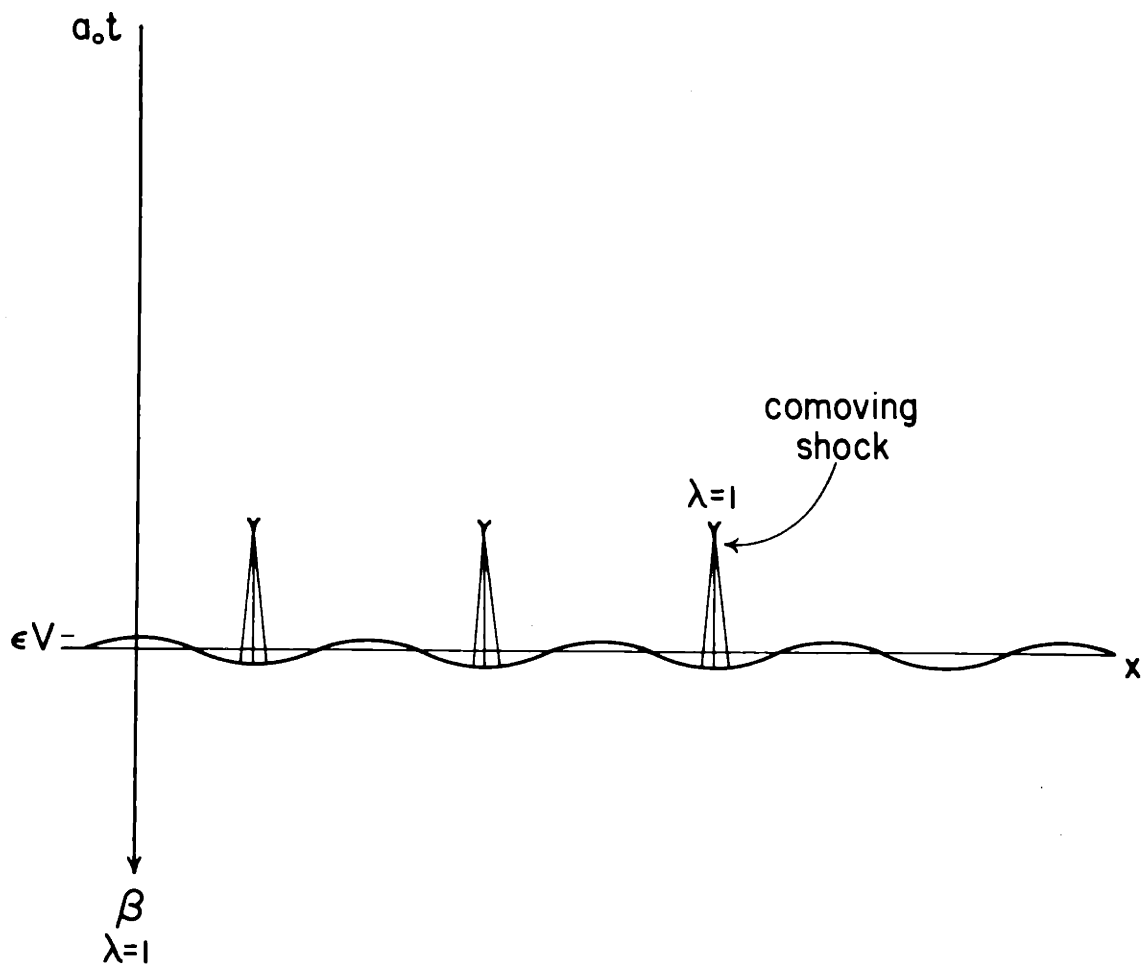


Figure (19.1)  
The Development of Comoving Shocks

The second possibility for which the Jacobian,  $J$ , equals zero is the case in which  $x_\beta = t_\beta = 0$ . In this case, we examine the explicit form of  $t_\beta$ :

$$t_\beta(\alpha, \beta) = -\frac{1}{a_0} + \epsilon \frac{kB_{1+}}{a_0^2} \left[ (\sin 2k\beta - \sin 2k\alpha) (\alpha - \beta) \right] + \dots$$

$$+ \mathcal{O}(\epsilon^n (\alpha - \beta)^n) + \dots$$

It is apparent that  $t_\beta$  cannot be made equal to zero until  $(\alpha - \beta)$  increases to  $\mathcal{O}(\epsilon^{-1})$ . It is when  $(\alpha - \beta)$  approaches  $\mathcal{O}(\epsilon^{-1})$  that all terms of the perturbation series approach unity. Therefore, the perturbation series breaks down before the formation of shocks of this type (i.e.,  $t_\beta = 0$ ) sets in.

#### Development of Isothermal Shocks

So far we have considered the flow of gas with an arbitrary adiabatic constant,  $\gamma$ . Suppose we now consider the situation for the flow of gas with a uniform mean turbulent dispersion speed (i.e.,  $\gamma = 1$ ).<sup>1</sup> In the limit as  $\gamma \rightarrow 1$ , the factor,  $(\gamma-1)/2 \rightarrow 0$  and

$$A_{1\pm} \rightarrow \frac{\frac{\lambda V}{a_0}}{\lambda^2 - 1} \quad B_{1\pm} \rightarrow \frac{\frac{V}{2a_0}}{\lambda + 1} \quad C_{1\pm} \rightarrow \frac{\frac{V}{2a_0}}{\lambda - 1}$$

---

<sup>1</sup>In Part II, we adopted a uniform mean turbulent dispersion speed.

Shock formation for the isothermal case,  $\gamma = 1$ , is therefore different from the more general case,  $\gamma \neq 1$ , only by the slight change in magnitude of these above constant factors.

## 20. Self gravitation of the gas

In reality the gas exerts a force on itself due to its own self gravitation. Suppose we include the effect of self gravitation and see how it influences the dynamics of the gas and the formation of shocks. It is to be expected that there is no major change in the general behavior of the gas, although quantitative modifications will appear.

The gas density is composed of a base state density,  $\sigma_0$ , together with a perturbation density,  $\sigma_1$ . Suppose we assume the perturbation density exhibits a simple sinusoidal variation (that is compatible with the perturbation solution in the case without self gravitational effects in the preceding sections). In this case, we follow an asymptotic analysis similar to the asymptotic scheme of Lin and Shu (1964) for a thin disk of gas and obtain a relation describing the force field of the gas in terms of its (simple sinusoidal) density variation:

$$f_g = \frac{2\pi G}{|k|} \frac{\partial \sigma_1}{\partial x}$$

Incorporating this additional force into the equations of motion, (16.1) and (16.2), we proceed with an analysis similar to the

analysis in the preceding sections, and we derive a perturbation series solution and determine the consequences of self gravitation of the gas on shock formation.

We find that the new effective base state dispersion speed is given by:

$$s^{(0)} = s_0 = \left( a_0^2 - \frac{2\pi G \sigma_0}{|k|} \right)^{1/2}$$

and we define:

$$\lambda = \frac{u_0}{s_0}$$

When self gravitation of the gas is included in the case,  $\lambda \neq 1$ , there are two types of shocks possible just as when self gravitation is absent. The density wave propagating at a speed,  $(u_0 - s_0)$ , gives rise to shocks propagating at the same speed in a time period for shock formation on the order:

$$t_s = \frac{2s_0 |\lambda - 1|}{\epsilon k V \left( 1 + \frac{\gamma-1}{2} \frac{a_0^2}{s_0^2} - \frac{\pi G \sigma_0}{|k| s_0^2} \right)} \quad (20.1)$$

The density wave propagating at a speed  $(u_0 + s_0)$  gives rise to shocks propagating at the same speed in a time period for shock formation on the order:



$$t_s = \frac{2s_o (\lambda + 1)}{\epsilon k V \left( 1 + \frac{\gamma-1}{2} \frac{a_o^2}{s_o^2} - \frac{\pi G \sigma_o}{|k| s_o^2} \right)} \quad (20.2)$$

These two types of shocks are of the same nature as those two types of shocks that develop in the case when self gravitation is not included.

When self gravitation of the gas is included in the case,  $\lambda = 1$ , only comoving shocks (similar to the ones possible in the case,  $\lambda = 1$ , without self gravitation) are possible. Indeed, when self gravitation of the gas is included, the comoving density wave gives rise to comoving shocks in a time period for shock formation on the order:

$$t_s = \frac{1}{(\epsilon V)^{1/2}} \frac{2}{k \left( 1 + \frac{\gamma-1}{2} \frac{a_o^2}{s_o^2} - \frac{\pi G \sigma_o}{|k| s_o^2} \right)^{1/2}} \quad (20.3)$$

### Part III B. Unsteady Gas Flow about a Spiral Galaxy

Now that we have seen the behavior of unsteady one dimensional gas flow and shock formation in the presence of a sinusoidal perturbation gravitational field, we would like to consider the more complicated problem of unsteady gas flow about a model spiral galaxy. When we refer to a spiral galaxy, we are speaking primarily of the grand design of spiral structure that extends over the galactic disk. Since most spiral galaxies exhibit a two-armed grand design, we consider a galactic model in which a small two-armed spiral gravitational field associated with the two spiral arms is superposed on the Schmidt model of the Milky Way System.

The asymptotic theory developed in Part II for the facilitation of numerical solution of the problem of steady gas flow and steady shock formation will also be applied in this analytical investigation of unsteady gas flow about a model spiral galaxy. The asymptotic gas dynamical equations (5.2), (5.3), and (5.4) therefore constitute the equations from which we begin this analysis. The time dependence however is retained in the following treatment.

In the asymptotic picture, the coordinate normal to the contours of constant phase of the spiral pattern is the most important spatial coordinate. Just as in the steady gas flow of Part II, it is to be expected in the present case that the direction of maximum variation of the perturbation quantities of density and velocity induced by the perturbation field is perpendicular to the contours of constant phase.

Differential rotation of the galactic disk and self gravitation of the gas are effects that are included at the outset, and we shall be concerned throughout with their influence on the time evolution of the nonlinear dynamics of the gas and on the possible formation of shocks in the spiral-armed disk.

It is natural to expect (in accordance with the results of Part III A) that the sinusoidal spiral field, which is initially superposed on the gaseous disk, gives rise to (at least) two density waves. The crucial question concerns the formation of galactic shocks: After a sufficiently long time is it possible for the spiral density waves to grow into shocks?<sup>1</sup> Our first goal in Part III B therefore is to determine how the formation of galactic shocks is possible and to determine the influence of the galactic parameters on the evolution and development of galactic shocks. One further goal is to determine what type of galactic shock is preferred by a spiral disk-shaped galaxy.

We consider three ranges of the base state flow: subcritical, critical, and supercritical (all of which will be properly defined), and we determine the nature of the formation of shocks in each of these cases.<sup>2</sup> In the critical speed case, a corotating galactic shock

---

<sup>1</sup>The time for the formation of a shock (in accordance with the results of Part III A) may be expected to depend on certain physical parameters such as the amplitude of the spiral field, the magnitude of the base state density of gas, and the differential rotation of the disk.

<sup>2</sup>These considerations in Part III B parallel the considerations of subsonic, sonic, and supersonic base state flow in Part III A.

(i.e., one that travels with the spiral pattern) is the only shock possible. It is shown that the theoretical Lin-Shu picture of spiral disk-shaped galaxies dictates that the base state flow be the critical speed and thereby selects the corotating galactic shock as the type of shock that eventually develops.

Our attention is then directed toward the initial value problem in which a sinusoidal spiral perturbation gravitational field is superposed from some time onwards on the gaseous component of the Schmidt model of our Galaxy.<sup>1</sup> If  $\Omega(\varpi)$  is the angular velocity of the gas at radius  $\varpi$  about the disk, and if  $\Omega_p$  is the pattern speed, then  $(\Omega(\varpi) - \Omega_p)$  is the basic circular velocity of the gas relative to the spiral pattern. Since the spiral contours of constant phase are everywhere inclined at an angle  $i$  to the circumferential direction, the base state gas velocity normal to the contours of constant phase is  $(\Omega(\varpi) - \Omega_p) \varpi \sin i$ , whereas the base state velocity parallel to the contours of constant phase is  $(\Omega(\varpi) - \Omega_p) \varpi \cos i$ . Since in the first order of the asymptotic approximation there is no variation of the perturbation field along constant phase contours, it is natural to expect the density waves and the developing shocks which are induced by the spiral field likewise to exhibit contours of constant phase which parallel those of the spiral field.

---

<sup>1</sup>In the Schmidt model, the basic equilibrium state of gas moves in purely circular streamtubes about the galactic center at given angular velocities dependent on the distances of the given streamtubes from the galactic center.

21. Initial value problem for galactic gas flow through a sinusoidal spiral perturbation gravitational field

We consider the initial value problem in which a sinusoidal spiral perturbation gravitational field is superposed from a time,  $t = 0$ , onwards on the gaseous component of the Schmidt model of the Galaxy. The asymptotic equations developed in Part II (with time dependence retained) serve as the equations governing the dynamics of the gas. These asymptotic equations (where  $\eta$  represents the coordinate normal to the spiral equipotential curves and where  $w_{\perp}$  and  $w_{\parallel}$  are the perturbation velocity components perpendicular and parallel to this coordinate,  $\eta$ , and where all the other variables are the same as those in Part II) may be written as:

$$\varpi \frac{\partial \sigma_1}{\partial t} + (w_{\perp 0} + w_{\perp}) \frac{\partial \sigma_1}{\partial \eta} + (\sigma_0 + \sigma_1) \frac{\partial w_{\perp}}{\partial \eta} + (\sigma_0 + \sigma_1 + \varpi \frac{d\sigma_0}{d\varpi}) \chi_1 = 0 \quad (21.1)$$

$$\varpi \frac{\partial w_{\perp}}{\partial t} + (w_{\perp 0} + w_{\perp}) \frac{\partial w_{\perp}}{\partial \eta} - 2\Omega \varpi w_{\parallel} + \frac{a^2}{\sigma_0 + \sigma_1} \frac{\partial \sigma_1}{\partial \eta} + \frac{\partial U}{\partial \eta} g_1 + \frac{\partial U_1}{\partial \eta} + \chi_2 = 0 \quad (21.2)$$

$$\varpi \frac{\partial w_{\parallel}}{\partial t} + (w_{\perp 0} + w_{\perp}) \frac{\partial w_{\parallel}}{\partial \eta} + \left(\frac{K^2}{2\Omega}\right) \varpi w_{\perp} + \chi_3 = 0 \quad (21.3)$$

where

$$w_{\perp 0} = (\Omega - \Omega_p) \varpi \sin i \quad w_{\parallel 0} = (\Omega - \Omega_p) \varpi \cos i$$

$\chi_1$ ,  $\chi_2$ , and  $\chi_3$  are defined by equations (5.6), (5.7), and (5.8); and  $U_1$  is the imposed sinusoidal potential. As in Section 20, we describe the self-induced force field of the gas in terms of its (assumed, simple sinusoidal) density variation:

$$-\frac{\partial U}{\partial \eta} g_1 = \frac{2\pi G \varpi}{|k|} \frac{\partial \sigma_1}{\partial \eta}$$

The initial value problem to be investigated consists of these three nonlinear equations, (21.1) - (21.3), for the unknown quantities  $w_{\perp}$ ,  $w_{\parallel}$ , and  $\sigma_1$  together with the equation:

$$a^2 = \kappa \gamma \sigma^{-1}$$

and the initial conditions at  $t = 0$ :

$$w_{\perp}(n,0) = 0 \quad w_{\parallel}(n,0) = 0 \quad \sigma_1(n,0) = 0$$

and the condition for the imposition of the sinusoidal potential. With the assumption that the gas streamtubes under the influence of a spiral field do not deviate significantly in the course of time from purely circular streamtubes of the base state, the equilibrium quantities,  $w_{\perp 0}$ ,  $w_{\parallel 0}$ , and  $\sigma_0$ , which are dependent only on the radius  $\varpi$ , may be

taken as constant quantities throughout the motion of the gas along each particular streamtube. This approximation is also made for the numerical calculations of Part II. Both the approximations of the small deviation of the gas streamtube from a circular orbit and of the small variation of the perturbation quantities along the contours of constant phase with respect to the variation of the same quantities across the contours of constant phase have been verified by the numerical calculations for the problem of steady gas flow in Part II. These approximations may be expected to hold equally well for the problem of unsteady gas flow considered here in Part III B.

If higher order terms are neglected, the equations (21.1), (21.2), and (21.3) may be rewritten in characteristic form as:

$$\begin{aligned}
 & \left\{ \omega \frac{\partial}{\partial t} + (w_{\perp 0} + w_{\perp} + s) \frac{\partial}{\partial \eta} \right\} \left\{ \omega \frac{\partial}{\partial t} + (w_{\perp 0} + w_{\perp} - s) \frac{\partial}{\partial \eta} \right\} w_{\perp} \\
 & = \left\{ \omega \frac{\partial}{\partial t} + (w_{\perp 0} + w_{\perp}) \frac{\partial}{\partial \eta} \right\} f - \frac{2\pi G \omega}{|k|} \frac{\partial}{\partial \eta} (\sigma_0 + \sigma_1) \frac{\partial}{\partial \eta} w_{\perp}
 \end{aligned} \tag{21.4}$$

$$\begin{aligned}
 & \left\{ \omega \frac{\partial}{\partial t} + (w_{\perp 0} + w_{\perp} + a) \frac{\partial}{\partial \eta} \right\} \left( w_{\perp} + \frac{2a}{\gamma - 1} \right) \\
 & = \left\{ \omega \frac{\partial}{\partial t} + (w_{\perp 0} + w_{\perp} - a) \frac{\partial}{\partial \eta} \right\} \left( w_{\perp} - \frac{2a}{\gamma - 1} \right)
 \end{aligned} \tag{21.5}$$

$$\left\{ \omega \frac{\partial}{\partial t} + (w_{\perp 0} + w_{\perp}) \frac{\partial}{\partial \eta} \right\} w_{\parallel} + \left( \frac{k^2}{2\Omega} \right) \omega w_{\perp} = 0 \quad (21.6)$$

$$\left\{ \omega \frac{\partial}{\partial t} + (w_{\perp 0} + w_{\perp}) \frac{\partial}{\partial \eta} \right\} \sigma_1 + (\sigma_0 + \sigma_1) \frac{\partial w_{\perp}}{\partial \eta} = 0 \quad (21.7)$$

where

$$s = \left[ a^2 + \frac{k^2 \omega^2}{k^2} - \frac{2\pi G \omega}{|k|} (\sigma_0 + \sigma_1) \right]^{1/2}$$



22. Perturbation theory in characteristic coordinates for galactic gas flow

Initial Value Problem in Characteristic Coordinates

By introducing the characteristic coordinates,  $\alpha$  and  $\beta$ , defined by:

$$s \frac{\partial}{\partial \alpha} = \varpi \frac{\partial}{\partial t} + (w_{\perp 0} + w_{\perp} + s) \frac{\partial}{\partial \eta}$$

$$-s \frac{\partial}{\partial \beta} = \varpi \frac{\partial}{\partial t} + (w_{\perp 0} + w_{\perp} - s) \frac{\partial}{\partial \eta}$$

where  $\varpi = \text{constant}$ ,

we may write the initial value problem considered in the preceding section as:

$$-s^2 \frac{\partial^2}{\partial \alpha \partial \beta} w_{\perp} = \frac{s}{2} \left( \frac{\partial}{\partial \alpha} - \frac{\partial}{\partial \beta} \right) f$$

$$- \frac{\pi G \varpi}{2 |k|} \left[ \left( \frac{\partial}{\partial \alpha} + \frac{\partial}{\partial \beta} \right) (\sigma_0 + \sigma_1) \right] \left[ \left( \frac{\partial}{\partial \alpha} + \frac{\partial}{\partial \beta} \right) w_{\perp} \right] \quad (22.1)$$

$$s \left( \frac{\partial}{\partial \alpha} - \frac{\partial}{\partial \beta} \right) a + \frac{\gamma-1}{2} a \left( \frac{\partial}{\partial \alpha} + \frac{\partial}{\partial \beta} \right) w_{\perp} = 0 \quad (22.2)$$

$$\frac{s}{2} \left( \frac{\partial}{\partial \alpha} - \frac{\partial}{\partial \beta} \right) w_{\parallel} + \left( \frac{K^2}{2\Omega} \right) w_{\perp} = 0 \quad (22.3)$$

$$s \left( \frac{\partial}{\partial \alpha} - \frac{\partial}{\partial \beta} \right) \sigma_1 + (\sigma_0 + \sigma_1) \left( \frac{\partial}{\partial \alpha} + \frac{\partial}{\partial \beta} \right) w_{\perp} = 0 \quad (22.4)$$

and

$$\frac{\partial \eta}{\partial \alpha} = (w_{\perp 0} + w_{\perp} + s) \frac{1}{\omega} \frac{\partial t}{\partial \alpha} \quad (22.5)$$

$$\frac{\partial \eta}{\partial \beta} = (w_{\perp 0} + w_{\perp} - s) \frac{1}{\omega} \frac{\partial t}{\partial \beta} \quad (22.6)$$

with initial conditions:

$$t = 0 \quad \eta = 2\alpha = 2\beta$$

$$a = a_0 \quad \sigma = \sigma_0 \quad w_{\perp} = 0 \quad w_{\parallel} = 0$$

### Solution by Perturbation Series

A solution to this initial value problem will be attempted in the form of a perturbation series in which each of the quantities,  $w_{\perp}$ ,  $w_{\parallel}$ ,  $a$ ,  $s$ ,  $\sigma_1$ ,  $t$ , and  $\eta$ , is expressed in the form:

$$q(\alpha, \beta) = q^{(0)}(\alpha, \beta) + \epsilon q^{(1)}(\alpha, \beta) + \epsilon^2 q^{(2)}(\alpha, \beta) + \dots \quad (22.7)$$

At this point we adopt an approximate form of the imposed spiral perturbation force field which will be adequate for our purposes of determining possible shock formation about the spiral galactic model. We take  $f$  of the form:

$$f(\alpha, \beta) = \begin{cases} 0 & t(\alpha, \beta) < 0 \\ \epsilon k V \sin k \eta^{(0)}(\alpha, \beta) & t(\alpha, \beta) \geq 0 \end{cases} \quad (22.8)$$

where  $\epsilon, k, V = \text{constants}; \quad \epsilon \ll 1.$

Expansion of  $s$  yields:

$$s^{(0)} = s_0 = (a_0^2 + \frac{K^2 \omega^2}{k^2} - \frac{2\pi G \omega \sigma_0}{|k|})^{1/2}$$

If equations (22.1) - (22.6) are written in the form of the perturbation series (22.7), and if terms of like powers of  $\epsilon$  are equated, these nonlinear equations (22.1) - (22.6) reduce to a series of systems of six linear equations each. The solution of this series of systems of linear equations to  $\mathcal{O}(\epsilon^2)$  for the physical quantities may be written in the form of the perturbation series (22.7):

$$\begin{aligned} w_{\perp 0} + w_{\perp}(\alpha, \beta) &= w_{\perp 0} + \epsilon \frac{V}{2s_0} \left[ \frac{1}{\lambda + 1} \cos 2k\beta + \frac{1}{\lambda - 1} \cos 2k\alpha \right. \\ &\quad \left. - \frac{2\lambda}{\lambda^2 - 1} \cos k((\lambda + 1)\alpha - (\lambda - 1)\beta) \right] \\ &+ \mathcal{O}(\epsilon^2) \end{aligned} \quad (22.9)$$

$$\begin{aligned}
w_{II0} + w_{II}(\alpha, \beta) &= w_{II0} + \varepsilon \left( \frac{K^2}{2\Omega} \right) \frac{\omega V}{2ks_0^2} \left[ \frac{1}{\lambda + 1} \sin 2k\beta \right. \\
&\quad \left. - \frac{1}{\lambda - 1} \sin 2k\alpha + \frac{2}{\lambda^2 - 1} \sin k((\lambda + 1)\alpha - (\lambda - 1)\beta) \right] \\
&\quad + \mathcal{O}(\varepsilon^2) \tag{22.10}
\end{aligned}$$

$$\begin{aligned}
a(\alpha, \beta) &= a_0 + \varepsilon \left( \frac{\gamma - 1}{2} \right) \frac{a_0 V}{2s_0^2} \left[ \frac{1}{\lambda + 1} \cos 2k\beta - \frac{1}{\lambda - 1} \cos 2k\alpha \right. \\
&\quad \left. + \frac{2}{\lambda^2 - 1} \cos k((\lambda + 1)\alpha - (\lambda - 1)\beta) \right] \\
&\quad + \mathcal{O}(\varepsilon^2) \tag{22.11}
\end{aligned}$$

$$\begin{aligned}
\sigma(\alpha, \beta) &= \sigma_0 + \varepsilon \frac{\sigma_0 V}{2s_0^2} \left[ \frac{1}{\lambda + 1} \cos 2k\beta - \frac{1}{\lambda - 1} \cos 2k\alpha \right. \\
&\quad \left. + \frac{2}{\lambda^2 - 1} \cos k((\lambda + 1)\alpha - (\lambda - 1)\beta) \right] \\
&\quad + \mathcal{O}(\varepsilon^2) \tag{22.12}
\end{aligned}$$

$$\begin{aligned}
\frac{1}{\omega} t(\alpha, \beta) &= \frac{1}{s_0} (\alpha - \beta) + \varepsilon \frac{1}{2s_0^2} \left\{ (C_{1+} \cos 2k\alpha - B_{1+} \cos 2k\beta)(\alpha - \beta) \right. \\
&+ \frac{1}{2k} (B_{1-} - C_{1-})(\sin 2k\alpha - \sin 2k\beta) \\
&+ \frac{1}{k} \left( \frac{A_{1+}}{\lambda - 1} \sin 2k\alpha - \frac{A_{1-}}{\lambda + 1} \sin 2k\beta \right) \\
&+ \left. \frac{1}{k} \left( \frac{A_{1-}}{\lambda + 1} - \frac{A_{1+}}{\lambda - 1} \right) \sin k((\lambda + 1)\alpha - (\lambda - 1)\beta) \right\} \\
&+ \dots + \mathcal{O}(\varepsilon^2(\alpha - \beta)) + \dots
\end{aligned} \tag{22.13}$$

$$\begin{aligned}
n(\alpha, \beta) &= (\lambda + 1)\alpha - (\lambda - 1)\beta \\
&+ \varepsilon \frac{1}{2s_0} \left\{ ((\lambda + 1)C_{1+} \cos 2k\alpha - (\lambda - 1)B_{1+} \cos 2k\beta)(\alpha - \beta) \right. \\
&+ \frac{1}{2k} ((\lambda + 1)B_{1-} - (\lambda - 1)C_{1-})(\sin 2k\alpha - \sin 2k\beta) \\
&+ \frac{1}{k} \left( \frac{\lambda + 1}{\lambda - 1} A_{1+} \sin 2k\alpha - \frac{\lambda - 1}{\lambda + 1} A_{1-} \sin 2k\beta \right) \\
&+ \left. \frac{1}{k} \left( \frac{\lambda - 1}{\lambda + 1} A_{1-} - \frac{\lambda + 1}{\lambda - 1} A_{1+} \right) \sin k((\lambda + 1)\alpha - (\lambda - 1)\beta) \right\} \\
&+ \dots + \mathcal{O}(\varepsilon^2(\alpha - \beta)) + \dots
\end{aligned} \tag{22.14}$$

where

$$A_{1\pm} = \frac{V}{s_0} \left( \frac{\lambda \pm \Delta}{\lambda^2 - 1} \right) \quad B_{1\pm} = \frac{V}{2s_0} \left( \frac{1 \pm \Delta}{\lambda \pm 1} \right) \quad C_{1\pm} = \frac{V}{2s_0} \left( \frac{1 \pm \Delta}{\lambda - 1} \right)$$

and

$$\Delta = \frac{\gamma-1}{2} \frac{a_0^2}{s_0^2} - \frac{\pi G \omega \sigma_0}{|k| s_0^2}$$

This solution for the problem of unsteady gas flow about a spiral galaxy is similar to the solution for the problem of unsteady one dimensional gas flow with self gravitation considered in Part III A. We could go ahead and calculate the  $\mathcal{O}(\epsilon^2)$  terms and higher order terms of the perturbation series solution; however, the  $\mathcal{O}(\epsilon)$  terms will be sufficient for indicating the formation of shocks. In general, the higher order terms of  $t(\alpha, \beta)$  and  $n(\alpha, \beta)$  depend on  $(\alpha - \beta)$  only to the first power. Therefore, the perturbation series remains valid up to the shock region and a little beyond just as in the case of one dimensional gas flow.

### 23. Shock development in a spiral galaxy

In the preceding section we have determined a perturbation series solution for an initial value problem of gas flow about a spiral galaxy. Now we wish to look for possible shock development in the galaxy as the outgrowth of such gas flow.

The perturbation series solution for the case,  $\lambda \neq 1$ , may be described by three density waves: one corotating density wave and two density waves which propagate through the pattern. It is evident that shocks cannot develop from the corotating density wave. As in the one dimensional gas flow problem, we are then left with the alternative of considering the two other portions of the solution and of determining what influence they may have on shock development. Both of these density waves contain compression and rarefaction regions. As each plane wave propagates, the compression portions tend to steepen and develop into shock fronts, whereas the rarefaction portions tend to smooth out more continuously. Therefore, after a long enough time has elapsed, we might expect shock fronts to develop periodically along the  $\eta$  direction.

Two types of shocks therefore develop in the initial value problem in which the base state flow is not equal to the dispersion speed. Figures (23.1) and (23.2) illustrate the nature of these two types of shocks for both subcritical<sup>1</sup> and supercritical base

---

<sup>1</sup>"Critical" refers to base state flow in which  $\lambda (= w_o/s_o) = 1$ . Critical base state flow is actually supersonic in the Galaxy.

state gas flow. After a sufficiently long time on the order:

$$t_s = \frac{2s_o \omega |\lambda - 1|}{\epsilon k V \left( 1 + \frac{\gamma - 1}{2} \frac{a_o^2}{s_o^2} - \frac{\pi G \omega \sigma_o}{|k| s_o^2} \right)} \quad (23.1)$$

the density wave propagating at a speed  $(w_o - s_o)$  gives rise to shocks propagating at the same speed. After a somewhat longer time on the order:

$$t_s = \frac{2s_o \omega (\lambda + 1)}{\epsilon k V \left( 1 + \frac{\gamma - 1}{2} \frac{a_o^2}{s_o^2} - \frac{\pi G \omega \sigma_o}{|k| s_o^2} \right)} \quad (23.2)$$

the density wave propagating at a speed  $(w_o + s_o)$  gives rise to shocks propagating at the same speed. The time it takes for the formation of shocks becomes longer; the smaller the amplitude of the spiral field, or the larger the base state turbulent dispersion speed.



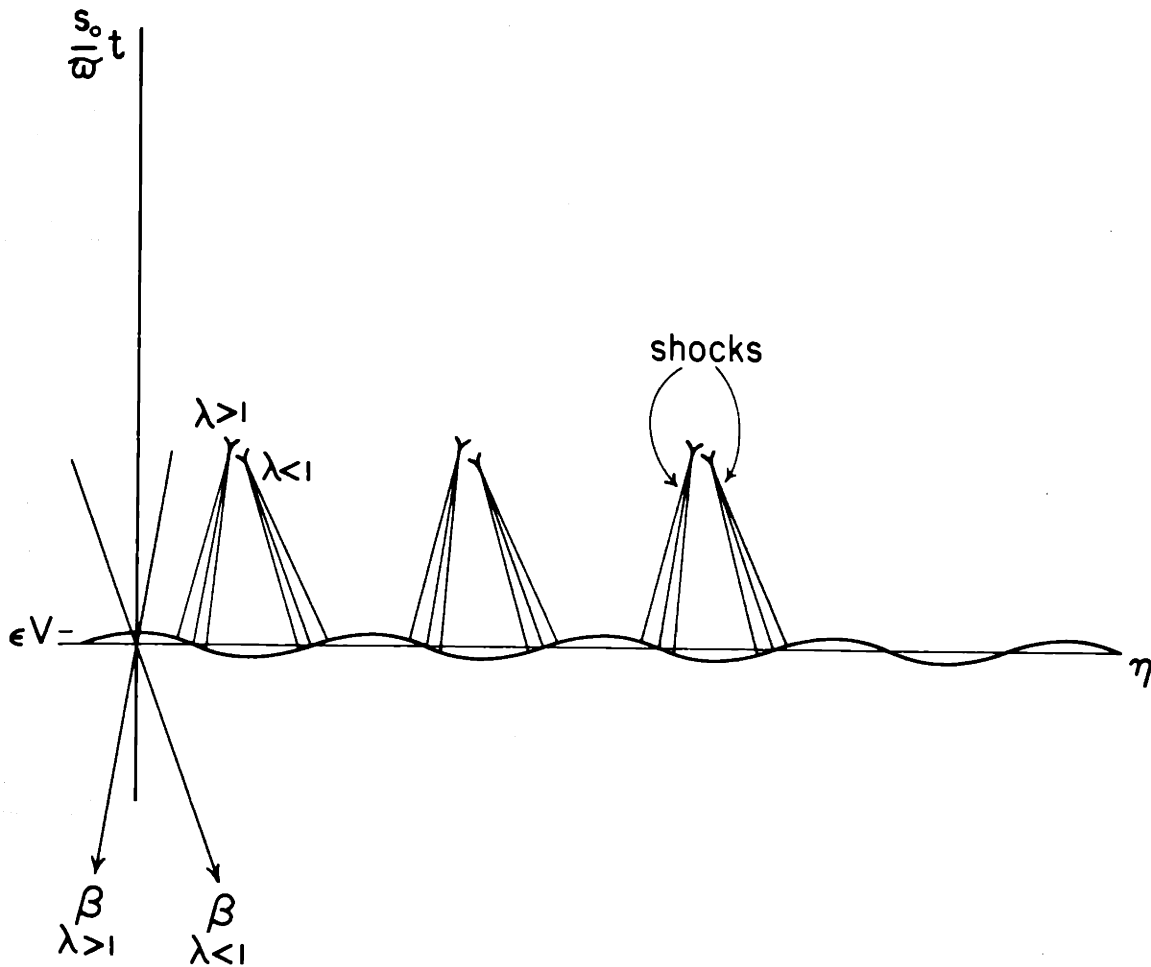


Figure (23.1)  
 The Development of Galactic Shocks Propagating at a  
 Speed ( $W_{10} - S_0$ ) Through the Field

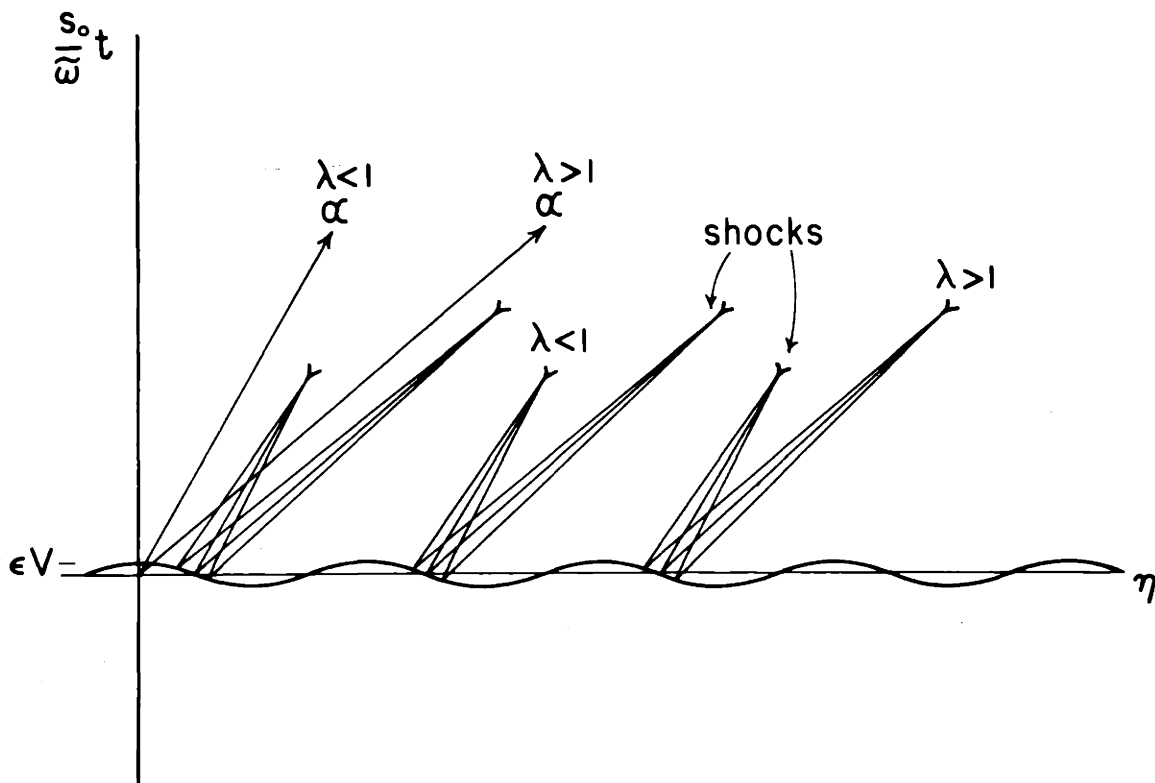


Figure (23.2)  
 The Development of Galactic Shocks Propagating at a  
 Speed  $(W_{\perp 0} + S_0)$  Through the Field

24. Spiral shock of most rapid development; the Lin-Shu neutral density wave mode

So far we have not examined the possibility for the formation of corotating shocks in the Galaxy. In the initial value problem for the cases of subcritical and supercritical base state flow, we have only shown that the development of non-corotating shocks is possible. Suppose we now consider the case in which the base state flow is equal to the dispersion speed (i.e.,  $\lambda = 1$ ). The perturbation series solution for this case is:

$$\begin{aligned}
 w_{\perp 0} + w_{\perp}(\alpha, \beta) &= w_{\perp 0} + \epsilon \frac{V}{4s_0} \left\{ 2k \sin 2k\alpha (\alpha - \beta) - \cos 2k\alpha \right. \\
 &\quad \left. + \cos 2k\beta \right\} + \dots + \mathcal{O}(\epsilon^n (\alpha - \beta)^n) + \dots \\
 n &= 2, 3, \dots \quad (24.1)
 \end{aligned}$$

$$\begin{aligned}
 w_{\parallel 0} + w_{\parallel}(\alpha, \beta) &= w_{\parallel 0} + \epsilon \left( \frac{K^2}{2\Omega} \right) \frac{\omega V}{4ks_0^2} \left\{ -2k \cos 2k\alpha (\alpha - \beta) \right. \\
 &\quad \left. + \sin 2k\alpha - \sin 2k\beta \right\} + \dots + \mathcal{O}(\epsilon^n (\alpha - \beta)^n) + \dots \\
 &\quad (24.2)
 \end{aligned}$$

$$\begin{aligned}
 a(\alpha, \beta) &= a_0 + \epsilon \frac{\gamma-1}{2} \frac{a_0 V}{4s_0^2} \left\{ -2k \sin 2k\alpha (\alpha - \beta) - \cos 2k\alpha \right. \\
 &\quad \left. + \cos 2k\beta \right\} + \dots + \mathcal{O}(\epsilon^n (\alpha - \beta)^n) + \dots \quad (24.3)
 \end{aligned}$$

$$\begin{aligned} \sigma(\alpha, \beta) = & \sigma_0 + \epsilon \frac{\sigma_0 V}{4s_0^2} \left[ -2k \sin 2k\alpha (\alpha - \beta) - \cos 2k\alpha \right. \\ & \left. + \cos 2k\beta \right] + \dots + \mathcal{O}(\epsilon^n (\alpha - \beta)^n) + \dots \end{aligned} \quad (24.4)$$

$$\begin{aligned} \frac{1}{\omega} t(\alpha, \beta) = & \frac{1}{s_0} (\alpha - \beta) + \epsilon \frac{1}{2s_0^2} \left[ kB_{1+} \sin 2k\alpha (\alpha - \beta)^2 \right. \\ & \left. - B_{1+} \cos 2k\beta (\alpha - \beta) + \frac{B_{1+}}{2k} (\sin 2k\alpha - \sin 2k\beta) \right] \\ & + \dots + \mathcal{O}(\epsilon^n (\alpha - \beta)^{1+n}) + \dots \end{aligned} \quad (24.5)$$

$$\begin{aligned} n(\alpha, \beta) = & 2\alpha + \epsilon \frac{1}{s_0} \left\{ kB_{1+} \sin 2k\alpha (\alpha - \beta)^2 - B_{1-} \cos 2k\alpha (\alpha - \beta) \right. \\ & \left. + \frac{B_{1-}}{2k} (\sin 2k\alpha - \sin 2k\beta) \right\} + \dots + \mathcal{O}(\epsilon^n (\alpha - \beta)^{1+n}) + \dots \end{aligned} \quad (24.6)$$

Upon examination of this perturbation series solution we find that corotating shocks may develop. Figure (24.1) illustrates the nature and the location of these shocks. Such corotating shocks develop in a time of the order:

$$t_s = \frac{1}{(\epsilon V)^{1/2} k \left( 1 + \frac{\gamma-1}{2} \frac{a_0^2}{s_0^2} - \frac{\pi G \sigma_0}{|k| s_0^2} \right)^{1/2}} \quad (24.7)$$

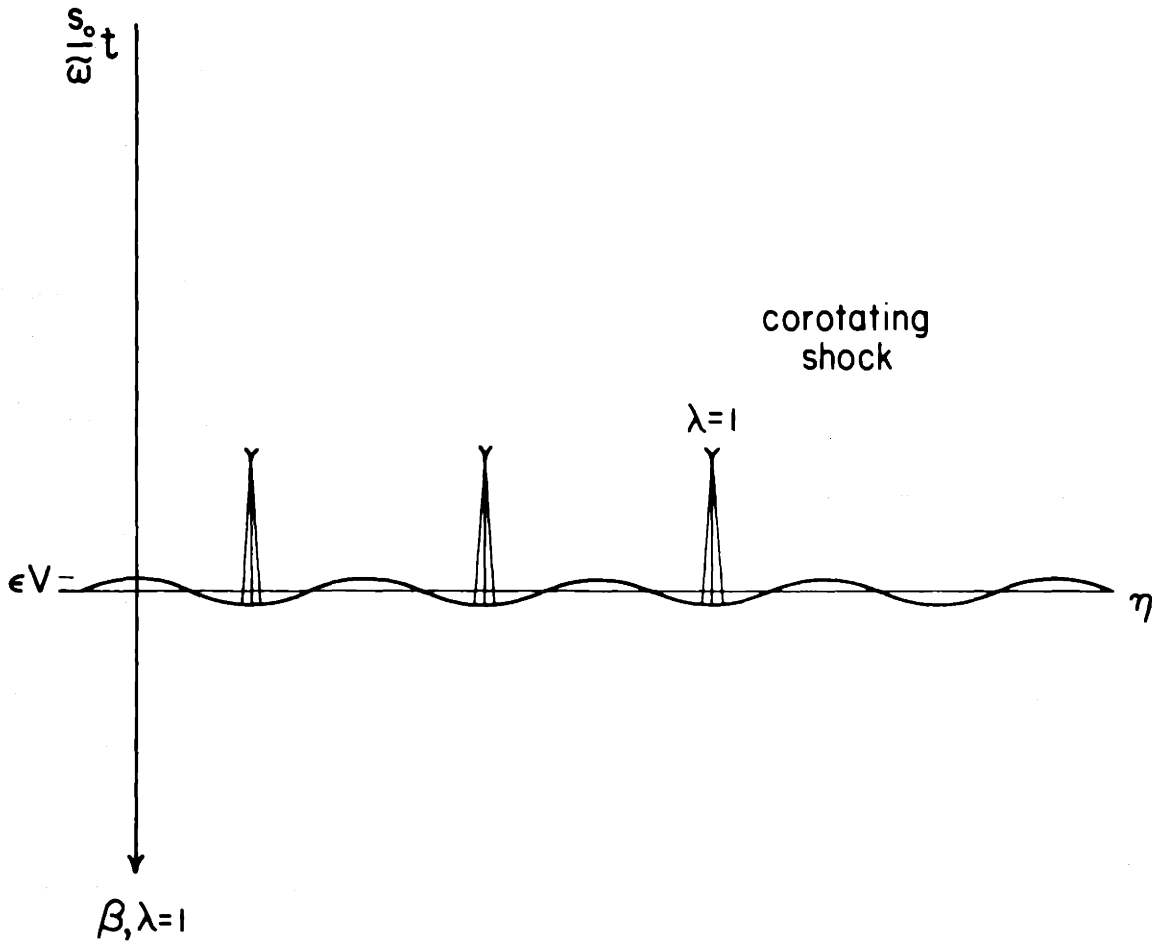


Figure (24.1)  
 The Development of Corotating Shocks in the Galaxy

If one encounters just two peaks of the spiral perturbation field as one moves in a complete cycle circumferentially about the galactic disk, then the number of corotating shocks to be expected would be two.

### Development of Isothermal Galactic Shocks

In the isothermal limit of  $\gamma = 1$ , those terms of the perturbation series solutions for both cases,  $\lambda \neq 1$  and  $\lambda = 1$ , which contain the factor,  $(\gamma-1)/2$ , approach zero. These isothermal solutions may well complement the numerical calculations of Part II. We shall see just how well they complement the TASS picture of the Galaxy in the following consideration of the type of shock preferred by a spiral disk-shaped galaxy.

### Theoretical Lin-Shu Picture of a Disk-Shaped Galaxy

We have seen the possibility for the formation of galactic shocks of various types: two types of non-corotating shocks (for subcritical and supercritical base state flow) and one corotating shock (for critical base state flow). In general, the base state gas flow predetermines what types of shocks may form.

Now that we have seen the various types of shocks possible under the various circumstances involved, we ask what type of initial value problem (subcritical, critical, or supercritical) is actually the one that may best characterize a spiral galaxy and what type of shock thereby may be preferred by the spiral galaxy. To determine such a preference for one or another of the types of shock waves, the base

state flow characteristic of a spiral galaxy must be determined.

Suppose we consider the theoretical Lin-Shu picture of spiral disk-shaped galaxies in which the spiral grand design is composed of density waves of gas and stars obeying the Lin-Shu dispersion relationship:

$$|k_{L-S}| = \frac{K^2 - 4(\Omega_p - \Omega)^2}{2\pi G [\sigma_0 F_v(x_g) + \sigma_* \bar{F}_v(x)]} \quad (24.8)$$

where

$k_{L-S}$  is the dimensional wave number of the spiral pattern; i.e.,  $k_{L-S} = \frac{k}{\omega}$ ,  
 $F_v(x_g)$  and  $\bar{F}_v(x)$  are gaseous and stellar reduction factors, and  
 $\sigma_*$  is the stellar base state density.

Suppose a spiral galaxy contains a density wave of small amplitude that satisfies this dispersion relationship. We may ask what type of shock formation, if any, is preferred. If we retain for the moment only the gaseous component, and if we rewrite the dispersion relationship in terms of  $k$  and  $w_{\perp 0}$ , we have:

$$w_{\perp 0}^2 - \left( \frac{K^2 \omega^2}{k^2} + a^2 - \frac{2\pi G \omega \sigma_0}{|k|} \right) = 0 \quad (24.9)$$

Since the terms making up the large bracket have been defined earlier as  $s_o^2$ , this relation is precisely the relation:

$$w_o^2 = s_o^2$$

or

$$\lambda = 1 \tag{24.10}$$

The initial value problem, in which the base state flow is "critical", is in fact the initial value problem most characteristic of and preferred by the theoretical Lin-Shu picture of spiral disk-shaped galaxies. This leads us to the important conclusion that a spiral galaxy may actually prefer the formation of corotating shocks rather than any other type of shocks (i.e., non-corotating shocks). The neutral density wave mode making up the grand design of spiral structure in the linear density wave theory is therefore a special mode; for, it is precisely this density wave mode and no other that can insure the case,  $\lambda = 1$ , and can provide for the formation of the corotating shock wave.

In addition, since the corotating shock is the most rapidly developing shock, it may be expected to dominate over any non-corotating shocks which might arise extraneously. For a small field of 1% of the axisymmetric field and a spiral pattern spacing between



arms that is consistent with  $\tan i = 1/7$ , the time scale for the formation of the corotating shock is equivalent to the time period of a few rotations of the grand design about the disk.

## Part IV - Star Formation

In Part II, we have seen that a stationary TASS pattern is compatible with the general nature of gas flow about the galactic disk. On the other hand, in Part III, we have seen how spiral galactic shock waves may evolve from density waves during a few rotations of the disk. Now we direct our attention toward the physical phenomena which the TASS pattern might trigger. We ask if the luminous spiral pattern outlined by the newly-born luminous stars and brilliant H II regions in our Galaxy might be a direct consequence of the galactic shock pattern.

In Part IV, we explore this question. First, a picture of the gaseous mass distribution in the interstellar medium is envisaged. Next we investigate two mechanisms which may very likely contribute toward star formation in our Galaxy: accretion and the galactic shock wave. Once we see how these mechanisms may provide for star formation, we construct a cloud-subcloud model of the interstellar medium on which these two mechanisms may act to form stars. Some classic problems associated with star formation are next investigated. In the final two sections, the essence of star formation appears: the candidates for proto-stars are envisaged; newly-born stars are found to be present only in stellar associations in general agreement with observations; and the brilliant grand design of spiral structure in the Galaxy comes to light.

25. Gas clouds: the constituents of the interstellar medium

From observational studies of our Milky Way System (for example, the photographs of Morgan, Stromgren, and Johnson (1955), it is apparent that the actual space distribution of interstellar matter is extremely irregular. In reference to these particular photographs, Spitzer (1968) points out that irregularities of all discernible scales are evidently present, ranging from globules a few thousand astronomical units across to complexes of clouds extending over several hundred parsecs. Possessing such an irregular structure, the gaseous disk exhibits the characteristics of a nonquiescent gaseous continuum<sup>1</sup> in a state of turbulent motion; and the individual gaseous mass elements comprising this continuum exhibit the character of turbulent eddies and fragments.<sup>2</sup> Therefore, the processes of fragmentation and disintegration of the turbulent fragments as well as the reverse process of reassociation may be well at work throughout the Galaxy as in any gaseous medium in turbulent motion at velocities exceeding that of sound.

We envisage gas concentrations of dimensions covering the entire spectrum of scales that may be maintained throughout the interstellar medium. Such a situation may be realized if an approximate statistical

---

<sup>1</sup>The mean-free-path of the atomic particle is still small compared with 1 pc. even when the gaseous density is as low as 1 H/cc.

<sup>2</sup>The scale of an eddy or fragment may be taken as the distance over which the velocity or density varies appreciably.

equilibrium exists among the turbulent fragments of all scales. In reality, the spectrum of turbulence however may be such that we may distinguish two ranges of scale, one much larger than the other. In this picture, we visualize the existence of large clouds and large cloud complexes, both covering the range of larger scale, and also smaller clouds and subclouds, each on the much smaller scale in the interstellar medium.

A number of models have been proposed to account for this picture of the turbulent galactic interstellar medium. Of these, the discrete-cloud model is perhaps the simplest and most widely used. In this model, spherical clouds on the galactic scale serve the same function as molecules in an ordinary laboratory gas. Just as the molecular mean-free-path is an important length-scale in an ordinary laboratory gas, the mean-free-path of a cloud is the important characteristic length-scale in the interstellar medium. First, when compared to the length-scale of the whole system, it provides a measure of the degree of rarefaction of the medium; and secondly, if a shock wave is present on a galactic scale, it provides a characteristic scale for the shock width.<sup>1</sup>

The model we shall consider is a modified version of the discrete-cloud model and consists of two basic portions: first, the discrete nonquiescent large clouds,<sup>2</sup> all of the same radius dispersed throughout space; and second, the nonquiescent intercloud medium filling the

---

<sup>1</sup> Later we shall see that a large-scale galactic shock wave may serve as an essential triggering mechanism for the collapse of gas clouds and the formation of stars along a grand design of spiral structure.

<sup>2</sup> These large clouds may be referred to as cloud complexes according to one's preference.

total volume of space apart from that of the large clouds.<sup>1</sup> If the total volume of large clouds is small compared with the intercloud volume, the local galactic picture is one of an isolated gas cloud of relatively high density embedded in a rarefied medium of gas, all in turbulent motion. In this nonquiescent picture, spatial inhomogeneities of density in the interstellar medium (e.g. clouds versus intercloud space) are accounted for by turbulence rather than by thermal instabilities. In order for the maintenance of pressure equilibrium on the cloud envelope between interior and exterior portions, the density contrast between cloud and intercloud space must be proportional to the square of the Mach number corresponding to the mean supersonic motion of the clouds throughout the interstellar medium.<sup>2</sup> Due to the relatively rapid radiation of thermal energy by the gas inside a cloud, a whole local neighborhood containing a cloud and its surrounding intercloud medium may be kept at a fairly uniform kinetic temperature. If the state of turbulence in the local neighborhood does not change appreciably, and the effective turbulent temperature remains uniform and unchanged, the local picture may be taken to consist of an isothermal sphere of gas

---

<sup>1</sup>In later investigation of protostar formation, we shall envisage these two portions, the large clouds and the intercloud volume, to consist of dense and rarefied concentrations of small clouds (subclouds).

<sup>2</sup>A crude approximation to the pressure inside a cloud is given by the product of the mean density of the cloud and the square of the mean acoustic speed inside the cloud. A crude approximation to the pressure outside a cloud is given by the product of the mean density of intercloud space and the square of the mean turbulent dispersion speed of the clouds themselves. The density contrast between cloud and intercloud space is therefore (in this crude sense) proportional to the square of (mean turbulent dispersion speed of clouds/mean acoustic speed inside the clouds.)

(at an equivalent temperature, partly kinetic and partly due to turbulence) in thermal equilibrium with the surrounding rarefied gaseous medium. Before specifying values for the dimensions, densities, temperatures, etc. of the components of our gas cloud model, we shall first discuss various processes contributing to gas cloud collapse and possibly to star formation in order to determine what values are most likely.

## 26. Accretion

A process that may enhance the prospects for the collapse of a large gas cloud over a relatively long time period<sup>1</sup> is the well known process of accretion. All massive clouds and cloud complexes, which are large enough, tend to accrete more mass by inelastic collisions with smaller clouds and subclouds of smaller masses. In this picture all clouds above a certain (vaguely defined) mass tend to become more massive. If indeed the spectrum of turbulence in the interstellar medium is such that we may distinguish two ranges of scale, one much larger than the other, then the process of accretion may provide the answer to the problem of how two diverse ranges of scale may have evolved in the first place. In any case, we have in mind a picture in which the large gas clouds during their motions in the interstellar medium tend to accrete the immediately surrounding smaller scale masses and grow in mass themselves until they eventually reach their verges of gravitational collapse.

While these accretion and condensation processes of the large clouds may play their roles in star formation, so also will the processes of fragmentation and disintegration play their roles. The feature of dissociation and fragmentation on the large scale as well as on all the

---

<sup>1</sup>Kahn (personal communication) estimates that 50 million years may be a typical time scale for the evolution of gas clouds to their verges of gravitational collapse by accretion only (in a gaseous medium with mean density of about 1 H/cc).

other scales possibly causes all gas concentrations and rarefactions to exhibit a rather temporary and nonpermanent character. Although some of the largest clouds may undergo appreciable mass accretion despite their tendencies toward fragmentation, only a few (some small fraction of the total number of clouds) would be able to grow in size and concentration and reach their verges of gravitational collapse under accretion before dissociation processes dispersed the concentrations. More definitely, even fewer turbulent subclouds would be able to reach their verges of gravitational collapse in this picture since gravitational collapse is even less easily accessible for smaller masses.

On the other hand, if a large cloud were to pass through a large-scale galactic shock wave which could help trigger the gravitational collapse of the massive cloud, then perhaps the processes of fragmentation and disintegration, which counterbalance the process of accretion throughout the journey of the cloud, could be swiftly overcome inside the shock region. In this situation, the process of accretion<sup>1</sup>, which acts to increase the mass of a large cloud throughout its prior journey before reaching the shock, and the galactic shock wave combine toward bringing about the gravitational collapse of the large cloud. Either mechanism may be sufficient by itself in achieving gas cloud collapse under particular circumstances. Whereas accretion may occur continuously over the entire disk providing for a homogeneous distribution of

---

<sup>1</sup>Accretion by large clouds most certainly speeds up inside the shock region and in the subsonic region behind the shock.



collapsing gas clouds, the galactic shock<sup>1</sup> provides for a narrow spiral band of collapsing gas clouds only in the spiral pattern along which it lies. The process of accretion and the galactic shock, acting together, may well enhance star formation in an outstanding grand design of spiral structure in the Galaxy.<sup>2</sup>

---

<sup>1</sup>This is the large-scale shock comprising the two-armed spiral galactic shock pattern of Part II.

<sup>2</sup>The grand design of spiral shock structure as well as the interior region of the shock will be investigated in later sections (see Sections 28 and 31).

27. Shock wave-triggered gravitational collapse of a large gas cloud

The process of gravitational collapse of an isolated system similar to a cloud of our model but containing no turbulence is well known (see Chandrasekhar, 1942; Ebert, 1955; and Spitzer, 1968). The system generally considered and outlined in these references contains a quiescent isothermal sphere of gas, embedded in a rarefied gaseous medium maintained at constant pressure. Qualitative results for the gravitational instability of a nonquiescent cloud in our model (analogous to the well known results for a quiescent cloud model whose total temperature is the kinetic temperature) may be stated in summarized form in the following way. For a given cloud (in our nonquiescent model) of mass  $M$ , at a kinetic temperature  $T$ , and with an internal root mean square turbulent dispersion speed,  $(\overline{v^2})^{1/2}$ , corresponding to an effective turbulent temperature, there is a maximum surface pressure,  $p_{\max}$ , dependent on the total equivalent temperature (partly kinetic and partly due to turbulence) which the isothermal cloud can withstand. For a surface pressure somewhat less than  $p_{\max}$  two equilibrium configurations are possible: first, an extended configuration, with relatively uniform density, which is stable; and second, a compact configuration, much more centrally condensed, which is unstable. If the surface pressure were increased to a value exceeding  $p_{\max}$ , no equilibrium configuration would be possible, and the cloud would be forced into rapid gravitational collapse. It is this latter situation of no equilibrium configuration into

which the large clouds may be forced by a galactic shock wave.

In this picture, turbulence endows the gas cloud with an effective turbulent temperature and pressure in addition to the quiescent kinetic temperature and pressure, which together provide the cloud with an equivalent temperature and pressure. Whereas the kinetic temperature and pressure are the significant variables for a quiescent gas cloud, it is the equivalent temperature and pressure that are the significant variables for the nonquiescent system. A few essentials of the nonquiescent cloud picture will be given in order (1) to demonstrate the importance and necessity of a triggering mechanism for gas cloud collapse such as a shock wave and (2) to illustrate an important difference between the quiescent and nonquiescent pictures that bears directly on the continual formation of young stellar associations in the present day as well as throughout the history of the Galaxy.

The maximum pressure and minimum radius of all equilibrium configurations which the cloud with mass  $M$  and equivalent temperature  $T_{\text{equiv}}$  can endure are given by the relations:<sup>1</sup>

$$p_{\text{max}} = 1.4 \frac{\left(\frac{kT_{\text{equiv}}}{m_p}\right)^4}{G M}$$

$$R_{\text{min}} = 0.41 \frac{GM}{\left(\frac{kT_{\text{equiv}}}{m_p}\right)}$$

---

<sup>1</sup>These results are analogous to the well known results of a quiescent cloud model where  $T_{\text{equiv}}$  is replaced by  $T$ , the kinetic temperature. c.f. Spitzer (1968).

where  $k$  is the Boltzmann constant and  $m_p$  denotes the mean particle mass.  $T_{\text{equiv}}$  may be taken of the form:

$$T_{\text{equiv}} = (a^2 + k_1 \overline{v^2})$$

where  $a$  is the ordinary acoustic speed, and  $k_1$  is a constant of order unity. The equivalent temperature is taken constant during the collapse process. This may be a valid approximation if two requirements are satisfied: first, if turbulent dissipation is sufficiently rapid to maintain a uniform and unchanged state of turbulence; and second, if the cloud medium is transparent to the internally-generated radiation, thereby insuring no appreciable internal heating due to absorption of radiation by interior portions of the cloud.

#### Typical large galactic gas clouds

Spitzer (1968) discusses some typical large galactic gas clouds taken from observational studies. Table (27.1) lists some of these typical large clouds. The kinetic temperatures of clouds of these types have been generally determined to lie within the range of 60°K to 120°K. A value of 100°K might be a reasonable estimate for the mean kinetic temperature characteristic of this group of clouds as a whole.

Clark, Radhakrishnan, and Wilson (1962) in their observations of the Orion Nebula and the Omega Nebula among other regions of the sky discovered absorption profiles for the clouds that seem to indicate the

Table (27.1)

Typical Large Galactic Gas Clouds

Cloud Type	$M/M_{\odot}$	R(pc)	n(H/cc)
"large" cloud	$1.8 \times 10^4$	20	20
large cloud	$10^4$	17	20
"typical large" cloud	$7 \times 10^3$	15	20

existence of internal turbulent fragments, a few parsecs in size and having dispersion velocities of a few kilometers per second. Of the Orion Nebula, they suggest: "the clouds consist of small wisps of the order of size of a few minutes of arc, moving with a velocity of a few kilometers per second with respect to each other." Of the Omega Nebula, they state: "there are large scale motions in the cloud with a typical length of at least 5' (or 3 parsecs)." Other observers have also made estimates of the state of turbulence in galactic gas clouds, and it appears a root mean square turbulent dispersion speed between .5 and 2 km/s would signify a typical estimate of the state of turbulence.

#### Numerical results

A criterion for determining those clouds which are beyond their verges of gravitational collapse may be written in terms of  $\bar{n}$ ,  $M$ , and  $T_{\text{equiv}}$  as follows:

$$\bar{n}_{\text{crit}} = \mathcal{O}(10^3) \frac{(T_{\text{equiv}})^3}{\left(\frac{M}{M_{\odot}}\right)^2}$$

Those clouds with mean density  $\bar{n} > \bar{n}_{\text{crit}}$  are in the collapsing stage, whereas those with mean density  $\bar{n} < \bar{n}_{\text{crit}}$  are not so compact as to lie beyond their verges of gravitational collapse. For example, clouds of mass  $M = 10^4 M_{\odot}$  with equivalent temperature = 300°K require a critical density of about 270 H/cc for collapse under the influence

of their self gravitation without the influence of external compressive effects. Only those clouds of this type with a higher density than 270 H/cc are capable of collapsing themselves. This critical density represents a fairly high density; for, large clouds observed in the interstellar medium generally have densities nowhere near this large a value. It is, therefore, rather difficult to explain star formation and the present day formation of young stellar associations on the basis of the self gravitation of gas clouds alone without some other triggering mechanism.

On the other hand, suppose a galactic shock wave exists in the galactic disk. A criterion for determining those clouds which may reach their verges of gravitational collapse under the influence of a shock with a compression ratio of  $\lambda^2$  may be written:

$$\bar{n}_{\text{crit}} = 0 \left( \frac{10^3}{\lambda^2} \right) \frac{(T_{\text{equiv}})^3}{\left( \frac{M}{M_{\odot}} \right)^2}$$

Clearly, the stronger the shock strength, then the smaller the critical density and the greater the spectrum of large clouds which may be compressed beyond their verges of gravitational collapse in passage through the shock. For example, clouds of mass =  $10^4 M_{\odot}$  with an equivalent temperature of 300°K require a critical density of only about

19 H/cc for gravitational collapse under an 8:1 shock compression.<sup>1</sup> In their passage through the shock, all large clouds with a mean density  $\bar{n} < \bar{n}_{\text{crit}}$  will adjust into a new equilibrium state before reaching their verges of gravitational collapse and will not be candidates for young stellar associations. On the other hand, those large clouds with a mean density  $\bar{n} > \bar{n}_{\text{crit}}$  are likely candidates for young stellar associations. Therefore, unlike the nonshock picture, a definite spectrum of gas clouds, which can reach their verges of gravitational collapse, is present in this galactic shock picture.

Figures (27.1), (27.2), and (27.3) illustrate the criteria for gas cloud collapse under various shock compressions for each of the typical clouds listed in Table (27.1). Each figure considers clouds of a given mass and covers the spectrum of density and equivalent temperature. Several critical curves indicating the critical density for compressions of 1:1, 8:1, and 100:1 are sketched in each figure. In addition, several curves for different constant surface pressures on the clouds are sketched. All clouds that lie to the left of the 1:1 critical curve are already in a state of collapsing. In passage through a shock wave of 8:1 compression, all clouds that lie between the 1:1 and 8:1 critical curves are likely to reach their verges of gravitational collapse, whereas those that lie to the right of the 8:1 critical curve will not. We see that the large clouds listed in Table (27.1) may possess equivalent temperatures as high as 250°K, 307°K, and 460°K corresponding their respective masses of  $7 \times 10^3$ ,  $10^4$  and  $1.8 \times 10^4 M_{\odot}$  and still be capable of reaching their verges of gravi-

---

<sup>1</sup>An 8:1 compression is a typical shock strength for the large-scale galactic shock waves that may participate in the TASS pattern of our Galaxy (see Part II).



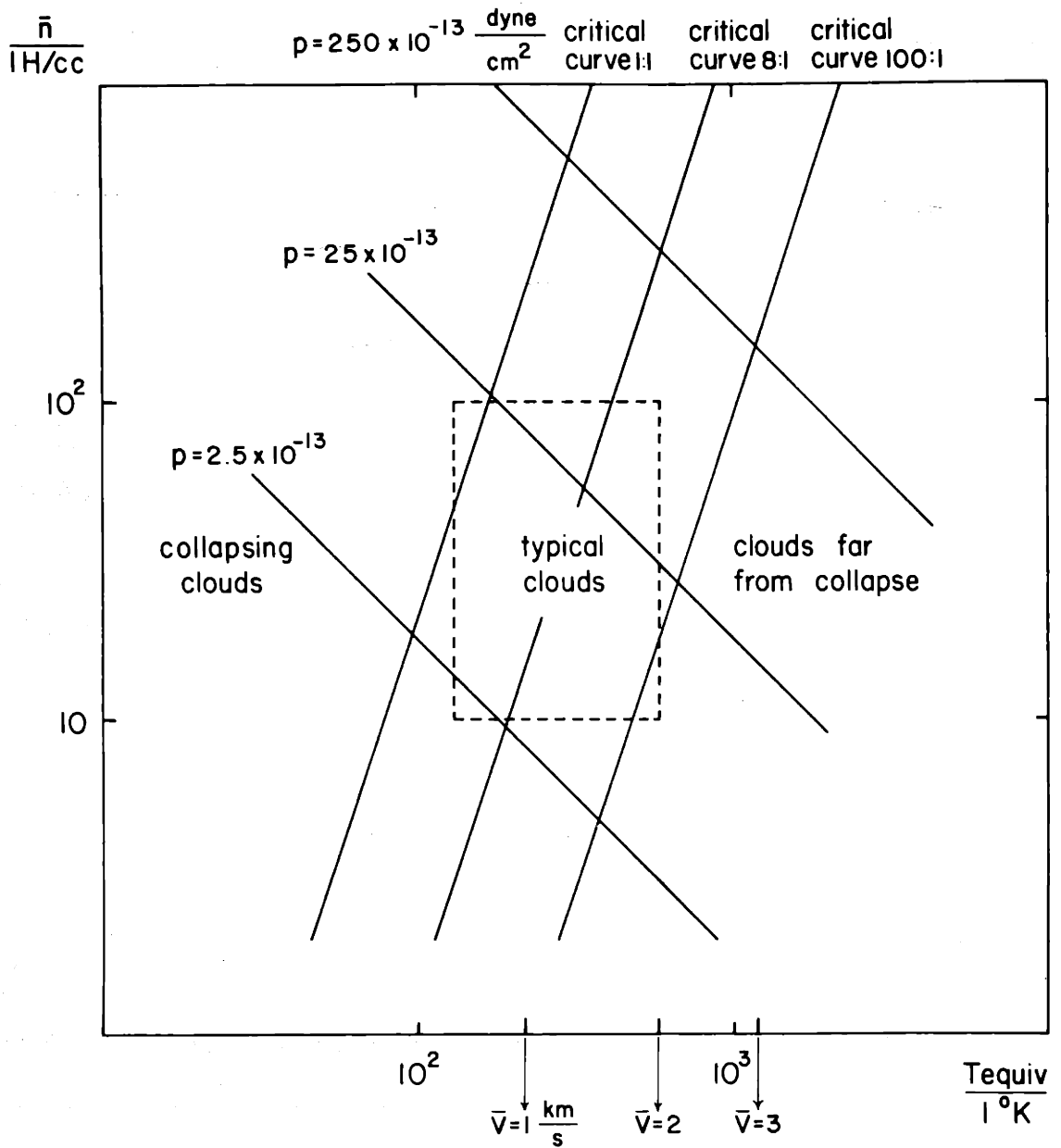


Figure (27.1)

The Collapse of Gas Clouds of Mass =  $7 \times 10^3 M_\odot$  Under Various Shock Strengths

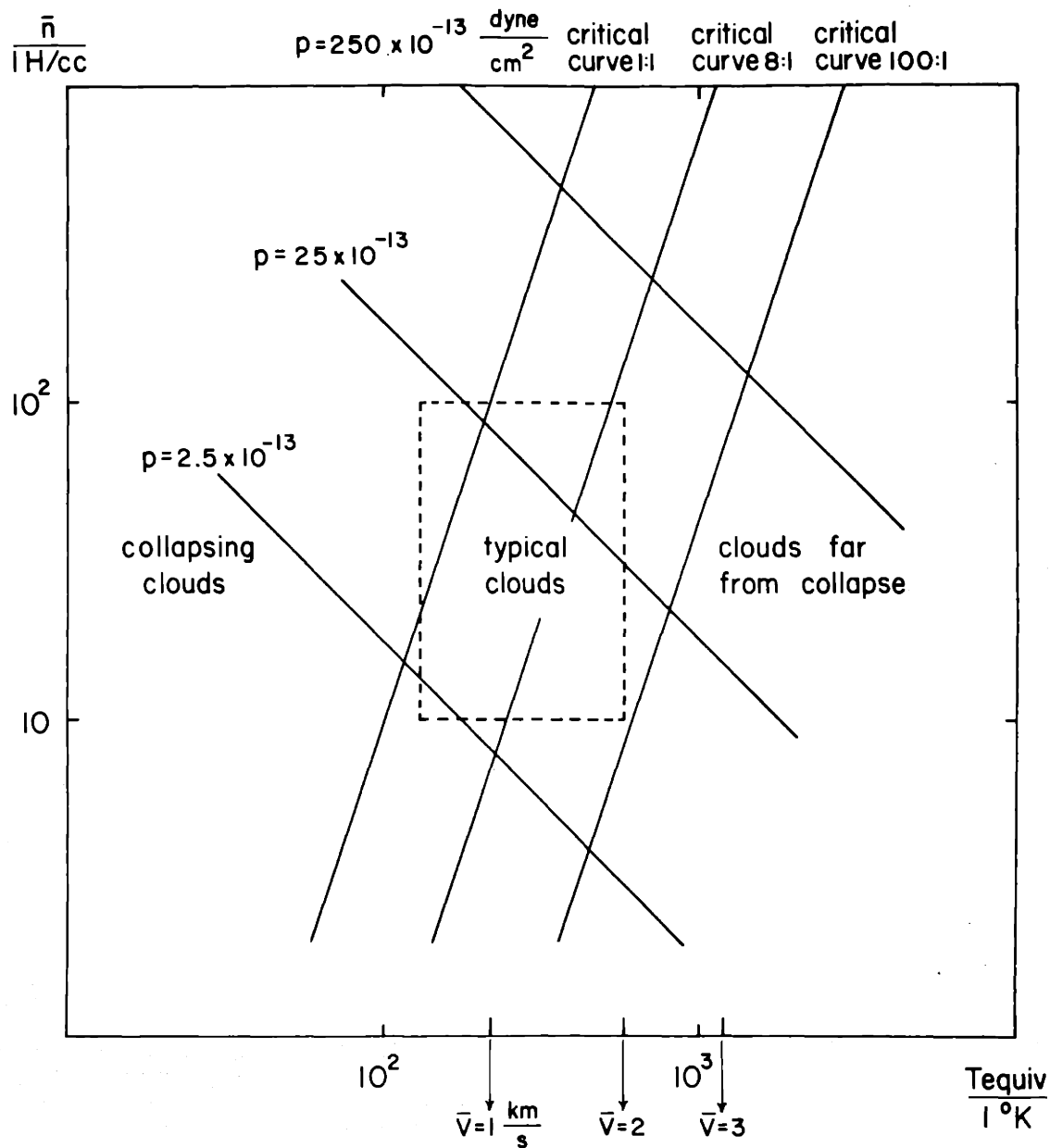


Figure (27.2)

The Collapse of Gas Clouds of Mass =  $10^4 M_{\odot}$  Under Various Shock Strengths

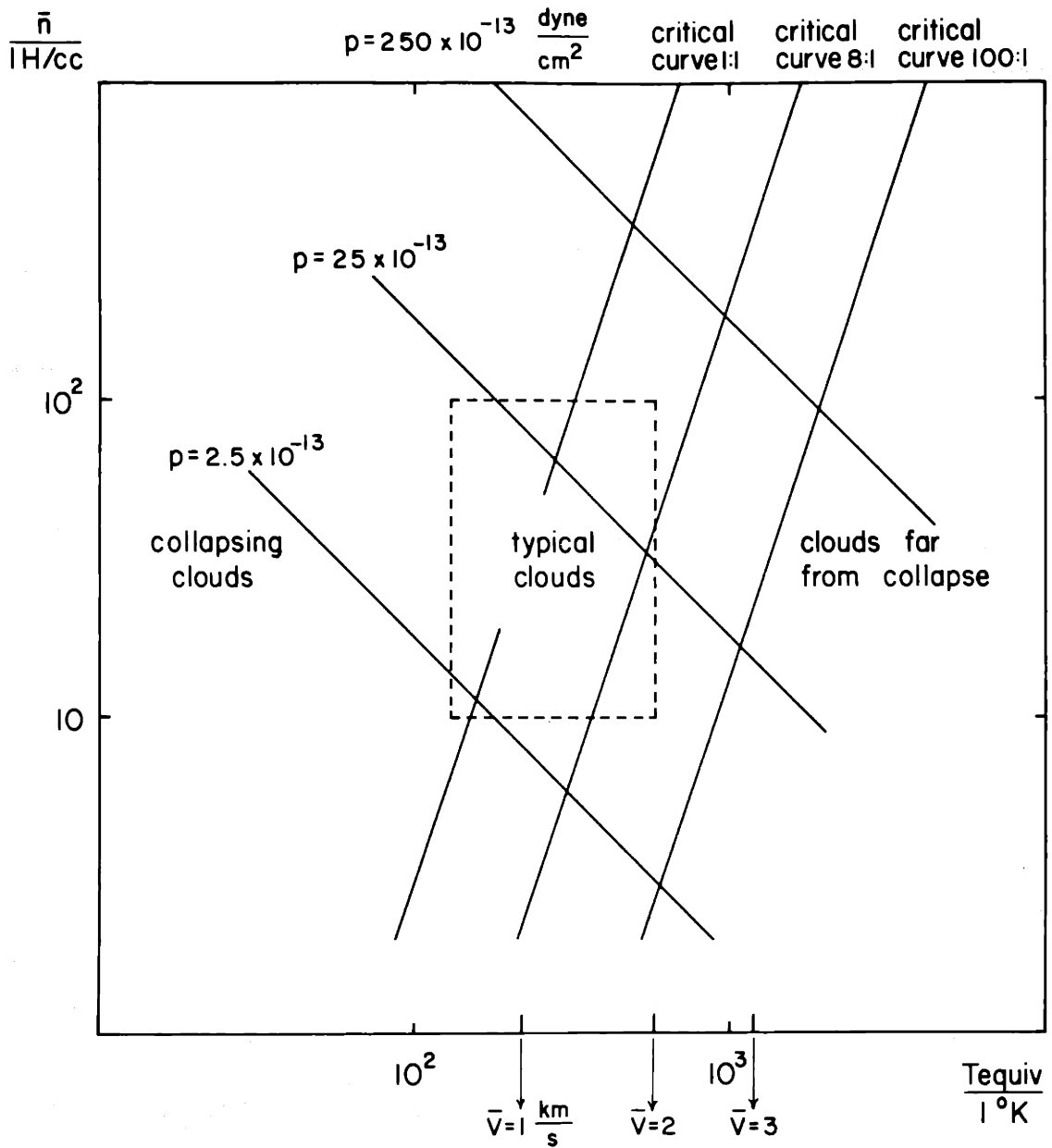


Figure (27.3)

The Collapse of Gas Clouds of Mass =  $1.8 \times 10^4 M_\odot$  Under Various Shock Strengths

tational collapse under an 8:1 shock compression. The mean turbulent dispersion speeds that correspond to these respective equivalent temperatures are 1.1, 1.3 and 1.7 km/s; and the corresponding equivalent surface pressures before and after compression for each of the respective clouds are  $6 \times 10^{-13}$  to  $48 \times 10^{-13}$ ,  $7 \times 10^{-13}$  to  $56 \times 10^{-13}$  and  $8 \times 10^{-13}$  to  $64 \times 10^{-13}$  dynes/cm<sup>2</sup>.

Figure (27.4) illustrates in a slightly different manner the criterion for determining what clouds may be placed on their verges of gravitational collapse by a fixed 8:1 shock compression. A cloud of a given mass that lies to the left of its critical curve will collapse under an 8:1 shock compression. On the other hand, if it exhibits too much internal turbulence or is not of sufficient density, an 8:1 shock compression is not sufficient to place it on its verge of gravitational collapse. The "outlined box" in the figure indicates the region of density and equivalent temperature space where most galactic gas clouds probably lie.

When little or no turbulence is present, the collapse of a large cloud may easily be triggered by a galactic shock wave of 8:1 strength. With too great a degree of turbulent dispersion, even the collapse of the largest galactic gas clouds may be prohibited. Yet turbulence has further significance in our Galaxy; for, without a nonquiescent interstellar medium all large clouds in the presence of a shock wave would have collapsed into stellar associations long ago. In such a situation neither the observed large clouds nor the young stellar associations would be in existence today.

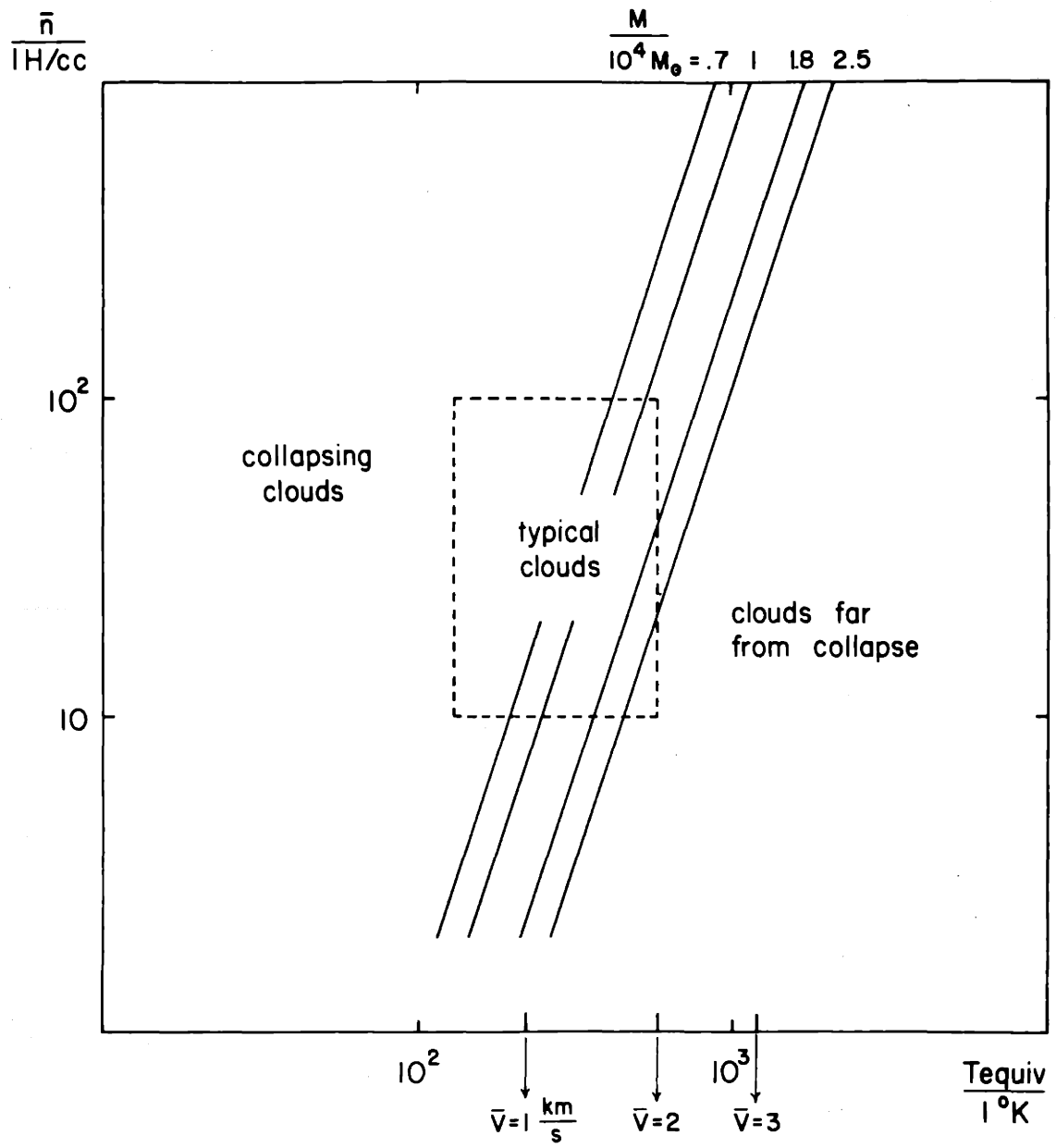


Figure (27.4)

The Collapse of Gas Clouds Under an 8:1 Shock Compression

28. Gas cloud model; internal region of a galactic shock

Suppose we adopt a cloud with a mass of  $10,000 M_{\odot}$ , a mean density,  $\bar{n}_c$ , of 20 H/cc, and a radius,  $R_c$ , of 17 pc as the constituent cloud of our model.<sup>1</sup> For the intercloud medium a typical estimate of the mean density,  $\bar{n}_{ic}$ , might be .5 H/cc. The mean turbulent dispersion speeds in the cloud and intercloud medium to account for this density contrast lie in the ranges of 1-2 km/s and 7-14 km/s respectively. If the overall mean density of the interstellar medium,  $\bar{n}$ , is about 1 H/cc, the fractions of the total volume occupied by clouds,  $V_c'$ , and intercloud space,  $V_{ic}'$ , in our model are about 1/39 and 38/39 respectively:

$$V_c' = \frac{\bar{n} - \bar{n}_{ic}}{\bar{n}_c - \bar{n}_{ic}} = \frac{1}{39}$$

$$V_{ic}' = \frac{\bar{n}_c - \bar{n}}{\bar{n}_c - \bar{n}_{ic}} = \frac{38}{39}$$

---

<sup>1</sup>The shape of the constituents of the interstellar medium is uncertain. Quasi-spherical and spherical shapes are a rather natural choice for our model. These may be contrasted with planar gas sheets or other shapes of the gaseous masses.

An important characteristic scale for the cloud model is the mean-free-path of a large gas cloud:

$$L_{\text{m.f.p.}} = \frac{R_c}{3V_c^1}$$

Before compression, a value of 240 pc is a typical estimate for the mean-free-path of a large cloud. After an 8:1 compression<sup>1</sup> of a given volume of interstellar space the new mean-free-path of a large cloud may range between 30 pc and 120 pc: the lower limit corresponding to a contraction of intercloud volume only, with clouds remaining about the same size; the upper limit corresponding to a homologous contraction of cloud and intercloud volume together.<sup>2</sup> The actual shock compression will evidently take the form of a contraction lying somewhere in the range between these two limiting contractions. A mean-free-path of 100 pc of the large cloud after compression would not be an unreasonable estimate. The mean-free-path between clouds also gives a characteristic scale for the shock width; and therefore, a scale of 100 pc, which is the estimate of mean-free-path after compression, might be a typical "shock thickness."

Gas enters and leaves the shock region at mean velocities perpendicular to the shock of about 28 km/s and 3.5 km/s respectively when the

---

<sup>1</sup>An 8:1 compression may be a typical shock strength (see the calculations of Part II).

<sup>2</sup>If clouds could be regarded as "billiard balls," a contraction of a volume of space would constitute a contraction of intercloud space only. On the other hand, since clouds in the interstellar medium probably have no sharply defined boundaries, a contraction of a volume of space may actually involve a more or less homologous contraction of the whole volume.

mean turbulent dispersion speed is about 10 km/s. The passage across the 100 pc shock thickness might take about 10 million years if a mean gas velocity of 10 km/s across the shock is assumed. The collision times in the regions in front of and behind the shock are on the order of 24 million years and 10 million years respectively. Hence, the times of adjustment of large gas clouds in passage across and behind the shock are comparable time scales, both on the order of 10 million years.

As we indicated in Section 25, the large cloud-intercloud model may be decomposed into further more basic components: the small clouds or subclouds and the intersubcloud medium.<sup>1</sup> These smaller gas masses lying in the range of smaller scale in the spectrum of turbulence (which may or may not be discernible) will serve as the candidates for proto-stars. Small clouds (subclouds) with masses of  $50 M_{\odot}$ , densities of 40 H/cc, and radii of 2.3 pc are reasonable candidates for proto-stars. In this subcloud picture, we allow for the formation and existence of large clouds and large cloud complexes of the sizes of  $10^4 M_{\odot}$  by distributing the  $50 M_{\odot}$  clouds in clumps of sufficient concentration. The fractions of the total volume occupied by subclouds,  $V_{sc}$ <sup>1</sup> and intersubcloud space,  $V_{isc}$ <sup>1</sup> in this picture are about 1/79 and 78/79 respectively. Therefore, the mean-free-path of a subcloud before and after compression varies from 60 pc before to the range of 8-30 pc after; again the mean-free-path after compression depends on the type of contraction. A value of 20 pc may be a reasonable estimate for the mean-free-path of subclouds after compression as

---

<sup>1</sup>It will be convenient to consider the subcloud picture in an investigation of the internal region of a shock.



well as the distance over which subclouds may travel between collisions in the shock region. In this picture, the turbulent adjustment time for subclouds in the shock region is on the order of a few million years. Although the actual interstellar medium would be best described by a model containing clouds of all scales, the realistic picture may be roughly approximated by this model of clouds and subclouds.<sup>1</sup>

With this cloud-subcloud model in mind, we now turn our attention to the picture of the interior region of a galactic shock wave. Whereas on the large scale of the TASS pattern, the shock resembles a discontinuity in mean density, velocity, and pressure; on the smaller scale characteristic of the size of gas clouds, the shock encompasses a broad region, six times the radius of a large cloud and almost fifty times the radius of a subcloud.

In the shock region there are possibly two types of compressive mechanisms that act on any given large gas cloud during its passage through the shock. The first is the collision of a large cloud with other large clouds. In the passage of a given large cloud through a shock thickness of 100 pc, an average of one such collision is likely. Such a collision of large clouds tends to flatten both participants although the process of "rebound" (personal communication with Kahn, 1968) may help clouds, which have been flattened, to become more spherical once again.

The second mechanism involves the composite effect of collisions of several subclouds with a large cloud. In the time period between

---

<sup>1</sup>In a later section we return to a discussion of subclouds as the possible candidates for protostars.

collisions of a given large cloud with other large clouds, five collisions of subclouds with the large cloud occur on the average in our model. In general, when a subcloud collides with a large cloud, the large cloud tends to absorb the smaller clouds and to become more massive.<sup>1</sup> Indeed, the process of accretion by the more massive large clouds may be enhanced considerably inside the shock region and in the subsonic region behind the shock. The extensiveness of the bombardment of a given large cloud by smaller subclouds may determine in part how isotropic is the compression felt by the large cloud.<sup>2</sup>

Undergoing these two types of collisions, large clouds may be compressed to varying degrees. Of especial interest are those clouds which may have reached their verges of gravitational collapse through the processes of pancake-like flattening and "rebound" (personal communication with Kahn, 1968). Also, of especial interest are those large clouds that undergo no collisions with other large clouds over a time period which is sufficient for subcloud bombardment to compress them (with little pancake-like flattening) beyond their verges of gravitational collapse. Statistically, a small fraction of all large clouds

---

<sup>1</sup>Accretion is discussed in Section 26.

<sup>2</sup>Another factor may play a role in determining how isotropic is the compression. A massive large cloud may be less easily decelerated in the shock region than a small cloud due to the contrast in momenta between the two. The less isotropic will be the compression of a large cloud due to subcloud bombardment, the larger is the difference between the mean velocities of the large and small clouds in the shock region.

may be triggered into gravitational collapse in these ways. It is this fraction that may account in large measure for the newly-born stellar associations<sup>1</sup> lying within the grand design of spiral structure in our Galaxy and in other spiral galaxies.

---

<sup>1</sup>Section 30 considers the formation of protostars from subclouds and the formation of stellar associations from large clouds and cloud complexes.

29. Classic problems associated with star formation

Fragmentation

On the one hand, it appears from observational studies that no stars of mass greater than  $70 M_{\odot}$  are in existence; on the other hand, it is evident that in order to initiate the collapse of a gaseous mass its mass must be on the order of  $10^4 M_{\odot}$ . Therefore, the formation of stars<sup>1</sup> must be accounted for by some process of fragmentation of the large clouds before or during their collapse into smaller collapsing submasses that may serve as the candidates for protostars. Why a large massive cloud should dissociate before or during its collapse so as to give rise to an association of smaller collapsing subclouds rather than just one large collapsing mass constitutes the classic problem of fragmentation.

Hunter (1964) has treated this problem of fragmentation in the collapse of a quiescent gas sphere and has shown that during the spherically symmetric collapse of the gas cloud the cloud shows a preference not toward condensation as a single entity but rather toward fragmentation into a number of subcondensations. In fact, Hunter demonstrates that density perturbations grow faster than the

---

<sup>1</sup>A mass loss  $> 99\%$  of the mass of a large cloud for the formation of a protostar of mass  $< 70 M_{\odot}$  is not easily accounted for. In Section 30, we discuss this possibility and find it an unlikely one.

uniformly contracting background of density, and that the relatively rapid growth of density perturbations perpetrates the fragmentation of the large gas cloud during collapse.

In the nonquiescent picture of the interstellar medium that we envisage, the process of fragmentation is evident throughout. Indeed, the processes of fragmentation and disintegration play their continual roles not only on the large scale that encompasses turbulent motions of large clouds and cloud complexes over the interstellar medium but also on the small scale that encompasses turbulent motions of subclouds in the interiors of large clouds themselves. Therefore, the usual problem of how fragmentation may arise is not a real one in this nonquiescent picture (since fragmentation is present even before the collapse of clouds). Turbulence provides for internal fragmentation of a large cloud but at the same time hinders the overall compression toward its verge of gravitational collapse. In this picture the formation of many protostars which lie in association<sup>1</sup> rather than the formation of one overly-massive supergiant protostar can be realized.

### Turbulence

Heretofore, we have made the assumption that a gas cloud during compression may be characterized as isothermal at an equivalent temperature (partly kinetic and partly due to turbulence). Indeed, the kinetic temperature may remain virtually unchanged if the cloud is optically thin and heat energy can be radiated away in a time period much shorter

---

<sup>1</sup>The internal subcloud picture will be discussed in more detail in a later section.

than the dynamical time scale of a few million years. On the other hand, it is possible that turbulent dissipation may not be sufficient to restrain the effective temperature due to turbulence from appreciably rising during compression. If this be the case, the gas may not be characterized as an isothermal gas at an unchanging equivalent temperature during compression.

By the law of conservation of circulation during cloud contraction:

$$\Gamma \propto \oint (\overline{v^2})^{1/2} ds$$

the mean turbulent dispersion speed (if the turbulent velocities are primarily rotational) may be expected to rise with decreasing cloud radius as:

$$(\overline{v^2})^{1/2} \propto R^{-1}$$

In the nonquiescent state, the equivalent temperature varies roughly as the square of the mean turbulent dispersion speed and therefore, the ratio of the rapidly increasing internal turbulent energy (when no

turbulent dissipation is present) and the gravitational energy is:

$$\frac{\frac{kT_{\text{equiv}}}{m_p}}{\frac{GM}{R}} \propto R^{-1}$$

With no other important effects present (such as turbulent dissipation) it therefore appears that a time will be reached during the collapse process when the pressure forces resisting compression will overcome the gravitational forces influencing collapse, and at this time further collapse will be hindered.

On the other hand, the process of turbulent dissipation must also be taken into account. To be sure, as the mean density increases during contraction, the collision rate of subclouds inside the large cloud also rises. Dissipation of turbulent energy by collisions therefore must increase, and this rate of increase of turbulent energy dissipation may be roughly approximated by:

$$\frac{1}{v^2} \frac{d(\overline{v^2})}{dt} \propto \frac{(\overline{v^2})^{1/2}}{R} \propto R^{-2}$$

Therefore, the dissipation of turbulent energy into heat energy which may then be radiated away, may be rapid enough to restrain the effective

temperature due to turbulence from rising appreciably, and, in particular, to restrain it from rising as fast as  $R^{-2}$ .

For example, if  $T_{\text{equiv}}$  rises only as fast as  $R^{-1}$  the ratio of turbulent pressure forces and gravitational forces remains unchanged during compression. In this situation, if the gravitational forces exceed the turbulent pressure forces initially, they will remain dominant; and gas cloud collapse will continue. If a simple polytropic law may be used to describe the gas cloud:

$$p = \kappa \rho^\gamma$$

then the ratio of turbulent pressure forces to gravitational forces will increase or decrease as  $\gamma$  is greater than or less than  $4/3$ , i.e., when  $\gamma = 4/3$ ,  $T_{\text{equiv}} \propto R^{-1}$ .

A typical estimate of the time scale for the dissipation of turbulent energy may be obtained from the dissipation rate of  $(\overline{v^2})^{1/2}/R$ . If  $(\overline{v^2})^{1/2} = 1\text{km/s}$  and  $R = 20\text{ pc}$ , then  $\tau_{\text{dissipation}} = 20\text{ million years}$ . Initially, a large cloud will tend toward collapse under a sufficient shock compression but will be hindered from complete collapse for a period of perhaps 20 million years or so during which enough dissipation of turbulent energy will have taken place and enough heat energy will have been radiated away so that collapse will no longer be discouraged. This time scale for the dissipation of turbulent energy may



be one of the longest time scales over which the cloud collapse process must be delayed before protostar formation may be realized. If a time period of 20 million years is allotted for the time scale of dissipation of turbulent energy, and if time periods of 10 million years are allotted for the time scales of passage through the shock and of adjustment of clouds (by turbulence) to the compressed medium behind the shock (all of which overlap somewhat since all three processes proceed simultaneously), then the process of protostar formation may evolve over a time period of 30 million years from the initial shock-triggering stage.

#### Rotation and Angular Momentum

Suppose we consider a gas cloud which rotates with a uniform angular velocity  $\omega$  about an axis through its center. If the cloud collapses isotropically, the law of conservation of angular momentum:

$$\text{Ang. Mom.} \propto \omega R^2 = \text{constant}$$

requires the centrifugal force, which is proportional to  $\omega^2 R$ , to increase as  $R^{-3}$ . Indeed, this represents a faster rate than the growth rate of  $R^{-2}$  for the gravitational force. Hence centrifugal effects though initially small will inevitably swamp gravitational effects. Since the rotation will halt the collapse perpendicular

to the axis of rotation but will not influence the collapse parallel to that axis, the cloud collapse will tend from one of a spherically symmetric nature to one of a pancake-like nature.

Once the collapse to a disk-like configuration has evolved, further collapse may be hindered in another way: the pressure force,  $\nabla p/\rho$ , which tends to prevent further collapse perpendicular to the plane of the disk, grows at the same rate as the gravitational force, which tends to influence further "pancaking" of the disk. In this situation, no strict verge of gravitational collapse may be realized. However, Hunter (1967) and Spitzer (1968) both have pointed out that the processes of fragmentation will not be significantly interfered with and that a hierarchy of fragmentating and contracting subdisks may evolve over the larger disk (if fragmentation is not already present).

Whereas those large clouds which are undergoing large rotations cannot be collapsed by the shock, those large clouds which possess little angular momentum may be. Statistically, there exists a small fraction of all clouds which possess no appreciable angular momentum, and these clouds are the ones that can be triggered into gravitational collapse by the shock. Since turbulence provides a transfer mechanism for angular momentum between internal subclouds and the intersubcloud medium inside the large cloud, no serious difficulty associated with internal rotational motions is visualized in the collapse picture of internal subclouds.

#### Magnetic Field

Suppose we consider a uniform sphere of radius  $R$  which contains a uniform magnetic field  $H$ . In a situation of equilibrium, the virial

theorem states:

$$0 = -\frac{3GM^2}{5R} + \frac{H^2R^3}{4}$$

Suppose we consider the isotropic contraction of the sphere. If the conductivity of the interstellar medium is high enough, magnetic lines of force remain frozen in the gas; and in this situation, the magnetic field intensity varies as  $R^{-2}$ , and the gravitational energy as well as the magnetic field energy varies as  $R^{-1}$  during the contraction. This picture of the collapse of a gas cloud in the presence of a magnetic field differs from the picture of collapse of a gas cloud under no magnetic field: when a magnetic field is present, the critical mass signifying the verge of gravitational collapse is unaltered by contraction; when no magnetic field is present, the critical mass steadily decreases during collapse. In the presence of a magnetic field, if the gas cloud is initially beyond its verge of gravitational collapse (i.e., it has a mass  $>$  the critical mass), it will remain there; and collapse will continue.

On the other hand, if the conductivity of the interstellar medium is low, then magnetic field lines cannot be frozen in the gas. For this reason alone, the influence of the magnetic field on gas cloud collapse may be of only secondary importance. To be sure, if the magnetic field strength is only of the order of a few microgauss, the magnetic field can play only a secondary role in gas cloud collapse. In addition,

in our nonquiescent picture of the interstellar medium, turbulence itself may be strong enough to appreciably diffuse magnetic field lines out of gas clouds; and in this situation, the influence of the magnetic field on gas cloud collapse may be even less. We have in mind a picture of this type where the magnetic field plays only a secondary role in the collapse of gas clouds and in the formation of stars.

### 30. Subclouds: the candidates for protostars

The dynamical picture for the spatial distribution of the interior portions of a large gas cloud may be much like the larger scale picture for the irregular spatial distribution of gaseous masses (large clouds and cloud complexes) over the interstellar medium. While the interstellar medium may be comprised of gaseous masses (large clouds and cloud complexes) in a state of turbulent motion, each of the gaseous masses may in turn be comprised of gaseous submasses (small clouds and subclouds) which experience their own state of turbulence. This picture of the interior regions of a large cloud may be particularly evident if the state of turbulence in the interstellar medium is such that we may indeed distinguish gaseous masses into two ranges of scale: the scale of the large cloud and cloud complex being much larger than the scale of the subcloud. In this picture, the process of gravitational collapse may be viewed.

As a large cloud contracts, the radiation originating from within the cloud tends to keep it in thermal equilibrium with its surrounding medium. If no appreciable absorption of the radiation by the interior takes place, and if turbulent dissipation is sufficiently rapid, the primary distortion to the internal turbulent fragments is their homologous contraction at a rate similar to the contraction of the cloud as a whole. As the volume shrinks, clumps of increasingly denser gas concentrations stand out and their self gravitation rises in increasing

proportions.<sup>1</sup> After sufficient contraction has taken place, the self gravitation of the most massive clumps of gas concentration becomes dominant over their internal turbulent pressure of dissociation. At this stage the most massive clumps are on the verge of gravitational collapse. As shrinkage progresses further, fragments of smaller and smaller scales succumb to their self gravitation and follow the largest fragments in a sequence along the path of collapse. As the gravitationally collapsing regions separate out from the remainder of the turbulent medium, the state of internal fragmentation assumes a more pronounced form. In this state of separation, the individual collapsing gas concentrations may be envisaged even more positively as nonquiescent subclouds.

This cloud-subcloud picture finds additional support in the fact that stars of mass greater than about  $70 M_{\odot}$  have not been found to exist in observational studies. With such an observational result in mind, we infer that either a large cloud during its collapse toward a protostar must lose over 99% of its mass or a star must be formed from a subcloud rather than directly from a large cloud whose mass must necessarily be of the order of  $10^4 M_{\odot}$  in order to be capable of collapsing in the first place. The first alternative which requires 99% mass loss is regarded as unfavorable since the mechanism for producing such

---

<sup>1</sup>In our nonquiescent picture of the interstellar medium, the process of fragmentation is evident throughout (see Section 29). Indeed, it is present even before any process of gas cloud collapse takes place. Therefore, during the process of gas cloud collapse (discussed herein, Section 30) fragmentation, which is already present, assumes a more pronounced form.

a mass loss appears to be lacking. The second alternative seems much more favorable, and we infer that subclouds as the constituents of large clouds may be the likely candidates for protostars.

### Stellar Associations

Before collapse, a large cloud (of our model) with a mass of  $10^4 M_{\odot}$ , a mean density of 20 H/cc, a radius of 17 pc, a kinetic temperature of 100°K, and an equivalent temperature of 300°K may contain, for example, 100 randomly dispersed subclouds with masses of  $50 M_{\odot}$ , mean densities of 40 H/cc, and radii of 2.3 pc. This is the cloud-subcloud model that is envisaged earlier in Section 28. If the balance of equivalent pressure between subcloud and intersubcloud medium is to be maintained in this picture, the intersubcloud medium must have a mean density of roughly 13 H/cc.<sup>1</sup> In such a model, the fraction of subcloud volume to intersubcloud volume is 1:3, whereas the total mass of the large cloud is distributed equally between subclouds and intersubcloud space.

Although the subcloud radius before compression is about 2.3 pc; when the subcloud is just at its verge of gravitational collapse, its radius is only .036 pc, and the mean intersubcloud distance between

---

<sup>1</sup>In order to have a mean intersubcloud density of 13 H/cc inside the large cloud, the basic intersubcloud density of .5 H/cc, which is adopted in Section 28 to represent the portions of the model of the interstellar medium apart from clouds, must be complemented with the gaseous mass, for example, of some 96 subclouds diffused throughout the intersubcloud volume. In this way, the large cloud may be formed from subclouds.

subclouds is about .1 pc. A compression of the subcloud on the order of 100,000: 1 is therefore necessary before an individual subcloud will reach its verge of gravitational collapse. The mean intersubcloud distance of .1 pc might be taken as a typical upper bound estimate<sup>1</sup> of the distances between newly-born stars in a stellar association at its birth. When the subclouds do reach their verges of gravitational collapse, the large cloud radius is about .27 pc. This large cloud distance of .27 pc may provide a typical upper bound scale for the size of a stellar association at birth. Although the large cloud already reaches its verge of gravitational collapse when its radius is as large as 7 pc, it is not until the large cloud collapses through an additional 10,000:1 contraction that subclouds reach their verges of gravitational collapse and a stellar association begins forming. The stellar dispersion inside a newly-born stellar association may be estimated by the mean subcloud dispersion speed inside a large cloud before contraction takes place. Since the mean dispersion speed before collapse has an upper bound of about 2 km/s, a typical estimate for the mean stellar dispersion speed in a newly-born stellar association might be a few kilometers per second. All these estimates are in general agreement with observations.

An important physical consequence of the cloud-subcloud picture in further agreement with observations requires that newly-born stars be found only in associations with other newly-born stars. Indeed,

---

<sup>1</sup>This is an upper bound estimate since more than 100 newly-born stars generally appear in a stellar association. As many as 1,000 to 10,000 stars might characterize a typical stellar association.



M. S. Roberts (1957) has confirmed through observational studies of many B stars in the solar neighborhood that they all appear to lie in stellar associations.

The necessity for stellar associations in the cloud-subcloud picture is apparent. Since the amount of compression necessary for triggering the gravitational collapse of a gas concentration varies inversely with the square of its mass, it is much easier to trigger the gravitational collapse of a large cloud rather than a subcloud. Indeed, a shock wave of 3:1 compression may be capable of triggering the gravitational collapse of a large gas cloud, whereas the triggering of the gravitational collapse of a gas subcloud requires a compression several orders of magnitude greater (100,000:1). The individual subclouds, that compose a large cloud, mutually attract one another by their gravitational forces, and this attraction is the factor that enables a large cloud to reach its verge of gravitational collapse under an 8:1 shock compression. It is only the rising pressure resulting from the contraction of the large cloud that eventually provides enough compression to place the subclouds on their verges of gravitational collapse. This compression and collapse of an individual subcloud forms a star, and this newly-born star lies in association with the stars formed from all the other subclouds inside the large cloud.

### 31. Galactic star formation in a grand design of spiral structure

After perhaps 30 million years from the shock triggering stage when an individual subcloud has become sufficiently compact, nuclear reactions inside the collapsing submass begin to take place, and the newly-born star begins to radiate. At this stage, the processes within each star become quite complicated. The radiation generated within each star is felt in the form of radiation pressure by all the other stars and masses in the association. In the early life of a young stellar association containing O and B stars, which were formed from the largest internal subeddies of the (ancestral) large cloud, the radiation pressure inside the association may be great enough to force some of the smaller gaseous masses (small subclouds) over their verges of gravitational collapse. In this situation, a secondary regeneration of star formation may take place.

At the same time that this secondary regeneration of star formation is occurring, the stellar association as a whole tends toward a state of expansion driven by the internal radiation pressure. Once a state of sufficient expansion is reached, the remaining gas masses of small scale (small subclouds) begin to decompress once again, and the possibility for further star formation ceases. Today, observational studies of stellar associations of newly-born stars indicate that the average distance between the stars is generally larger than the mean intersubcloud distance characteristic of the final stages of collapse

of the ancestral cloud prior to the formation of stars<sup>1</sup>; and the explanation for this is readily found in the expansion of young stellar associations driven by the excessive amounts of radiation pressure felt throughout.

A further stage of the stellar evolution process evidently follows. After a few more million years have passed, the relatively massive newly-born stars presumably explode in the form of supernovae. In addition to providing appreciable amounts of energy for the interstellar medium and brilliantly lighting up their environments, these explosions may also give rise to local small-scale shock waves of large shock strengths which propagate through the gaseous environment of the stellar association. It is conceivable that these small-scale shocks could in turn collapse still more small-scale gaseous masses (small subclouds) which never before quite reached their verges of gravitational collapse. In a situation where many supernovae evolve simultaneously in the association, further secondary star formation effects might therefore be present.

During these supernovae explosions most of the mass of the exploding stars returns to the interstellar medium once again and provides more gas clouds, together with all those that never reached their verges of gravitational collapse, and in this way enhances the gaseous medium for a repetition of the star formation process during the passage of the next large-scale galactic shock. Even when supernovae are evolving

---

<sup>1</sup>An upper bound estimate of the mean intersubcloud distance when a subcloud in our model is at its verge of gravitational collapse is about .1 pc (see Section 30).

over a region of the galactic disk, the next large-scale galactic shock still lies only a little less than half a revolution about the disk. Only a small fraction of the stellar mass is not exploded out from supernovae, and what remains assumes the form of a white dwarf.

The overall energy balance may be envisaged as a combination of all these processes which provide energy, together with the process of dissipation of turbulent energy by collisions. Over the 30 million years of travel from the shock, large amounts of energy are evidently made available to the interstellar gas by the radiation of the young stars and the supernovae explosions. Of this energy, perhaps 1% is converted into kinetic energy of the gas itself.<sup>1</sup> The region lying adjacent to a shock and extending approximately a distance of about  $1/8$  of the wavelength between successive spiral arms is the area where most of this energy is available to the gas and where the turbulence of the gas is likely to increase somewhat. Indeed, it is this portion of the galactic disk where the grand design of spiral structure stands out with such great brilliance and striking luminosity. In a disk-shaped galaxy, a luminosity contrast of many orders of magnitude may be maintained between these brilliantly luminous spiral arms and the interarm regions, which together compose the grand design of spiral structure. With the lack of sufficient radiation from young stars<sup>2</sup> (a

---

<sup>1</sup>Personal communication with Kahn, 1968

<sup>2</sup>Indeed, by the time the young stars which are formed in the shock region, have passed outside the spiral arms, they are no longer young.

scarcity compared to the exorbitant amounts of stellar radiation observed in the spiral arms) and the lack of supernovae explosions over the remaining  $7/8$  of the travel distance toward the next successive galactic shock, dissipation of turbulent energy is likely to predominate outside the spiral arms. At the next shock the regeneration and dissipation cycle for gaseous turbulent energy starts anew.

Part V. Conclusions and Implications

## 32. Summary of results

In this thesis, three basic problems have been investigated: (1) the gaseous response of the galactic disk to a spiral gravitational field and the compatibility for the existence and persistence of a two-armed spiral shock wave pattern, (2) the possible evolution and development of galactic shock waves over the disk, and (3) the possible implications of shock formation on star formation along the spiral arms.

### Stationary Two-Armed Spiral Shock Pattern

The compatibility of two periodically-located shock waves lying along and within the imposed two-armed spiral pattern has been confirmed for the Schmidt model of the Milky Way System. Figure (32.1) illustrates the position of the shock inside the imposed two-armed spiral pattern of trailing type. Arrowed streamlines which turn sharply at each shock are drawn for several typical radii. The imposed pattern is the composite pattern of all the moderately-old stars, of ages greater than perhaps 30 million years, and therefore does not stand out in observational studies. One basic feature of the shock pattern is the predetermined location of the shock which approximately coincides with the center axis of the imposed spiral arm and actually is shifted slightly to the inner side in the case of the trailing spiral arm.

This coincidence of the spiral shock, as well as the large induced

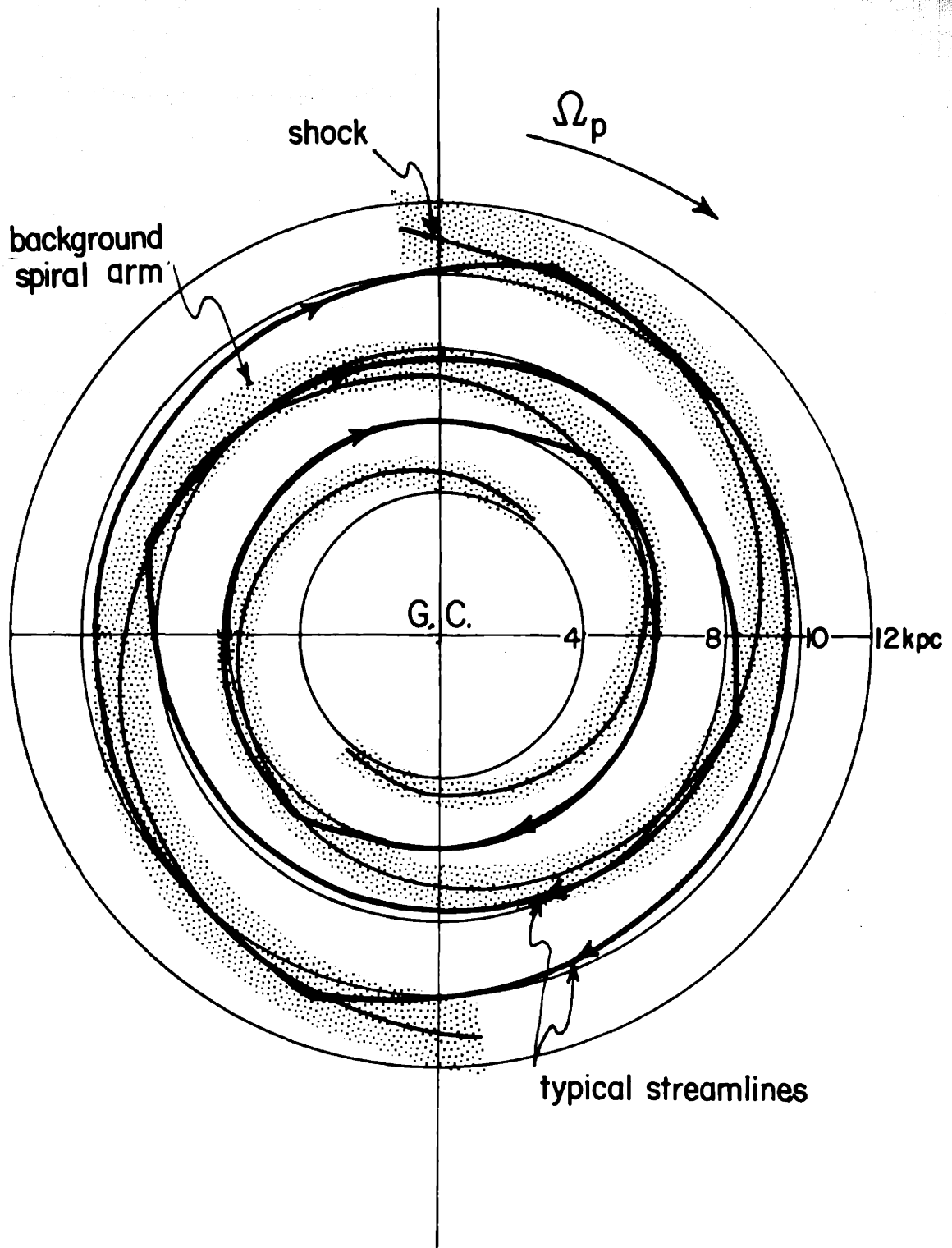


Figure (32.1)  
Shock and Background Spiral Pattern in the Galaxy



gaseous concentration just behind the shock, with the imposed (gravitational) spiral arm is favorable for the self consistency of the overall spiral field and the maintenance of the stationary shock pattern. Self consistency requires that the induced field due to the response in the gaseous and stellar components of the galactic disk be similar to the original imposed field which gives rise to the response. In fact, it has been shown that the fundamental component of the (non-linear) gas-induced field lies approximately in phase with the imposed field. Therefore, the imposed field may be regarded as the resultant spiral gravitational field of gas, young stars, and moderately-old stars. This compatible and self consistent coexistence of the (nonlinear) gaseous TASS pattern and the (linear) stellar density wave pattern has been confirmed between the radii of 3-4 kpc and 12 kpc over the galactic disk.

The shock determined by numerical calculations for a spiral galaxy of leading type again coincides approximately with the center axis of the imposed spiral arm but is shifted slightly to the outer side in the case of the leading arm. In general, for both leading and trailing spiral galaxies the shock wave occurs just before the gas flow reaches the minimum of the imposed spiral potential field.

Investigation of some typical gas clouds has shown that large clouds may not be far from the critical condition where gravitational collapse becomes possible. Indeed, it is suggested that galactic shock waves may very well form the triggering mechanism for the gravitational collapse of gas clouds, leading to star formation. Since newly-born luminous stars give rise to H II regions, galactic shocks may be visualized as the necessary forerunners of the large H II regions as well as

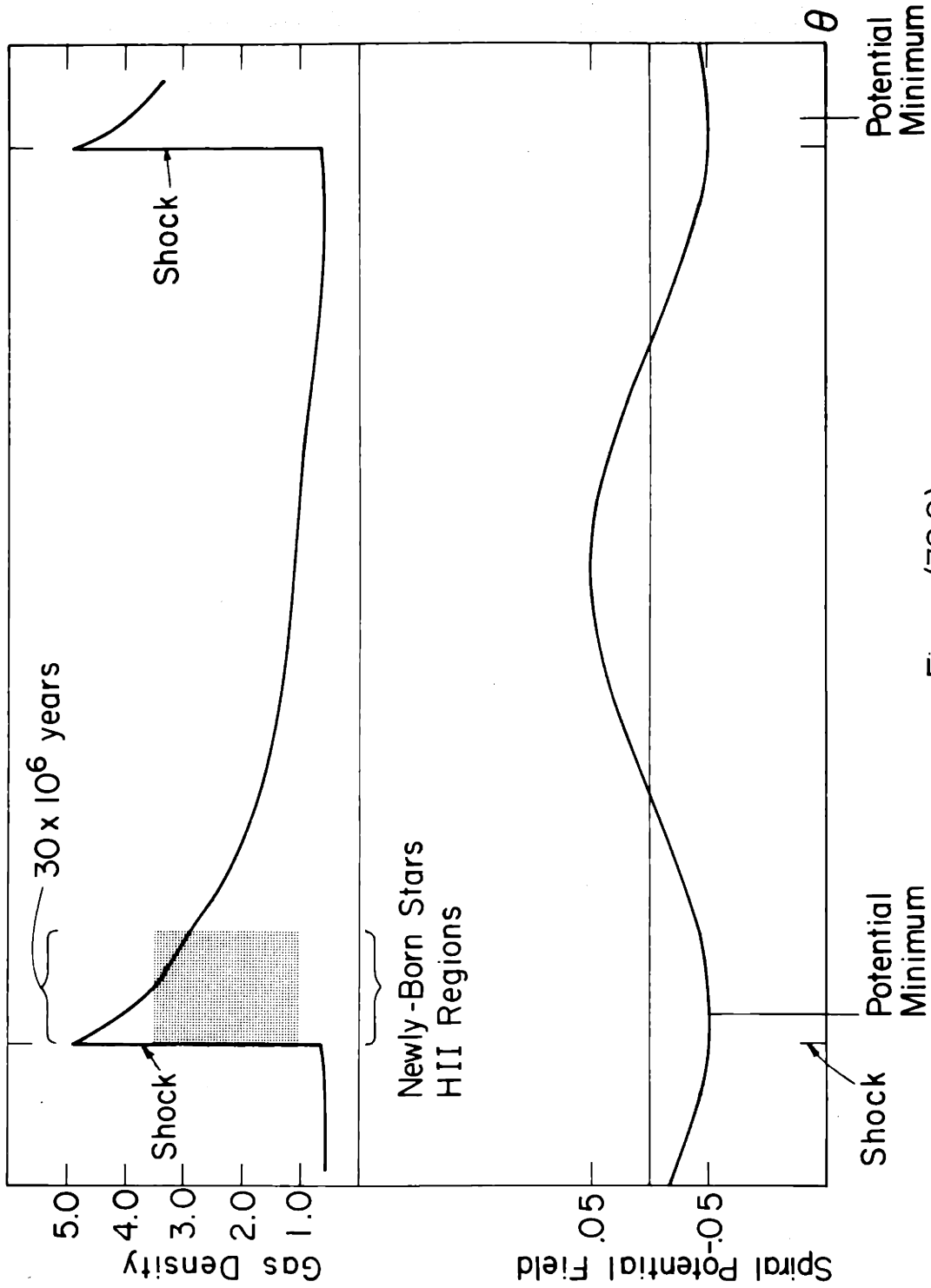


Figure (32.2)

Gas Density Distribution along a Typical Streamtube in the TASS Pattern

the newly-born stars. Figure (32.2) illustrates the behavior of the gas density along a typical streamtube of the TASS pattern. The imposed potential field due to the moderately-old stars is sketched at the bottom. The potential minimum corresponds to the density maximum and the center of the imposed spiral arm. A shock occurs slightly in front of the imposed arm's center axis. The region extending from the shock to the point where the gas density drops below its average value of unity corresponds to the observed gaseous spiral arm. If an upper bound of 30 million years is assumed for the process of formation and evolution of relatively massive stars initiated at the shock, the regions of newly-born luminous stars and H II regions lie on the inner side of the observed gaseous spiral arm, extending from the inner edge to approximately the middle of the arm.

We now visualize how the Galaxy may appear with shocks present. When observations of the galactic disk are made, the moderately-old star background distribution making up the imposed two-armed spiral pattern is not seen. Basically, what we do see are: (1) the observed gaseous spiral arms of H I, and (2) the newly-born luminous stars and H II regions. Figure (32.3) illustrates this observable physical picture according to the shock predictions. A shock occurs on the inner edge of the observed gaseous spiral pattern (the light-toned region). On the inside of this observable trailing spiral pattern lie regions of newly-born luminous stars and H II regions (the darkened area) extending from the shock on the inner edge to approximately the center of the arm.

Some quantitative features of this theoretical TASS picture are

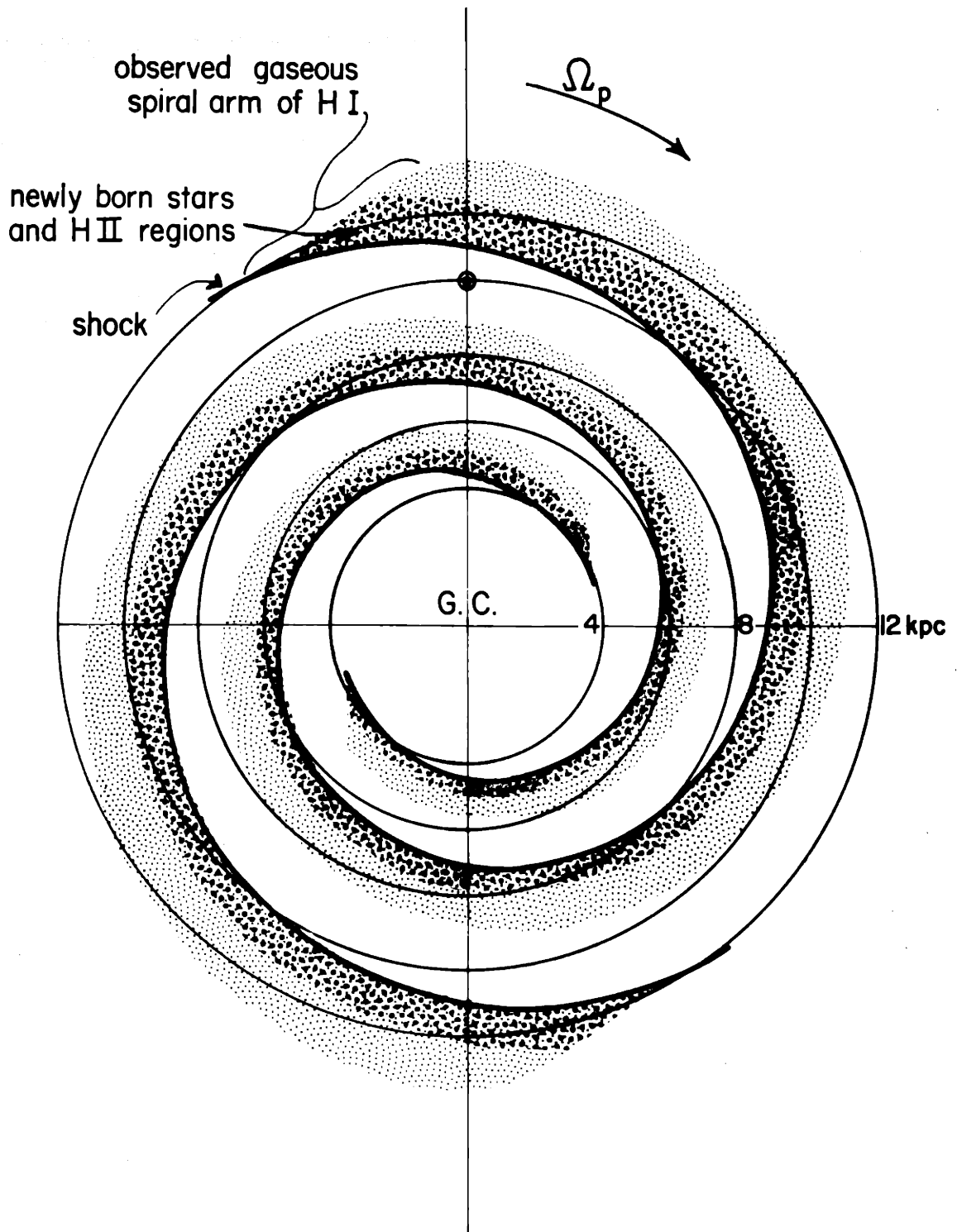


Figure (32.3)  
Spiral Pattern in the Galaxy

of especial interest. An imposed spiral gravitational field with a magnitude of about 5% of the symmetrical field is adopted,<sup>1</sup> although calculations for other spiral field strengths have been carried out also. In this picture, the effective shock compression along the shock wave pattern varies from about 5 in the 10 kpc region to approximately 8-10 in the 3-4 kpc neighborhood. Gas streamtubes themselves appear as sharp-pointed ovals with their two sharp turning points lying coincident with the shocks. Along each streamtube the radial velocity varies considerably; the maximum and minimum radial velocities which are attainable along the 10 kpc streamtube are about  $\pm 13$  km/s, whereas the maximum and minimum radial velocities which are attainable along a streamtube in the 3-4 kpc neighborhood are about  $\pm 20$  km/s.

In the linear density wave theory, the density wave pattern of spiral structure, which is composed of both gas and stars, terminates in inner Lindblad resonance at a distance of about 3.5 kpc from the galactic center. Such a lack of overall spiral structure within the radius of about 3.5 kpc signifies the absence of an overall spiral gravitational field in this region of the galactic disk.

An exciting theoretical feature of the galactic shock picture is therefore evidenced by the twice-periodic gas streamtube free mode discovered near the 3 kpc region of the Schmidt model. This free mode exhibits an effective compression over the streamtube of about 10, and

---

<sup>1</sup>In studies of the migration of moderately-young stars in our Galaxy, the spiral field is estimated at about 5% of the symmetrical field. (see Lin, Yuan, and Shu, 1968)

the maximum and minimum radial velocities along the free mode streamtube are about  $\pm 16-20$  km/s. Since the free mode is maintained with a zero imposed spiral perturbation field, such a free mode is evidently sustained entirely by resonance. The existence of this free mode therefore indicates in a positive manner the presence of resonance in the dynamics of the gaseous disk.

Some features of the "3 kpc arm" of observational studies are apparent in this "resonant" free mode. Large positive radial velocities (on the order of 16-20 km/s) occur over two short arcs<sup>1</sup> of length similar to the length of the "3 kpc arm." Large negative velocities of similar order of magnitude occur over two other short arcs of similar length. Since no imposed spiral field of leading or trailing type is present to influence the leading or trailing nature of the free mode, both a leading and a trailing free mode are possible.<sup>2</sup> Since the "3 kpc arm" of observational studies exhibits large positive radial velocities (of the order of 50 km/s), the free mode of leading type rather than the free mode of trailing type better characterizes high density arcs which undergo rapid outwards motion toward the solar neighborhood.<sup>3</sup> If the free mode were oriented in such

---

<sup>1</sup>These arcs of high radial velocity lie exactly  $\pi$  radians apart along the streamtube.

<sup>2</sup>Section 12 shows that the maximum positive radial velocity coincides with the maximum density along a streamtube in the shock pattern of leading type, whereas the maximum negative radial velocity coincides with the maximum density along a streamtube in the shock pattern of trailing type.

<sup>3</sup>If the "3 kpc arm" of observational studies were actually located on the far side of the galactic disk from the solar neighborhood, the free mode of trailing type would better characterize the high density region of rapid inwards motion towards the solar neighborhood.

a way that one of those high velocity arcs lies between the galactic center and the solar neighborhood, then in observational studies made from the solar vicinity, these large positive velocity arcs may well appear as material arms in rapid radial expansion with features strikingly similar to the "3 kpc arm" (although the theoretical free mode expansion is still only about 1/3 of the observed outwards expansion of the "3 kpc arm.")

Just as over other portions of the galactic disk, a spiral field enhances the shock pattern and increases the maximum radial velocity possible along a streamtube. Therefore, the effects of an imposed spiral gravitational field on the free mode are of interest also.<sup>1</sup> When spiral fields with strengths of 5%, 10%, and 15% of the symmetrical field are imposed, the maximum radial velocities induced along the 3 kpc streamtube are about 20 km/s, 30 km/s, and 40 km/s respectively. The high density regions coincide with the regions of large positive or negative radial velocity according as the shock pattern is of leading or trailing type. With a 15% field the value of 50 km/s for radial velocity in observational studies is almost attained, although there is lack of sufficient reason how a spiral field of such a great strength can exist in the 3 kpc region in the first place. On the other hand, if

---

<sup>1</sup>These calculations where a spiral field is imposed in the 3 kpc neighborhood of the Schmidt model are of general exploratory character since no such spiral field is possible in this region according to the linear theory. However, in the nonlinear theory, the gaseous component organizes itself into a free mode and maintains a shock pattern in the 3 kpc region without a supporting field. This nonlinear organization of a gaseous free mode signifies as well the organization of an induced gravitational field due to the gas alone, although this induced field due to the gas can be at most of the order of only a few percent of the symmetrical field.

the rotation curve of the Galaxy were actually shifted from its present shape in the 3 kpc neighborhood (and in the central regions) of the Schmidt model, then the possibility for continuation of the grand design into the 3 kpc region and for a spiral field and a forced mode, which might exhibit radial velocities of the order of 50 km/s, may be present.



## Evolution and Development of Galactic Shock Waves

The growth of galactic shock waves within a spiral galaxy has been investigated in Part III. It has been shown that the superposition of a spiral gravitational field on a disk-shaped galaxy is sufficient to induce the formation of large-scale galactic shocks within a few rotations of the disk. The greater the strength of the spiral field, the more rapidly are shocks induced.

Of the various shocks possible there exists one mode that evolves into a corotating shock. This mode grows at a more rapid rate than any of the others. With  $\epsilon$  as a measure of the perturbation field strength, the time for the formation of the corotating shock is of the order of  $\epsilon^{-1/2}$ , whereas the time for the development of all the other non-corotating shocks is of the order of  $\epsilon^{-1}$ . The most exciting feature of Part III is this most rapidly growing, corotating shock; for, it is shown that this shock is precisely the time-evolved, self-sustained density wave which comprises the quasi-stationary grand design of spiral structure in the Lin-Shu linear density wave theory.

Whereas the investigation of Part II provides for the existence and persistence of a stationary two-armed spiral shock wave pattern, the investigation of Part III indicates the possible evolutionary process of the development of a galactic shock pattern as an outgrowth of the grand design of spiral structure according to the linear density wave theory.

## Star Formation along Spiral Arms

The final area of investigation in this thesis has been the implication of the spiral galactic shock pattern on star formation along spiral arms. Encouragement for star formation along spiral arms in our theoretical picture has been provided by trial calculations for a simple gas cloud model consisting of an isothermal sphere of gas in thermal equilibrium with a surrounding medium of rarefied gas, all in turbulent motion. Although internal turbulence enhances the cloud with an equivalent temperature and pressure that tend to prevent self gravitational collapse, it also provides the cloud with internal fragmentation which influences the formation of many protostars inside the cloud once the collapse process has been triggered. A typical large gas cloud has a mass of 10,000 to 25,000  $M_{\odot}$ , a mean density of 20 H/cc, a radius of 17 to 25 pc, a kinetic temperature of 100°K, and an internal root mean square turbulent velocity between .5 km/s and 2 km/s, which is a typical estimate of internal turbulence according to observational studies. An 8:1 shock compression is just sufficient to trigger the gravitational collapse of a cloud of this size.

Due to internal turbulent eddies and fragments, the interior of the cloud may be visualized to consist of two distinct portions: (1) those regions consisting of clumps of gas concentration called subclouds which are the candidates for protostars; and (2) the inter-subcloud medium. Even though this model is somewhat of an idealization of the real physical picture, some basic features of star formation are apparent from such a cloud-subcloud model. With a subcloud

of an average mass of  $50 M_{\odot}$  and a mean density of  $40 \text{ H/cc}$ , a compression on the order of  $100,000:1$  is necessary to place the individual subcloud on its verge of gravitational collapse. Therefore, an  $8:1$  shock wave compression can trigger only the collapse of the large cloud, which in turn is capable of triggering the subsequent compression and collapse of the individual subclouds. Each subcloud may form a star, and this newly-born star lies in association with the stars formed from all the other subclouds inside the large cloud. The overall time of collapse of a typical large cloud from the shock-triggering stage to the formation of an association of newly-born stars is about 30 million years. It may be inferred that subclouds can form stars only if they are contained in large clouds or in large cloud complexes. In addition, newly-born stars must practically always be found in associations with other newly-born stars, and these newly-born stellar associations for the most part must lie along spiral arms. These implications from the shock theory and the cloud model are already generally well established by observational studies.

### 33. Comparison with observations

A comparison will now be made between the theoretical results of this thesis and observational studies of our own Milky Way System as well as other spiral galaxies.

#### Narrow Star Formation Regions

Observational studies of our Milky Way System have provided evidence that newly-born stars and luminous H II regions lie for the most part along narrow spirals<sup>1</sup> on the inside of the spiral arms making up the grand design of our Galaxy (personal communication of Westerhout to Lin and coworkers). In general agreement with these observational studies, the theoretical investigations of this thesis have confirmed that galactic shock waves may provide for the formation of stellar associations along narrow spirals similar to those of observational studies. This theoretical picture contains galactic shocks lying nearly along the center axes of the nonobservable background spiral arms and along the inner edges of the observable trailing gaseous spiral arms of the two-armed luminous grand design of our Galaxy.

Attention may be focused on the narrowness of the gas density peak located just behind the shock in Figures (32.2) and (32.3). Such

---

<sup>1</sup>see Morgan et al. (1952); and Sharpless (1965).

a narrow peak in pressure and density indicates appreciable star formation may take place only over the narrow spiral region lying just behind the large scale galactic shock. Over a time period for the formation and evolution of the relatively massive stars initiated at the shock, (on the order of 30 million years), matter traverses a distance normal to the spiral arm of only about  $1/8$  of the total wavelength separating successive arms. Therefore, the relatively massive and luminous newly-born stars are confined to the inner sides of the observed gaseous spiral arms; for, when they pass outside this region, they are no longer newly-born or luminous. The most luminous region of the disk is therefore the narrow spiral sector directly outside each galactic shock which itself lies on the inner edge of an observable gaseous spiral arm of trailing type. By the time the newly-born stars have travelled to the center of an observable gaseous spiral arm, their luminosity will have decayed appreciably because of their relatively rapid evolution.

#### H I versus H II Distributions

M. S. Roberts (1967) has shown for Sc-type galaxies that the regions of highest H I distribution do not coincide with and, in fact, lie significantly outside of the regions of the newly-born stars and the H II regions. For the several investigated Sc-type galaxies, the optical arms lie significantly interior to the H I peak. In close similarity to the distributions of H I and H II for Sc-type galaxies investigated by M. S. Roberts, this same feature is present for our own Milky Way System, as the Westerhout results (1958) for the distribu-

tions of H II and neutral hydrogen have confirmed.<sup>1</sup>

Since it would seem a priori that the distributions of H I and H II with respect to radius should have the same general character, with the peak of one coinciding with the peak of the other; the work of M. S. Roberts sheds a new light on the spiral galaxy picture: namely, a large shift in the peak of H II from the peak of H I seems to indicate a strong triggering mechanism which is capable of affecting the production of H II according to the mechanism's own pattern, considerably independent of the distribution of H I. In our own galaxy as well as the various Sc-type galaxies investigated by M. S. Roberts, not only is the mechanism apparently present, but also its strength must be considerable in order to produce such radial shifts of the H II distribution away from the basic sustaining H I distribution. The large supersonic Mach numbers and large compressions characteristic of the theoretical TASS picture demonstrate how powerful a mechanism the galactic shock pattern may be in governing the H II distribution at will. All this evidence then adds further support to a large-scale TASS pattern that can control to a large extent the star formation process as well as the radial distribution of H II over the galactic disk.

In the Schmidt model of our own Milky Way System the theoretical TASS pattern extends outwards to about a radius of 12 kpc. The extent of the shock pattern which is limited to within the 12 kpc region of the Schmidt model may therefore provide this limit on the radial

---

<sup>1</sup>Also, see Oort (1965).

extent of H II concentrations in our Milky Way System. Indeed, the reason why there are no newly-born stars and no H II regions coinciding with the regions of highest H I distribution in our own galaxy and in Sc-type galaxies may be that there are no shocks present at such large radii where the H I distribution is maximal.

### Recent H II Investigations

Further comparisons may be made between the theoretical shock picture and the recent observational studies of Burke, Mezger, Reifenshtein, and Wilson (1968), who have searched for H II regions in the galaxy. They have drawn the following picture of the distribution of H II: Within the nuclear region some H II regions exist, however outside the nucleus and out to about 4 kpc distance from the galactic center, few H II regions can be found. At about 4 kpc many giant H II regions begin to appear, and from 4 kpc to 6 kpc such H II regions are plentiful. They have found some H II in the 8 kpc region and smaller concentrations of H II in the solar neighborhood; however the highest density of H II regions appears to be concentrated from 4 kpc to 6 kpc in the galactic disk. The neutral hydrogen is more widely extended, and therefore the H II appears mainly in the inner parts of the H I disk. These more recently observed features even further demonstrate the general agreement between the theoretical TASS picture and observational studies of the Milky Way System.

There may be at least two basic effects in the theoretical TASS picture that help contribute to the rise in H II density inwards from 10 kpc toward the 4 kpc neighborhood. The first effect is the rise in

shock compression toward the galactic center; the second effect is the possible increase in turbulent dispersion toward the center. A typical galactic shock pattern has an effective compression of 5 in the 10 kpc radial region and 8-10 near the 4 kpc radial neighborhood. A shock pattern of such an inwards-increasing strength may well account for a rise in H II concentration by a factor of almost two between the 10 kpc and 4 kpc regions. The second effect of increasing gaseous turbulent dispersion (with the accompanying effect of increasing density variation in the gaseous clouds) toward the inner regions may contribute to a further relative rise in star formation and H II concentration in the 4 kpc neighborhood. From observational studies it appears the disk may retain a fairly constant thickness between 4 kpc and 10 kpc, whereas the gaseous density may rise somewhat toward the center. Since the gaseous turbulent dispersion gives rise to a pressure which helps support the gaseous disk against further self gravitational flattening, a rise in density encourages a corresponding rise in the turbulent dispersion in order to maintain the disk at fairly constant thickness. In this situation, larger amounts of turbulent pressure act on the cloud envelopes in the inner galactic regions; and less massive clouds which are not capable of reaching their verges of gravitational collapse in the solar neighborhood, for instance, may indeed surpass their verges of gravitational collapse in the 4 kpc neighborhood. A variation in turbulent dispersion speed of a few km/s from 10 kpc to 4 kpc may well enhance the relative abundance of star formation and H II concentration in the 4 kpc neighborhood in relation to that in the solar neighborhood.



### Free Mode and "3 Kpc Arm"

There is one further exciting feature of the theoretical shock pattern that helps to account for the remarkable "3 kpc arm" phenomenon of our own Milky Way System. This feature is the free mode discovered in the 3 kpc neighborhood of the Schmidt model of our Galaxy. The free mode itself contains large amplitude effects and high radial velocity expansion regions even in the presence of a zero spiral field. Such a free mode with positive radial velocities as high as 16-20 km/s provides a definite indication for the existence of non-linear gaseous resonance in the 3 to 4 kpc neighborhood of our Galaxy. Resonance alone without the influence of any spiral field is apparently capable of sustaining this free mode in the 3 kpc neighborhood of the Schmidt model.

Some curious features of the theoretical free mode in the 3 kpc region are also characteristic of the "3 kpc arm" of observational studies. The free mode contains streamtube arcs of high positive radial velocity (of about 16-20 km/s) located exactly  $\pi$  radians apart along the gas streamtube. If our solar neighborhood happened to lie along a radius vector which passes through one of these arcs in the 3 to 4 kpc neighborhood, then an arc of gaseous matter with high radial expansion would be a quite apparent feature in observational studies

from the solar neighborhood.<sup>1</sup> The observationally described "3 kpc arm" of expansion may well be in reality such an expansion arc of gas.

---

<sup>1</sup>The free mode itself can account for a radial expansion of about 16-20 km/s, whereas the "3 kpc arm" of observational studies in fact exhibits an expansion of about 53 km/s. If indeed the observational picture is correctly interpreted, some further aspect of the theoretical picture is needed to supply the extra outwards radial velocity of some 30 km/s. Sections 15 and 32 have discussed the possibility of an imposed spiral perturbation field in the 3 kpc region. Such an imposed field of 15% of the symmetrical field is shown in fact to give rise to a material arm of short arc length with almost 50 km/s radial expansion. However, a field of such great strength and in fact any field at all in the 3 kpc region above a few percent of the symmetrical field is difficult to account for in the linear density wave theory and in the nonlinear theory as well.

Appendices

## Appendix I. Comparison with earlier work

Although Fujimoto's calculations on gas flow through a model spiral arm (1966) may be regarded of general exploratory character, they nevertheless represent an important first step in the determination of the nonlinear dynamics of the gaseous disk. Fujimoto considers the motion of gas across a "gravitational washboard" (i.e., a gravitational potential of a sinusoidal form)<sup>1</sup> and demonstrates that a periodic shock solution is possible over the "washboard". One of the most important features of his shock solution is the strikingly-large density contrast of 5 or more<sup>2</sup> which the imposed perturbation field of moderate strength (7.5% of the symmetrical field) induces. Another important feature is evidenced by the fact that a shock generally occurs within the potential well of the imposed potential.

Understanding the importance of these results, we should discuss why Fujimoto's calculations must be regarded of general exploratory character and why further nonlinear investigation has been necessary.

---

<sup>1</sup>Fujimoto's multiarmed potential is similar to the two-armed potential adopted in this investigation; although it possesses no fewer than four, and in some of his calculations as many as ten or twenty arms.

<sup>2</sup>A density contrast of 5 to 10 is characteristic of the shock solutions of this investigation also.

At the time Fujimoto performed his calculations, it was evidently not clear what a typical estimate of the pattern speed for our Milky Way System should be. In the absence of any a priori determination of the pattern speed, Fujimoto adopted a value of about 45 km/s/kpc. This value presumably represents some kind of mean angular velocity of the matter in the galactic disk. Since the pattern speed determined from more recent observational studies is estimated at about 12.5 km/s/kpc,<sup>1</sup> the value for the pattern speed adopted by Fujimoto appears too large by a factor of almost 4. As a consequence of such a high pattern speed as 45 km/s/kpc, corotation in the Schmidt model occurs at about 5 kpc; and therefore, Fujimoto's calculations, which cover the range of radii between 6 and 11 kpc in the galactic disk, actually represent points lying outside corotation. In the present work, the more recent estimate of 12.5 km/s/kpc for the pattern speed is adopted, and thereby corotation lies at about 17 kpc from the galactic center. Therefore, all calculations in the present investigation which involve streamtubes lying within 12 kpc from the galactic center, represent gas flow lying within the corotation circle.

One further major difference stands out between Fujimoto's calculations and the present investigation. This difference is readily seen if we write the basic set of equations (4.4), (4.5), and (4.6) and compare them with Fujimoto's equations. If we write:

---

<sup>1</sup>This pattern speed is obtained from two studies - (1) the distribution of neutral hydrogen and (2) the migration of moderately-young stars (see Lin, Yuan, and Shu, 1968). The value used here is actually a compromise between 11.5 and 13.5.

$$\sigma_0 + \sigma_1 = \sigma$$

$$(\Omega - \Omega_p)\varpi \sin i + w_{\perp} = W_{\perp}$$

$$(\Omega - \Omega_p)\varpi \cos i + w_{\parallel} = W_{\parallel}$$

then the set of equations, (4.4), (4.5), and (4.6), may be rewritten in the form:

$$\frac{\partial \sigma}{\partial t} + \frac{1}{\varpi} \left( \frac{\partial(\sigma W_{\perp})}{\partial n} + \frac{\partial(\sigma W_{\parallel})}{\partial \xi} \right) + \frac{\sigma}{\varpi} (W_{\perp} \cos i - W_{\parallel} \sin i) = 0 \quad (I.1)$$

$$\begin{aligned} \frac{\partial W_{\perp}}{\partial t} + \frac{1}{\varpi} \left( W_{\perp} \frac{\partial W_{\perp}}{\partial n} + W_{\parallel} \frac{\partial W_{\perp}}{\partial \xi} \right) - 2\Omega_p W_{\parallel} + \frac{1}{\varpi} \left( \frac{a^2}{\sigma} \frac{\partial \sigma}{\partial n} + \frac{\partial U_{\perp}}{\partial \xi} \right) \\ = \frac{W_{\parallel}}{\varpi} (W_{\parallel} \cos i + W_{\perp} \sin i) - (\Omega^2 - \Omega_p^2)\varpi \cos i \end{aligned} \quad (I.2)$$

$$\begin{aligned} \frac{\partial W_{\parallel}}{\partial t} + \frac{1}{\varpi} \left( W_{\perp} \frac{\partial W_{\parallel}}{\partial n} + W_{\parallel} \frac{\partial W_{\parallel}}{\partial \xi} \right) + 2\Omega_p W_{\perp} + \frac{1}{\varpi} \left( \frac{a^2}{\sigma} \frac{\partial \sigma}{\partial \xi} + \frac{\partial U_{\parallel}}{\partial \xi} \right) \\ = -\frac{W_{\perp}}{\varpi} (W_{\parallel} \cos i + W_{\perp} \sin i) + (\Omega^2 - \Omega_p^2)\varpi \sin i \end{aligned} \quad (I.3)$$

Fujimoto's equations may be written in the form:

$$\frac{1}{\varpi} \left( \frac{\partial(\sigma W_{\perp})}{\partial \eta} + \frac{\partial(\sigma W_{\parallel})}{\partial \xi} \right) = 0$$

$$\begin{aligned} \frac{1}{\varpi} \left( W_{\perp} \frac{\partial W_{\perp}}{\partial \eta} + W_{\parallel} \frac{\partial W_{\perp}}{\partial \xi} \right) - 2\Omega_p W_{\parallel} + \frac{1}{\varpi} \left( \frac{a^2}{\sigma} \frac{\partial \sigma}{\partial \eta} + \frac{\partial U_{\perp}}{\partial \eta} \right) \\ = - [\Omega^2 - \Omega_p^2 - (\Omega - \Omega_p)^2] \varpi \cos i \end{aligned}$$

$$\begin{aligned} \frac{1}{\varpi} \left( W_{\perp} \frac{\partial W_{\parallel}}{\partial \eta} + W_{\parallel} \frac{\partial W_{\parallel}}{\partial \xi} \right) + 2\Omega_p W_{\perp} + \frac{1}{\varpi} \left( \frac{a^2}{\sigma} \frac{\partial \sigma}{\partial \xi} + \frac{\partial U_{\parallel}}{\partial \xi} \right) \\ = [\Omega^2 - \Omega_p^2 - (\Omega - \Omega_p)^2] \varpi \sin i \end{aligned}$$

Comparing Fujimoto's equations with the set of equations, (I.1), (I.2), and (I.3), term by term, we find that a significant term of first order is lacking in each of Fujimoto's velocity component equations. These missing terms are respectively:

$$2 (\Omega - \Omega_p) w_{\parallel}$$

$$- (\Omega - \Omega_p) w_{\perp}$$

The absence of these terms is readily seen if the right hand sides of equations (I.2) and (I.3) are expanded. For example, the right hand side of equation (I.2) becomes:

$$\begin{aligned}
& \frac{W_{\parallel}}{\sigma} (W_{\parallel} \cos i + W_{\perp} \sin i) - (\Omega^2 - \Omega_p^2) \sigma \cos i \\
& = - [\Omega^2 - \Omega_p^2 - (\Omega - \Omega_p)^2] \sigma \cos i + 2(\Omega - \Omega_p) W_{\parallel} \\
& \quad - (\Omega - \Omega_p) W_{\parallel} \sin^2 i + (\Omega - \Omega_p) W_{\perp} \sin i \cos i \\
& \quad + \frac{W_{\parallel}}{\sigma} (W_{\parallel} \cos i + W_{\perp} \sin i)
\end{aligned}$$

The second term in particular is non-negligible compared to  $2\Omega_p W_{\parallel}$  when the flow region does not encompass the corotation neighborhood.

In summary, the basic physical differences between the two analyses are:

- (1) Because of the high pattern speed of about 45 km/s/kpc adopted in Fujimoto's analysis, his calculations (which cover radii between 6 and 11 kpc) correspond to points in the disk lying outside corotation. In this work, the calculations (for portions of the galactic disk between 3-4 kpc and 12 kpc) for a pattern speed of 12.5 km/s/kpc correspond to points interior to corotation.
- (2) With the neglect of terms of  $\mathcal{O}(\Omega - \Omega_p)$ , Fujimoto's analysis is valid only near corotation in his model. The calculations of the present investigation, which are valid to first order in the asymptotic approximation, determine gas flow along streamtube bands which cover the entire disk between the radii of 3-4 kpc and 12 kpc.
- (3) A two-armed spiral shock pattern covering a large portion of the galactic disk is determined in this work. No two-armed shock pattern



is possible in Fujimoto's calculations (this is a consequence of differences (1) and (2) above).

Appendix II. Validity of the asymptotic approximation

In Section 5, we made an asymptotic approximation. We now demonstrate its validity. If we introduce the new independent variables:

$$\zeta = \delta_1 \xi$$

$$\tau = \delta_2 t$$

the nonlinear equations, (4.4), (4.5), and (4.6), may be written in the following form:

$$\begin{aligned} & \frac{\partial(\sigma_1 w_{\perp})}{\partial \eta} + \sigma_0 \frac{\partial w_{\perp}}{\partial \eta} + (\Omega - \Omega_p) \omega \sin i \frac{\partial \sigma_1}{\partial \eta} \\ & + (\sigma_0 + \sigma_1 + \omega \frac{d\sigma_0}{d\omega}) (w_{\perp} \cos i - w_{\parallel} \sin i) \\ & + [\delta_2 \omega \frac{\partial \sigma_1}{\partial \tau} + \delta_1 \{ \frac{\partial(\sigma_1 w_{\parallel})}{\partial \zeta} + \sigma_0 \frac{\partial w_{\parallel}}{\partial \zeta} + (\Omega - \Omega_p) \omega \cos i \frac{\partial \sigma_1}{\partial \zeta} \}] \\ & = 0 \quad (\text{II.1}) \end{aligned}$$

$$\begin{aligned}
& w_{\perp} \frac{\partial w_{\perp}}{\partial \eta} + (\Omega - \Omega_p) \varpi \sin i \frac{\partial w_{\perp}}{\partial \eta} - 2\Omega \varpi w_{\parallel} + \varpi^2 \frac{d\Omega}{d\varpi} \sin i (w_{\perp} \cos i - w_{\parallel} \sin i) \\
& - w_{\parallel} (w_{\perp} \sin i + w_{\parallel} \cos i) + \frac{a^2 \varpi \cos i}{\sigma_0 + \sigma_1} \frac{d\sigma_0}{d\varpi} + \frac{a^2}{\sigma_0 + \sigma_1} \frac{\partial \sigma_1}{\partial \eta} + \frac{\partial U_1}{\partial \eta} \\
& + [\delta_2 \varpi \frac{\partial w_{\perp}}{\partial \tau} + \delta_1 \{ w_{\parallel} \frac{\partial w_{\perp}}{\partial \zeta} + (\Omega - \Omega_p) \varpi \cos i \frac{\partial w_{\perp}}{\partial \zeta} \}] = 0 \quad (\text{II.2})
\end{aligned}$$

$$\begin{aligned}
& w_{\perp} \frac{\partial w_{\parallel}}{\partial \eta} + (\Omega - \Omega_p) \varpi \sin i \frac{\partial w_{\parallel}}{\partial \eta} + 2\Omega \varpi w_{\perp} + \varpi^2 \frac{d\Omega}{d\varpi} \cos i (w_{\perp} \cos i - w_{\parallel} \sin i) \\
& + w_{\perp} (w_{\perp} \sin i + w_{\parallel} \cos i) - \frac{a^2 \varpi \sin i}{\sigma_0 + \sigma_1} \frac{d\sigma_0}{d\varpi} \\
& + [\delta_2 \varpi \frac{\partial w_{\parallel}}{\partial \tau} + \delta_1 \{ w_{\parallel} \frac{\partial w_{\parallel}}{\partial \zeta} + \frac{a^2}{\sigma_0 + \sigma_1} \frac{\partial \sigma_1}{\partial \zeta} + \frac{\partial U_1}{\partial \zeta} \\
& + (\Omega - \Omega_p) \varpi \cos i \frac{\partial w_{\parallel}}{\partial \zeta} \}] = 0 \quad (\text{II.3})
\end{aligned}$$

The bracket, [ ], in each of the equations is regarded as influencing the gas flow to a secondary order in relation to the other terms in each equation although some small terms are also retained outside the bracket.

First,  $\delta_2$  is taken small enough for all time dependence to disappear to first order. Second, we take:

$$\frac{\delta_1}{\tan i} = \mathcal{O}(1)$$

In this case, the gradients,  $\frac{\partial}{\partial n}$  and  $\frac{\partial}{\partial \zeta}$ , of the quantities,  $\sigma_1'$ ,  $w_{\perp}'$ , and  $w_{\parallel}'$  (the nondimensional form of the physical quantities), may be directly compared for a determination of the importance of each term appearing in equations (II.1), (II.2), and (II.3). For example, the numerical calculations (of Part II) for the region of the galactic disk between the radii of 6 kpc and 10 kpc (excluding the shock neighborhood) yield:

$$\left. \frac{\frac{\partial \sigma_1'}{\partial \zeta}}{\frac{\partial \sigma_1'}{\partial n}} \right|_n = \mathcal{O}\left(\frac{1}{6}\right) \quad \left. \frac{\frac{\partial w_{\perp}'}{\partial \zeta}}{\frac{\partial w_{\perp}'}{\partial n}} \right|_n = \mathcal{O}\left(\frac{1}{5}\right) \quad \left. \frac{\frac{\partial w_{\parallel}'}{\partial \zeta}}{\frac{\partial w_{\parallel}'}{\partial n}} \right|_n = \mathcal{O}\left(\frac{1}{10}\right)$$

If we now write the largest term in the bracket, [ ], and the corresponding term outside the bracket of each of the equations, (II.1), (II.2), and (II.3) in nondimensional form, we have:

$$(\Omega - \Omega_p) \omega \sin i \left[ \frac{\partial \sigma_1'}{\partial n} + \frac{\delta_1}{\tan i} \frac{\partial \sigma_1'}{\partial \zeta} \right]$$

$$(\Omega - \Omega_p) \omega \sin i \left[ \frac{\partial w_{\perp}'}{\partial n} + \frac{\delta_1}{\tan i} \frac{\partial w_{\perp}'}{\partial \zeta} \right]$$

$$(\Omega - \Omega_p) \omega \sin i \left[ \frac{\partial w_{\parallel}'}{\partial n} + \frac{\delta_1}{\tan i} \frac{\partial w_{\parallel}'}{\partial \zeta} \right]$$

Since  $\delta_1$  and  $\tan i$  are of the same order, the second term in each bracket above is no larger than  $\mathcal{O}(1/5)$  of the corresponding first

term. In addition, all the other terms in the bracket, [ ], of each of the equations, (II.1), (II.2), and (II.3), are  $O((1/5)\delta_1)$  of their counterparts outside the bracket. Therefore, the asymptotic approximation for the region between the radii of 6 kpc and 10 kpc (and in general between the radii of 3-4 kpc and 10 kpc) is valid to  $O(1/5)$ .

### Appendix III. Sonic point conditions

A particularly convenient place to begin the numerical integration of equations (5.10) and (5.11) is the point in velocity space where  $w_{\perp 0}' + w_{\perp}' = a$ . This point is referred to as the sonic point because the velocity component,  $w_{\perp}'$ , changes from subsonic to supersonic at this point.

The first sonic point condition may be written in nondimensional form as:

$$w_{\perp}'|_{\eta=0} = a' - w_{\perp 0}' \quad (\text{III.1})$$

Examination of equation (5.10) leads us to the conclusion that unless the numerator of the right hand side is zero at the sonic point, the derivative,  $\frac{\partial w_{\perp}'}{\partial \eta}$ , will be infinite there. We therefore consider alternatives to the possibility of an infinite derivative,  $\frac{\partial w_{\perp}'}{\partial \eta}$ , at the sonic point. One possible way to avoid this unphysical situation is to set the numerator of the right hand side of equation (5.10) equal to zero at the sonic point. In this case, we have the condition (in nondimensional form):

$$(w_{\perp 0}' + w_{\perp}') (w_{\parallel}' + f' - \chi_2') + \left(1 + \frac{\pi}{\sigma_0 + \sigma_1} \frac{d\sigma_0}{d\bar{\omega}}\right) a'^2 \chi_1' = 0$$

From this relation we may determine  $w_{\parallel}'$  at the sonic point. Since the gradient of base state density with respect to radial distance,

$\omega$ , has been assumed of secondary importance in the numerical calculations, we disregard the term containing  $\frac{d\alpha_0}{d\omega}$  as well here. If  $x_1$  and  $x_2$  are expanded, this relation yields:

$$w_{11}'(n=0) = \frac{-b_1 + \{(b_1^2 - 4 \cos i b_2)\}^{1/2}}{2 \cos i} \quad (\text{III.2})$$

where

$$b_1 = \left[ 1 + \left( \frac{\omega \frac{d\Omega}{d\omega}}{2\Omega} - \frac{\Omega - \Omega_p}{2\Omega} \right) \sin^2 i \right]$$

$$b_2 = \left[ f' + \left( a' - \frac{\omega \frac{d\Omega}{d\omega}}{2\Omega} \sin i \right) \cos i w_{11}' \right] \Big|_{n=0}$$

Relation (III.2) comprises the second sonic point condition. The positive [+] square root in equation (III.2) provides the only physical result.

The third sonic point condition is easily obtained from equation (5.11):

$$\frac{\partial w_{11}'}{\partial n} \Big|_{n=0} = - \frac{\left( \frac{K}{2\Omega} \right)^2 w_{11}' + x_3'}{a'} \Big|_{n=0} \quad (\text{III.3})$$

The fourth sonic point condition for  $\frac{\partial w_{11}'}{\partial n}$  will now be determined. Since both the numerator and the denominator of equation (5.10) are equal to zero at the sonic point, a Taylor series expansion of both numerator and denominator about the sonic point is necessary. Expanding

all terms about the sonic point, we arrive at the following expression in the limit as  $\Delta\eta \rightarrow 0$ :

$$2\left(\frac{\partial w_{\perp}'}{\partial \eta}\right)^2 \Big|_{\eta=0} = \left[ \frac{\partial w_{\parallel}'}{\partial \eta} + \frac{\partial f'}{\partial \eta} - \frac{\partial \chi_2'}{\partial \eta} - \chi_1' \frac{\partial w_{\perp}'}{\partial \eta} + a' \frac{\partial \chi_1'}{\partial \eta} \right] \Big|_{\eta=0}$$

Upon substitution of the expressions for  $\chi_1'$  and  $\chi_2'$  we obtain a relation for  $\frac{\partial w_{\perp}'}{\partial \eta}$ :

$$\frac{\partial w_{\perp}'}{\partial \eta} \Big|_{\eta=0} = \frac{-b_3 + (b_3^2 + 8b_4)^{1/2}}{4} \quad (\text{III.4})$$

where

$$b_3 = [w_{\perp}' \cos i - 2w_{\parallel}' \sin i + \left(\frac{w}{2\Omega} \frac{d\Omega}{d\sigma} \sin i - a'\right) \cos i] \Big|_{\eta=0}$$

$$b_4 = \left[ \frac{\partial f'}{\partial \eta} + \left(1 + 2w_{\parallel}' \cos i + \left(\frac{w}{2\Omega} \frac{d\Omega}{d\sigma} - \frac{\Omega - \Omega_P}{2\Omega}\right) \sin 2i\right) \frac{\partial w_{\parallel}'}{\partial \eta} \right] \Big|_{\eta=0}$$

Relation (III.4) then is the fourth sonic point condition. The positive square root provides the only physical result since the negative [-] square root would provide for a change from supersonic flow to subsonic flow at the sonic point which is physically impossible except by means of a shock.



#### Appendix IV. Procedure of numerical integration

With the specification of all the parameters, the sonic point conditions are determined, and the numerical integration of the equations of motion may begin. We will concentrate here on the numerical integration of equations (5.10) and (5.11). These two equations contain the two dependent variables  $w_{\perp}$  and  $w_{\parallel}$  and the one independent variable  $\eta$ . With the sonic point as the starting point for the integration forwards and backwards in  $\eta$ , we have a problem similar in form to an initial value problem. We now describe the subroutine used for the integration.

We have used subroutine RKGS (see pp. 118-121 of System/360 Scientific Subroutine Package) which incorporates the Runge-Kutta method for the solution of initial value problems. The purpose of the Runge-Kutta method is to obtain an approximate solution of a system of first-order ordinary differential equations with given initial values. It is a fourth-order integration procedure which is stable and self-starting; that is, only the functional values at a single previous point are required to obtain the functional values ahead. For this reason it is easy to change the step size at any step in the calculations. On the other hand, each Runge-Kutta step requires the evaluation of the right-hand side of the system four times, which is a great disadvantage. Another disadvantage of the method is that neither the truncation errors nor estimates of them are obtained in the calculation procedure. Therefore control of accuracy and adjustment of the step size is done by

comparison of the results due to double and single step size. Actually, this RKGS subroutine contains Gill's modification of the classical Runge-Kutta formulas for the compensation of accumulated roundoff errors.

With these essentials of the RKGS scheme in mind we now describe how we have applied it to our problem. We numerically integrate the equations of motion both forwards and backwards in  $\eta$  from the sonic point. Both a supersonic branch and a subsonic branch of the solution are determined. Since we are interested in incorporating a shock which jumps appropriately between the two branches, we calculate as well a "shock jump curve", (see Figure (8.4) ). The point where the shock jump curve and the subsonic branch intersect is the point along the subsonic branch where a shock will be compatible. Therefore, the numerical integration is carried out until this intersection of the subsonic branch and the shock jump curve takes place. The resulting total solution curve represents periodic gas flow which may begin from a shock and pass along the subsonic branch toward the sonic point, become supersonic at the sonic point, and finally after remaining supersonic for a time reach the next successive shock along its path. Once it reaches the next shock, the cycle begins again. The cycle may be repeated as many times as is necessary in order to circle the galactic disk. Proper choice of the physical parameters will guarantee exactly twice-periodic streamtube flow through two periodically-located shocks.

## Appendix V. Closure of gas streamtubes about the galactic disk

We will now examine the STS solution more closely. We see from Figure (8.3) that the shock occurs in the imposed spiral potential well. This feature is characteristic of all STS solutions we have found. The gas on the supersonic side of the shock feels the pull of the spiral field forwards toward the shock, whereas the gas on the subsonic side of the shock feels the pull of the spiral field backwards toward the shock. Closure of the streamtube is insured only if the integrated effect of the forcing on a given fluid element over one cycle of the streamtube averages to zero.

Suppose we first deduce the sense of nonclosure due to a sinusoidal spiral field of trailing type. A gas element spends more time under an acceleration backwards along  $\eta$  than forwards along  $\eta$ , so that the net coriolis effect will provide for a net positive component of velocity  $w_{\parallel}$  along  $\xi$ . When the streamtube finally reaches the same radius from which it began, its variation in  $\xi$  will therefore be greater than  $\pi \cos i$  and its circumferential variation,  $\Delta\theta$ , will be greater than  $\pi$ . According to the numerical calculations,  $\Delta\theta$  varies from  $\pi$  by about 2% for a 5% field, and by about 3% for a 7.5% field. We therefore are interested in adding just a small positive correction force directed along  $\eta$  to the spiral perturbation field. A typical correction might

be:

$$-\frac{\partial U_2}{\partial \eta} = A_2 = \text{constant}$$

Figure (V.1) sketches two STS solutions in  $w_{\perp}'$ - $w_{\parallel}'$  space, one not closed for zero correction force, and the other closed with a correction force of a magnitude about 1/6 of the magnitude of the spiral field, i.e.,  $A_2 = 1/6A$ . In general, a correction of just 1/6 of the magnitude of the spiral field is enough to insure closure for the gas streamtube. It is important to note how similar are the two curves in Figure (V.1); the only difference being a slight shift of one with respect to the other along the  $w_{\parallel}'$  axis.

With  $A_2 = 1/6A$ , the correction force involves a percentage correction to the basic axisymmetric gravitational field of less than 1%. Suppose we ask what percentage error can be expected in the neglect of stellar dispersion, for instance, in the basic circular motion of the Schmidt model:

$$-\frac{\partial U}{\partial \varpi} + \varpi \Omega^2 \left[ 1 + \mathcal{O} \left( \frac{c}{\varpi \Omega} \right)^2 \right] = 0$$

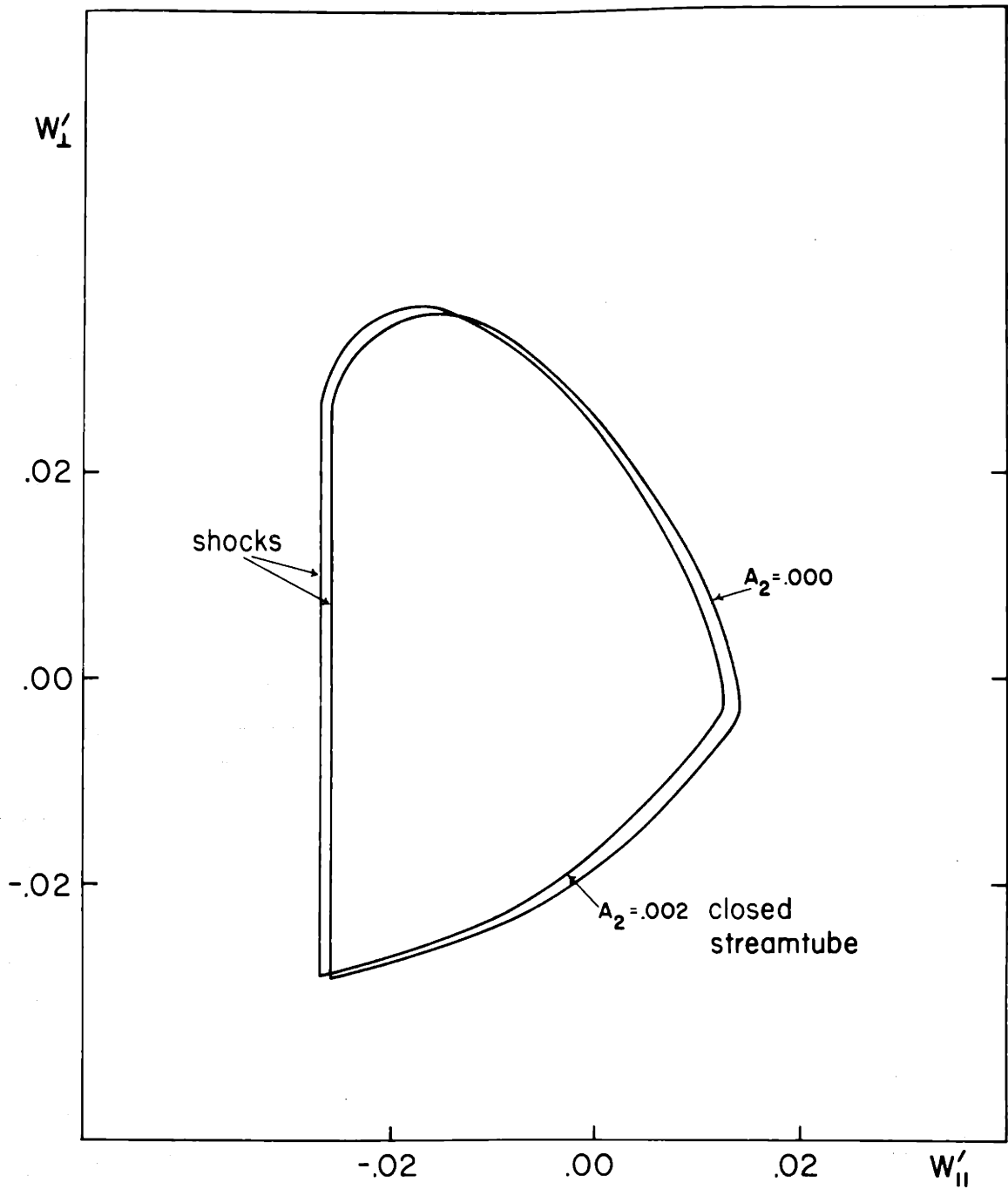


Figure (V.1)  
Closure of a Gas Streamtube

Assuming  $c_{\sigma} = 35$  km/s in the solar neighborhood, we have:

$$\left(\frac{c_{\sigma}}{\sigma\Omega}\right)^2 = .02$$

Therefore, a 2% error is already present in the base state motion in the Galaxy through the neglect of stellar dispersion; whereas only a 1% correction is involved in the problem of closure. Since the correction force is directed along  $\eta$ , it is practically equivalent to a small 1% correction to the basic centrifugal force in the galaxy.

For a spiral galaxy of leading type we may deduce much the same phenomenon. Similar to the trailing situation, the shock occurs in the potential well. With the shock in the potential well, the subsonic flow feels an acceleration backwards along  $\eta$ , and the supersonic flow feels an acceleration forwards along  $\eta$ . The times spent under each acceleration are unequal: the subsonic flow spending longer. The coriolis effect involves a net negative component of velocity  $w_{\parallel}$  along  $\xi$ . Hence, when a streamtube returns to the same radius at which it began, it will have travelled through a distance,  $\Delta\xi, < \pi \cos i$  and an angular variation,  $\Delta\theta$ , less than  $\pi$ . A small correction force directed along the  $\eta$  direction and with a magnitude about 1/6 of the magnitude of the spiral field will insure closure of the gas streamtube. Whereas the compensation involves a small subtraction from the basic gravitational field in the spiral galaxy of trailing type, the compensation involves a small addition to the basic gravitational field in the spiral galaxy of leading type.

### Bibliography

1. Axford, W.I., 1961, Phil. Trans. R. Soc. London A 253, 301.
2. Baade, W., Mayall, N.U., 1951, in Problems of Cosmical Aerodynamics, 165 (Dayton, Ohio: Control Air Documents Office).
3. Barrett, A.H., Meeks, M.L., Weinreb, S., 1964, Nature, 202, 475.
4. Burke, B.F., Mezger, P.G., Reifenstein, E.C., Wilson, T., 1968, A.A.S. meeting, Charlottesville, Va.
5. Chandrasekhar, S., 1942, in Principles of Stellar Dynamics (New York: Dover).
6. Clark, B.G., Radhakrishnan, V., Wilson, R.W., 1962, Ap. J., 135 151-174.
7. Ebert, R., 1955, Z. Astrophysics, 37, 217.
8. Field, G.B., Rather, J.D.G., Aannestad, P.A., and Orszag, S.A., 1967, Ap. J., 151, 953.
9. Fox, P., 1955, J. Math. Phys., XXXIV, 133-151.
10. Fujimoto, M., 1966 (preprint, Columbia University).
11. Hunter, C., 1964, Ap. J., 139, 570.
12. Hunter, C., 1967, Am. Math. Soc. Lectures in Applied Mathematics (1965): Relativity Theory and Astrophysics, 2, 169-194.
13. Kahn, F.D., 1960, in Die Entstehung von Sternen (Berlin: Springer-Verlag).
14. Kahn, F.D., 1968 (preprint, M.I.T.).
15. Kahn, F.D., 1968 (personal communication).
16. Kerr, F.J., Westerhout, G., 1965, in Galactic Structure, 196 (University of Chicago Press).

17. Lasker, B., 1966a, Ap. J., 143, 700.
18. Lasker, B., 1966b, Ap. J., 146, 471.
19. Lin, C.C., 1966, SIAM J. Appl. Math., 14, 876-921.
20. Lin, C.C., 1967, Am. Math. Soc. Lectures in Applied Mathematics (1965): Relativity Theory and Astrophysics, 2, 66-97.
21. Lin, C.C., 1967, Gen. Assembly IAU, Prague.
22. Lin, C.C., Shu, F.H., 1964, Ap. J., 140, 646.
23. Lin, C.C., Shu, F.H., 1966, Proc. Nat. Acad. Sci., 55, 229.
24. Lin, C.C., Yuan, C., Shu, F.H., 1968 (to be published.)
25. Lindblad, B., 1963, Stockholm Obs. Ann., 22, 3.
26. Lindblad, P.O., 1960, Stockholm Obs. Ann., 21, 3.
27. Lindblad, P.O., 1962, in Interstellar Matter in Galaxies, 222 (New York: W.A. Benjamin).
28. Mathews, W.C., 1965, Ap. J., 142, 1120.
29. Morgan, W.W., Sharpless, S., Osterbrock, D.E., 1952, A. J., 57, 3.
30. Morgan, W.W., Stromgren, B., Johnson, J.M., 1955, Ap. J. 121, 611.
31. Oort, J.H., 1962, in Interstellar Matter in Galaxies, 3-22, 234-244 (New York: Benjamin).
32. Oort, J.H., 1965, Gen. Assembly IAU, Hamburg, 789.
33. Roberts, M.S., 1957, Pub. A.S.P., 68, 59.
34. Roberts, M.S., 1962, A. J., 67, 437.
35. Roberts, M.S., 1967, Gen. Assembly IAU, Prague.
36. Roberts, W.W., 1968, A.A.S. meeting, Charlottesville, Va.
37. Sandage, A., 1961, in The Hubble Atlas of Galaxies (Washington, D.C., The Stinehour Press).
38. Schmidt, M., 1965, in Galactic Structure, 513-530 (University of Chicago Press).



39. Sharpless, S., 1965, in Galactic Structure, 131 (University of Chicago Press).
40. Shu, F.H., 1968, Ph.D. Thesis, Harvard University.
41. Spitzer, L., 1962, in Interstellar Matter in Galaxies, 98-107 (New York: Benjamin).
42. Spitzer, L., 1968, in Nebulae and Interstellar Matter, 1 (University of Chicago Press).
43. Wentzel, D.C., 1966, Ap. J., 145, 595.
44. Westerhout, G., 1958, B.A.N., 14, 215 and 261.
45. Westerhout, G., 1968 (personal communication).
46. Woerden, H. van, 1966, Gen. Assembly IAU.
47. Yuan, C., 1968 (to be published).

### Biographical Sketch

William W. Roberts was born on October 8, 1942 in Huntington, West Virginia. After graduating from Huntington High School as salutatorian of his class of 1960, he entered the Massachusetts Institute of Technology where he received the S.B. degree in mathematics in June, 1964. From the fall of 1964 to the fall of 1968, he has pursued graduate study in the Department of Mathematics at M.I.T. and has held teaching and research assistantships there. After receiving the Ph. D. degree in the fall of 1968, he will join the Department of Applied Mathematics and Computer Science at the University of Virginia as an Assistant Professor.

He has been employed by the RAND Corporation, Santa Monica, California, and by the M.I.T. Lincoln Laboratory, Lexington, Massachusetts, and by the U.S. Naval Underwater Weapons Research and Engineering Station, Newport, Rhode Island.

He is a member of The American Mathematical Society, The American Astronomical Society, The American Institute of Physics, and Sigma Xi.